Cláudia Alexandra Maia do Couto

B.Sc in Applied Chemistry

Active bionanoconjugates of laccase and gold nanoparticles: Kinetic and structural studies

Thesis for the master degree in Structural and Functional Biochemistry

Supervisor: Ricardo Franco, Assistant professor, FCT-UNL

Jury:

President: Prof. Isabel Borges Coutinho Medeiros Dias

Examiner: Prof. Eulália Fernanda Alves de Carvalho Pereira

Vowel: Prof. José Ricardo Ramos Franco Tavares

FACULDADE DE CIÊNCIAS E TECNOLOGIA
UNIVERSIDADE NOVA DE LISBOA

September 2012

Active Bionanoconjugates of laccase and gold nanoparticles: Kinetic and stuctural studies

Cláudia Couto

2012

Cláudia Alexandra Maia do Couto

B. Sc. in Applied Chemistry

Active bionanoconjugates of laccase and gold nanoparticles: Kinetic and structural studies

Thesis for the master degree in Structural and Functional Biochemistry

Supervisor: Ricardo Franco, Assistant professor, FCT-UNL

Jury:

President: Prof. Isabel Borges Coutinho Medeiros Dias

Examiner: Prof. Eulália Fernanda Alves de Carvalho Pereira

Vowel: Prof. José Ricardo Ramos Franco Tavares

Active bionanoconjugates of laccase and gold nanoparticles: Kinetic and structural studies

Acknowledgements

This dissertation would have not been possible without the guidance of Prof. Ricardo Franco as supervisor. I express the deepest gratitude to my supervisor for accepting me in his laboratory, not only this year, but in previous years as well, and to allow me to discover the fascinating world of nanoparticles. I am also grateful for the constant help and patience shown during this process. In addition, I would also like to thank Prof. Ludwig Krippahl for his help and support on the computational modelling studies.

The last eleven months were made of long hours of work and research, of successful moments and even draw backs. However, these were the times that encouraged me to move forward and accomplish the professional and personal objectives set in the beginning of this dissertation.
I personally want to thank Milton Silva, Tânia Monteiro, Diana Ribeiro, João Luz, Inês Gomes, Inês Osório, Isabel Silva, the remaining colleagues connected to Lab. 603 and degree colleagues. To them I owe many hours of friendly dedication and support. They have been with me throughout this process, always listening to both the frustrations and successes achieved.
Last, but not the least, I would like to thank to my family, especially my parents for their love, support and efforts to provide me with an academic education.

Abstract

The work presented here had the objective of using gold nanoparticles (AuNPs) functionalized with mercaptoundecanoic acid (MUA), or the peptide CALNN, to develop bionanoconjugates (BNCs) with the enzyme *Rhus vernicifera* (*Rv*) laccase. Laccases are multi copper oxidases able to catalyze the oxidation of a variety of phenolic compounds with the reduction of molecular oxygen to water, and conjugating this enzyme with AuNPs could potentially contribute to enhance its catalytic activity.

Spectroscopic, electrophoretic, kinetic, and computer modelling studies were carried out in order to characterize the enzyme structurally and investigate its stability and activity when conjugated with AuNPs.

The studies performed revealed that *Rv* laccase is a monomer with 5.65 ± 0.83 nm in diameter and presents an optimal activity at pH 7.5, when syringaldazine was used as substrate.

Laccase was successfully adsorbed to AuNP-CALNN but not to AuNP-MUA. BNCs with laccase and AuNP-CALNN remained active in the experimental conditions tested at pH from 6 – 8.5.

Laccase followed a Michaelis-Menten kinetic model using syringaldazine as a substrate, in the pH range 6 – 8.5. Parallel studies with free laccase were conducted to evaluate the influence of AuNP-CALNN on laccase activity. These kinetic studies were performed by following substrate consumption and product formation. The kinetic results with less error were obtained when the reaction of product formation was followed. Therefore, the results for product formation were considered to be more reliable than the results obtained for substrate consumption.

The results for product formation revealed that the catalytic efficiency of BNCs was more than 50% higher at pH 7, almost 100% higher at pH 7.5 and 30% higher at pH 8 in comparison with free laccase. At pH 6 there was a decrease of approximately 38% in the catalytic efficiency. The catalytic efficiency was similar in BNCs and free laccase at pH 6.5 and 8.5. In the pH range 6.5 to 8.5, AuNP-CALNN proved beneficial by either maintaining or increasing the catalytic activity of laccase. Using AuNP-CALNN to immobilize laccase might allow decreasing industrial costs, recycling the enzyme and improving the outcome of processes usually achieved with free laccase, such as delignification, wine clarification, textile dye bleaching or waste water detoxification.

Keywords: gold nanoparticles, laccase, bionanoconjugates, immobilization.

Resumo

O presente trabalho teve como objectivo o uso de nanopartículas de ouro (AuNPs) e a sua funcionalização com ácido mercaptoundecanoico (MUA), ou com o péptido CALNN. Estes ligandos conferem carga negativa às partículas e ajudam na imobilização de macromoléculas à sua superfície. Estas partículas foram posteriormente utilizadas para desenvolver bionanoconjugados (BNCs) com a enzima lacase de *Rhus vernicifera* (*Rv*). As lacases são oxidases que contêm cobre e que catalizam a oxidação de vários compostos fenólicos com redução de oxigénio molecular a água.

Efectuaram-se estudos espectroscópicos, electroforéticos, cinéticos e de modelação computacional com vista a caracterizar a enzima estruturalmente e compreender a sua estabilidade e actividade quando conjugada com AuNPs.

Os estudos efectuados revelaram que a lacase de *Rv* é um monómero de 5.65 ± 0.83 nm de diâmetro, e apresenta uma actividade óptima com o substrato siringaldazina a pH 7.5.

Esta enzima foi adsorvida à superficie de AuNP-CALNN com sucesso, mas não à de AuNP-MUA. Os BNCs produzidos a partir de laccase e AuNP-CALNN revelaram-se activos entre pH 6-8.5, nas condições experimentais ensaiadas.

A enzima laccase seguiu uma cinética típica de Michaelis-Menten na presença de siringaldazina. Todos os estudos cinéticos foram efectuados entre pH 6-8.5 com BNCs. Como termo de comparação, efectuaram-se também estudos cinéticos para enzima livre nas mesmas condições. Nestes estudos seguiram-se as reacções de consumo de substrato ou de formação de produto. Os resultados cinéticos mais fidedignos e com menor erro foram obtidos para a reacção de formação de produto.

Os resultados para formação de produto revelaram que a eficiência catalítica da lacase nos BNCs foi mais elevada a pH 7, 7.5 e 8. A pH 6 existiu um descréscimo na eficiência. No entanto, a eficiência catalítica foi semelhante à da enzima livre a pH 6.5 e 8.5. Entre pH 6.5 e 8.5 verificou-se que as AuNP-CALNN mantiveram ou melhoraram a actividade catalítica da lacase. A imobilização de lacase em AuNP-CALNN poderá assim vir a diminuir custos de processos, facilitar a reciclagem da enzima e poderá encontrar utilização em processos industriais de delinhificação, clarificação de vinho, descorar tintas em texteis, desintoxificação de águas residuais.

Termos chave: Nanopartículas de ouro, lacase, bionanoconjugados, imobilização.

Index

List of figures

List of tables

List of abbreviations and symbols

AuNPs	Gold nanoparticles
AuNP-CALNN	Gold nanoparticles functionalized with the ligand CALNN
AuNP-MUA	Gold nanoparticles functionalized with the ligand MUA
BNCs	Bionanoconjugates
BNC-CALNN	Bionanoconjugates with AuNP-CALNN
BNC-MUA	Bionanoconjugates with AuNP-MUA
BSA	Bovine serum albumin
Cys	Cysteine
DLS	Dynamic Light Scattering
EDC	Ethyl(dimethylaminopropyl) carbodiimide
I	Ionic strength
Lac	Laccase
MUA	Mercaptoundecanoic acid
NHS	N-Hydroxysuccinimide
PAGE	Polyacrylamide gel electrophoresis
PDB	Protein data base
pI	Isoelectric point
Rv laccase	*Rhus vernicifera* laccase
SDS	Sodium Dodecyl Sulfate Sodium
SDS-PAGE	Dodecy Sulfate Polyacrylamide gel electrophoresis
SPR	Surface plasmon resonance
SYR	Syringaldazine
TMAMQ	Tetramethoxy azobismethylene quinone
Tv laccase	*Trametes versicolor* laccase

Chapter I: Introduction

1.1. Bionanotechnology

Biotechnology, a researching field with high interest nowadays, is considered to be an area that is able to use materials available in the living cells to build custom-designed molecules to atomic specifications[1]. The characteristics of this investigation area provided a wide field of applications. They include commercial production of hormones and drugs, methods for diagnosing several diseases and engineering organisms for specialized tasks, such as bioremediation and disease resistance[1]. Biotechnology took several decades to develop. The main impediment for a fast development in this area was the lack of basic knowledge of biomolecular processes and mechanisms[1].

While biotechnology rapidly advanced over the last decades it also opened an opportunity window for new technologies to grow and become the focus of attention inside the scientific community. This opportunity made it possible for other investigation fields to progress even further and to be recognized as containing valuable knowledge for biology and medicine. It also allowed branching into other areas, such as nanotechnology.

Nanotechnology is the ability to build and shape matter one atom at a time, manipulating structures or particles with less than 100 nm[1,2]. In this size range, scientists are able to build molecules that have proprieties that can be tuned depending on the size, like the fluorescence of certain semi-conductive particles[2], and design atomic structures that have specific applications.

Nanotechnology expanded into bionanotechnology with the necessity to design molecular machinery to atomic specifications, and create bionanomachines capable of performing specific nanoscale tasks[1]. Nanomedicine takes the majority of the profits of this field. Bionanomachines work in the living cell environment and are tailored for medical applications. Complex molecules seek out diseased or cancerous cells, sensors are used for diagnosing diseases, and custom-built molecules are used for therapy[1].

Biomaterials are also an important application and address the growing ecological sensitivity of humankind. These are materials that, not only are strong, but also biodegradable and ideal to use as day to day materials. In addition, nanomaterials also have medical applications as well[1]. Other developments include the future possibility of production of hybrid machines, part biological and part inorganic[1], which will be able to encompass the characteristics of both materials and assemble into a new product with specific applications at the atomic scale.

Within this research area, nanoparticles became attractive inorganic materials with a wide variety of applications in Bionanotechnology. Nanoparticles have been the focus of many research groups ever since the pioneer work of Michael Faraday and its massive research and development later in the 1980s[3].

1.2. Gold nanoparticles

Metal nanoparticles are generally produced from noble metals, such as, gold, silver, and platinum[4]. These particles present sizes ranging up to 100 nm, and their size grants them distinct and improved proprieties when compared to the materials that originated them[4]. They encompass unique electronic, optical and catalytic properties. Nowadays, their use is so widely spread in industry that they can usually be found in common products, such as shampoos, soaps, detergents, shoes, cosmetic products, toothpaste, and in both medical and pharmaceutical applications.

The optical proprieties of nanoparticles rise from the electromagnetic surface waves that propagate in the interface between the conducting material and a dielectric in a wide range of frequencies[3]. Thus there is an electromagnetic field coupled to the conductive electrons called surface plasmons[3]. At reduced dimensions, as seen for nanoparticles, boundary and surface effects become extremely important.

Gold nanoparticles (AuNPs) encompass the phenomenon called surface plasmon resonance (SPR), which occurs when light is dispersed by a nanometric metallic material[5]. It occurs when the collective oscillation of these electrons is in resonance with the incident electromagnetic radiation[5]. The electric field of the radiation induces a dipole in the nanoparticle that leads to the production of a restoring force to compensate the dipole formation so that a unique resonance frequency matches the electron oscillation within the particles[3].

This phenomenon provides the distinct optical proprieties of nanomaterials that are mostly dependent on the size, but also on their shape and on the nature of the media[3,5].

The goal in AuNPs preparation is to obtain a material with good homogeneity in physical proprieties, which leads to a tight control over size, shape and surface proprieties.

Spherical AuNPs are usually synthesised by the method described by Turkevich *et al.*[6,7], based in the chemical reduction of a gold (III) precursor in an aqueous solution. Citrate is used to efficiently reduce gold and as a capping agent. The size of the final particles is directly related to the concentration of citrate added to the synthesis. These citrate-reduced AuNPs are very stable in aqueous solution. AuNPs synthesised with this method are red and show a typical plasmonic band in the UV-Visible spectrum with maximum extinction around 520 nm for particles with 5 – 30 nm in diameter[8,9].

AuNPs stability, and the possibility of aggregation, is an important parameter to evaluate when investigating the behaviour of these nano-systems and their characteristics. Aggregation of these AuNPs can occur in the presence of cationic or oligocationic species in solution. In these conditions, AuNPs will be closer to each other and a red-shift in the plasmonic absorbance will occur to higher wavelengths[10] resulting in purple coloured solutions (Figure 1.1).

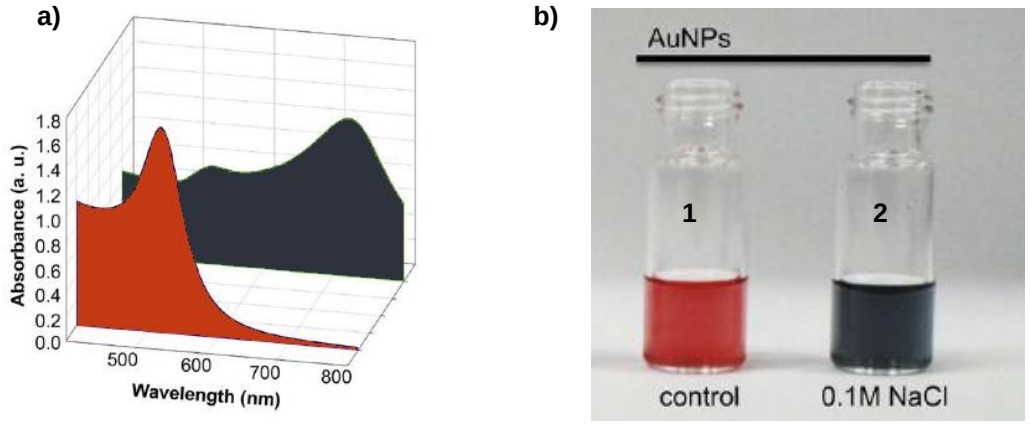

Figure 1.1. a) UV-Visible spectroscopy study of the spectral changes in the SPR of 16 nm AuNP-Citrate particles: Spectrum of AuNP-Citrate (red), spectrum of AuNP-Citrate with the addition of 0.1 M NaCl (dark blue); **b)** AuNP-Citrate solutions: 1) AuNP-Citrate solution related to the red spectrum, 2) AuNP-Citrate solution related to the dark blue spectrum[11].

1.2.1. Functionalization of gold nanoparticles

Preparation of AuNPs in solution rely on the use of capping agents, that adsorb to their surface and form a dense monolayer around the particles[12] (Figure 1.2). This adsorption can usually occur by chemisorption, electrostatic interaction, or hydrophobic interaction, and is a dynamic and reversible process[12].

The role of the capping agent is to both prevent the uncontrolled growth of the particles and convey surface proprieties that stabilize and protect nanoparticles against irreversible aggregation[12]. It is very common for the citrate-stabilized AuNPs to undergo changes to their functionalization by the exchange of citrate by another capping agent. This exchange occurs by the addition of a capping agent with higher affinity for AuNPs than the one already functionalizing the particles[12].

The usual capping agents are nonpolar, alkanethiol-capped molecules of 1-4 nm in diameter. Most functionalization strategies rely on thiol ligands with a hydrophilic terminal group[13]. These thiolated ligands, of various compositions, can either be charged or simply neutral. In the case of charged capping agents, ionic strength and pH of the media have a major influence in colloidal stabilization. This leads to the AuNPs to be soluble only in a limited pH range dependant on the isoelectric point of the capped AuNPs[12].

Capping agents are not only required for the AuNPs to remain stable and soluble in aqueous media, but also to convey controllable chemical reactivity and high optical detectability to the individual AuNPs[13].

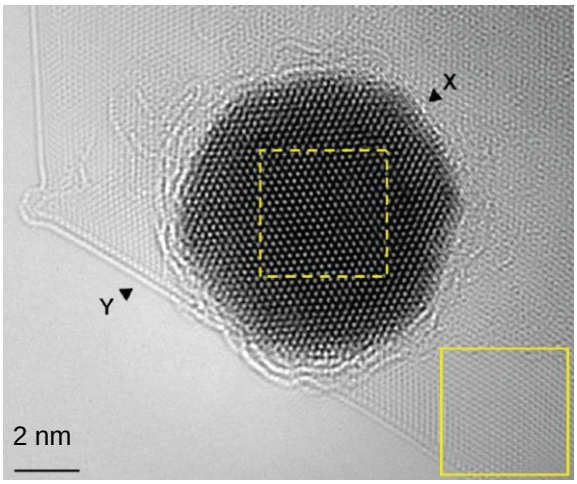

Figure 1.2. Atomic-resolution imaging of a gold nanoparticle with the surrounding citrate capping agent[14].

Various ligands for AuNPs were developed in the last 10 years[13]. Few have successfully been considered to bring advantages, such as improved colloidal stabilization, to the AuNPs. Among them are oligopeptides, like the pentapeptide CALNN (Cysteine, Alanine, Leucine, Asparagine, Asparagine)[13], or simple molecules like mercaptoundecanoic acid (MUA). At pH above 4 both are negatively charged and the preferential ligands that were used in the experimental procedures of this dissertation (Figure 1.3).

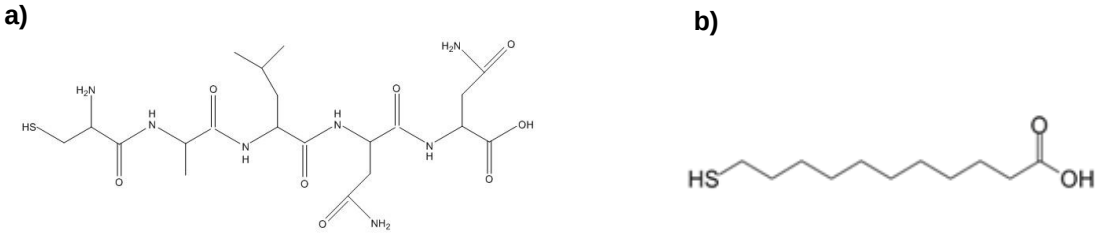

Figure 1.3. a) Structure of the pentapeptide CALNN, **b)** Structure of mercaptoundecanoic acid (MUA)

When ligands, such as CALNN, are added to citrate-capped AuNPs solutions, a shift of approximately 2 nm occurs in the maximum absorbance wavelength[13]. The plasmon band extinction increases slightly in just seconds after the addition[13]. This effect occurs because of the local change of dielectric permittivity that is the direct result of the formation of a peptide layer on the surface of the particles[13]. The reaction is instantaneous, first by electrostatic interaction of the opposite charged ligand to the negatively charged AuNPs, followed by the binding of the thiol group due to its high affinity for gold[13]. Ligands not only offer protection to the particles against electrolyte induced aggregation, but they also offer new proprieties and increased surface area. They have been found to be of aid in the immobilization of biomolecules in AuNPs surface with minimal activity loss[13,15].

1.2.2. Applications of gold nanoparticles

One of the major applications of AuNPs, mostly due to their size, is, as referred above, the immobilization of biomolecules[16]. Since biomolecules generally range in sizes from 2 – 20 nm themselves, they are able to cover the AuNPs surface[16].

One of the factors that influence the immobilization process is the functionalization of the AuNPs surface, thus the choice of capping agent is critical[12]. For example, AuNPs functionalized with charged capping agents can selectively bind to the opposite charge residues, in the case of proteins, or opposite charges in other molecules. Several types of biomolecules can be immobilized in AuNPs and form bionanoconjugates (BNCs).

The bond between AuNPs and biomolecules can be made by electrostatic adsorption of the macromolecule to the AuNP surface, or provided by chemical covalent bond with a cross-linking agent, such as EDC/NHS (Figure 1.4). Other strategies encompass affinity-based systems, with the attachment of a protein cofactor, and chemisorption by the thiolated amino acids of the protein (Figure 1.4).

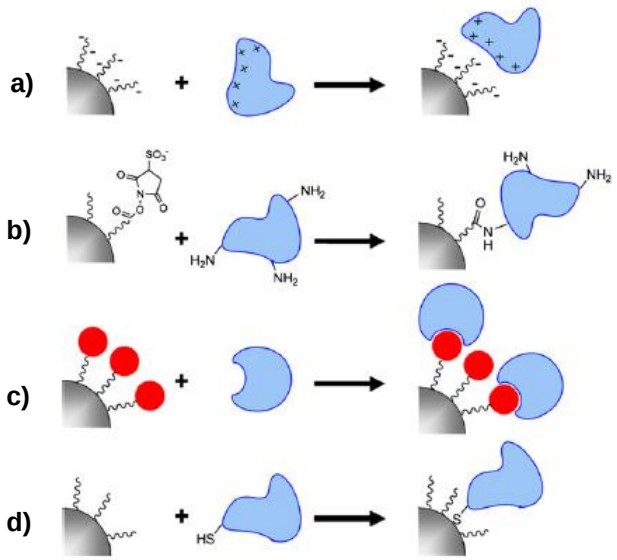

Figure 1.4. Schematic representation of nanoparticle-protein labelling strategies: **a)** electrostatic attachment, **b)** covalent attachment, **c)** attachment to a protein cofactor, **d)** direct binding of thiolated amino acid[15].

Additionally, there are several parameters that can also influence the structure and activity of proteins when linked to nanoparticles. These parameters are the characteristics of the nanoparticle itself (material, ligand, size, shape), the labelling site and the protein coverage (Figure 1.5)[15].

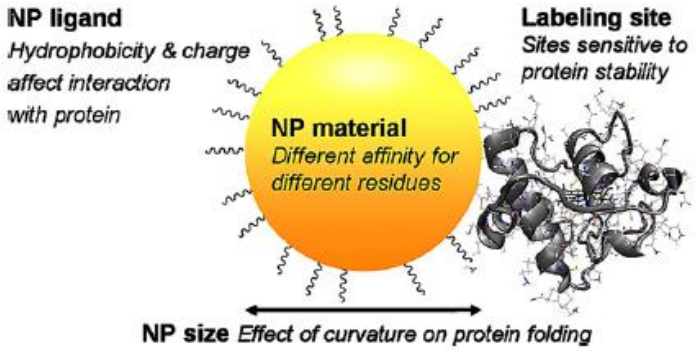

Figure 1.5. Schematic representation of the parameters that affect the interaction between protein and nanoparticles[15].

Enzyme immobilization has attracted interest in biotechnological processes due to the high operational stability and durability of this system[17]. In industrial biotechnology, the option to re-use an enzymatic catalyst through immobilization has proven to be one of the key steps in rendering an enzymatic process economically viable[18]. The immobilization process has also been used to enhance enzyme activity and stabilization in both aqueous and non-aqueous media[17].

Nanostructured materials, such as AuNPs, have been found to be a useful matrix for enzyme immobilization. They present a large surface area and good electronic proprieties that provide a stable surface for immobilization and act as conduction centres to facilitate transfer of the electrons[17]. Also, the high curvature of spherical AuNPs might be able to help preserving the three-dimensional structure of the enzyme[19], by decreasing the number of contact points between the enzyme and the highly electronical charged AuNP metallic surface.

After the formation of the AuNPs-enzyme complex, not only AuNPs might be able to confer extra stability to the enzyme, but the enzyme is also known to favour colloidal stability[20]. However the structure, stability and reactivity of the enzyme may vary during conjugation[20]. Since the enzyme's three-dimensional structure is essential to its activity, any structural alterations, such as the unfolding of the structure, are responsible for activity loss[17].

Often, AuNPs are able to bind to the active site, or promote conformational changes that completely inactivate some enzymes[15,16]. On the other hand, AuNPs might also be able to enhance the catalytic activity of an enzyme by linking to surface residues, far from the active site, increasing the exposure of the active site to substrate molecules [16]. The immobilization of redox enzymes with colloidal gold is thought to either help the protein to assume a favourable orientation or to make possible conducting channels between prosthetic groups and the gold surface[17]. In either case, it is important to keep in mind that inactivation or activation of an enzyme is not subjective and depends on the strategy required for a given system.

Special care should be taken during the process of conjugation to prevent denaturation and oversaturation of protein at the particles' surface that leads to the formation of multilayers[20].

In this case, diffusion limitations of the reactants to the inner layers of protein or even the inactivation of the enzyme may occur[20].
The goal for enzymatic immobilization in AuNPs is to find an ideal arrangement to achieve high selectivity, stability, reliability and low detection limits, preserving or enhancing the catalytic activity[21].

AuNPs with carboxyl terminated thiol groups have been used to successfully immobilize the enzyme glucose oxidase[22]. This system was found to confer higher thermal stability to this enzyme when immobilized[22]. Another successful immobilization was found to be between AuNPs and trypsin. In this case, these BNCs were found to have higher enzyme activity and stability than the free enzyme in the conditions tested[23]. Tyrosinase has also been found to form stable and active BNCs to be used in the biosensing of phenolic compounds[24].
Enzymatic immobilization in AuNPs has also been achieved with other enzymes such as lysozyme, aminopeptidase and alcohol dehydrogenase[17].

In electrochemical bioassays, AuNPs are used to connect enzymes to electrode surfaces and are able to mediate electrochemical reactions as redox catalysts. The particles also amplify recognition signals for biological processes[12]. Such electrodes include tyrosinase electrodes for phenol detection. There are also electrodes that aid in the electrocatalysis of molecules such as H_2O_2, O_2 or NADH that are involved in several biological processes[25].
The fact that AuNPs can be used as an ideal support for enzyme immobilization provides an advance for enzymatic biosensor construction. These biosensors are very useful in several biotechnological processes in food and environmental fields[22].
AuNPs are also used in drug delivery systems[26] and molecular diagnosis enabling early diagnosis and more effective therapies[12].
There are three main approaches when AuNPs are used in biodiagnosis: colorimetric sensing, surface functionalized AuNPs that provide highly selective probes used in fluorescence quenching-based assays, and electrochemical detection methods based on electrical signal enhancement provided by AuNPs[12]. The most developed is colorimetric sensing depending on inter-AuNP distance[12]. This type of approach has been applied in the detection of specific DNA/RNA sequences as well as for proteins/antigens and sugars in solution[12]. It is a method based on the colour change from red to blue as spherical AuNPs change from dispersed to aggregated.
With AuNPs new biosensors with improvements in sensibility, selectivity, easy fabrication and low cost have been developed.[25]
Sensitive immunoassays can be constructed with the conjugation between AuNPs and antibodies[12]. Detection relies mostly on electrochemical methods by using the advantages of increased surface area of AuNPs. These bionanoconjugates with antibodies, such as immunoglobulin G (IgG), can be immobilized onto an electrode surface, increasing detection sensibility[12].

In addition, since these particles are highly sensitive as transducers of target binding events, they have been applied in real-time immunoassays[12].
AuNPs have also brought added sensitivity to already existing techniques such as enzyme-linked immunosorbent assay (ELISA) as, for example, in the research to detect breast cancer biomarkers[27].

All the excellent characteristics of AuNPs, and the diversity of functions they can perform, make the field of nanotechnology one of the most interesting and rapidly developing fields of investigation in this century. They have been applied in biodiagnosis, cancer therapy, detection of pathogenic agents, textile industry, and even bioremediation.

1.3. Laccase

Some of the most attractive enzymes in the field of biotechnology are laccases. Laccases (EC 1.10.3.2, p-diphenol:dioxygen oxidoreductase) are multicopper proteins that belong to the blue-copper family of oxidases and have been studied since the nineteenth century. They can be found in a wide variety of higher plants, vegetables, fungi, bacteria[28] and recently were identified in insects and prokaryotes as well[29]. Laccases can be secreted or intracellular. Even though their function is different in the various organisms, all of them can catalyse polymerization or depolymerisation processes[29]. Frequently, some organisms produce isoforms of laccase with the same or even different features than the primary enzyme[28].
Fungal laccases have isoelectric points (pI) that range from 3 to 7, while plant laccases have pI values that can go up to 9[28].
Laccase activity also varies depending on the organism. For example, fungal laccases are well adapted to acidic conditions while plant laccases, being intracellular, have their optimal pH in the physiological range[28]. Fungal laccases usually have their optimal pH between 3.6 and 5.2. Other laccases, such as *Rhus vernicifera* (*Rv*) laccase that is found in a lacquer plant, has an optimal pH between 6.8 and 7.4[30]. It has also been reported that this laccase can also present maximal activity in a more alkaline medium.
In plants, laccases are involved in cell wall formation and lignifications processes, while in fungus, laccases are an important virulence factor[29] and remove toxic phenols from the medium[28]. It was also discovered that laccases are involved in various cellular and microbial activities. They are responsible for pigment formation in mycelia and fruiting bodies, improve cell-to-cell adhesion, and assist in the formation of rhizomorphs. They are also responsible for the formation of the polyphenolic glue that binds hyphae together[28]. Some other functions include insect sclerotization, bacterial melanisation, and melanin related virulence for humans[28].

1.3.1. Structural and functional features of laccase

Laccases occur as glycosilated monomers or homodimers, depending on the organism. Laccases' molecular weight ranges from 60 to 100 kDa with 10-50% of the weight attributed to the presence of monosaccharides (hexoseamine, glucose, mannose, galactose, fucose and arabinose)[28,31]. Glycosylation is extremely important to these enzymes since it is responsible for secretion, proteolytic susceptibility, activity, copper retention and thermal stability[28].

Besides the generic 280 nm protein band, the UV-Visible spectra of these enzymes also shows two maxima around 600 nm and 330 nm, characteristic of the copper centres[28]. The protein copper centres were classified by their redox, optical and magnetic proprieties[32]. Laccases contain four copper atoms per monomer and no other co-factor[32].

Type I copper (T1) is responsible for the absorbance band around 600 nm originating from the Cys → Cu^{2+} charge transfer[33]. Laccases also contain one type II copper (T2) and two type III coppers (T3). The T2 and T3 sites form the trinuclear active site[28] (Figure 1.6b).

The redox potential (E^o), the energy required to capture one electron from a reducing substrate with the corresponding formation of a cation radical, is determined in laccases by the T1 centre and can vary widely between laccases of different sources. The E^o of fungal laccases is higher than the ones for plant or bacterial laccases, therefore laccases can also be classified according to their high or low redox potentials (Table 1.1)[32]. The fungal *Trametes versicolor* laccase has a redox potential of +0.79 V and is considered a high redox enzyme, while the plant *Rhus vernicifera* laccase, with a redox potential of +0.43 V, is considered a low redox enzyme[32].

The reactivity of laccases has been correlated with their redox potentials and plays a major role in the enzyme performance, since the oxidation rate depends on the E^o difference between the reducing substrate and the T1 centre[32]. A hydrophobic residue, a leucine or phenylalanine, at the axial position of T1 copper is implicated in the high redox potentials, but it is not the sole contributor for this feature[32].

Table 1.1. Redox potential (E^o) values of laccases and other multi-copper enzymes from different origins[32].

Species	Organism	Enzyme	CuT1 E^o(V)	Potential axial ligand	Ref
Trametes versicolor	Basidiomycete	Laccase	+0.79	Phe	(Alcalde *et al.*, 2002)
Trametes villosa	Basidiomycete	Laccase	+0.79	Phe	(Kumar *et al.*, 2003)
Neurospora crassa	Ascomycete	Laccase	+0.78	Leu	(Piontek *et al.*, 2002)
Rhizoctonia solani	Deuteromycete	Laccase	+0.71	Leu	(Kumar *et al.*, 2003)
Coprinus cinereus	Basidiomycete	Laccase	+0.55	Leu	(Kumar *et al.*, 2003)
Scytalidium thermophilum	Basidiomycete	Laccase	+0.51	Leu	(Kumar *et al.*, 2003)
Homo sapiens	Mammalian	Ceruloplasmin	+0.49	Met	(Kumar *et al.*, 2003)
Myrothecium verrucaria	Fungi mitosporic	Bilirubin oxidase	+0.48	Met	(Kumar *et al.*, 2003)
Myceliophthora thermophila	Ascomycete	Laccase	+0.47	Leu	(Alcalde *et al.*, 2002)
Rhus vernicifera	Plant	Laccase	+0.43	Met	(Yaropolov *et al.*, 1994)
Zucchini (Cuburbita pepo)	Plant	Ascorbate oxidase	+0.34	Met	(Kumar *et al.*, 2003)

Three-dimensional structures of several laccases obtained by X-ray crystallography have already been reported. Most of the structures obtained are from fungal laccases, such as the one from *Trametes versicolor* (*Tv*) (Figure 1.6)[32].

Tv laccase is a monomer that consists in three domains[32]. Domain 3 contains T1 copper, domain 2 contains residues that participate in substrate binding and the T2 and T3 coppers are situated between domain 1 and 3[32]. The structure of this laccase is stabilized by two disulfide bonds. The T2 and T3 coppers are arranged in an almost perfect regular triangle shape. In addition, there are two channels, one broad and one narrow, which facilitate the access of solvent molecules to the trinuclear active site[32].

The electrostatic surface potential distribution for this enzyme has been reported to have a dominance of negative charges at pH 5.6 (above the pI of 3.5)[34]. It is known that the substrate binds to a small negatively charged cavity near the T1 copper site[34]. This negative pocket might help stabilize the cation product formed during the catalytic activity[34].

These crystallographic studies and others lead to the conclusion that the active site and its environment are structurally highly conserved[32].

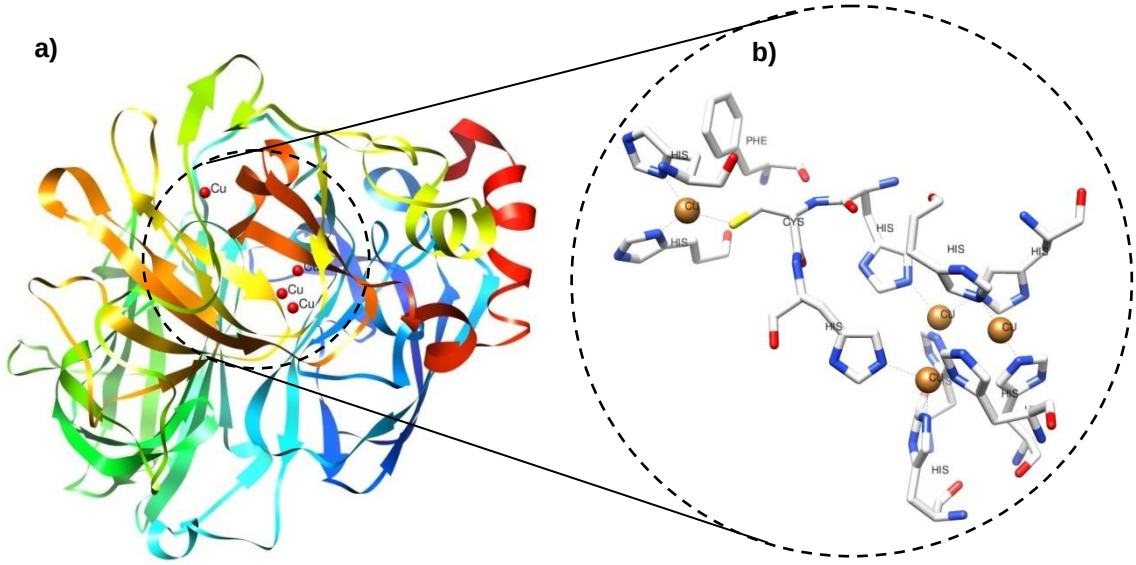

Figure 1.6. a) Three-dimensional X-ray molecular structure of laccase from *Trametes versicolor* with full copper content at 1.90 Å (PDB code: 1GYC[34]). Structure produced with the software Chimera[35]. Secondary structure represented with flat ribbon and coloured with the rainbow code from blue to red (N-terminal in blue to C-terminal in red); copper atoms represented in red; **b)** Zoom of the active site region: Copper atoms (orange) and the amino acids that coordinate each copper.

To this day, the three-dimensional structure of *Rhus vernicifera* laccase, used in the experimental procedures in this dissertation, remains unknown.

In 2002, Nitta *et al.*, reported that the *Rhus vernicifera* tree has at least three laccase isozymes[36]. Yet only the cDNA fragment for one isozyme was obtained from both stems and leafs. This isozyme, laccase-1 (Genbank: AB062449), was used to study the structure and similarities with laccase isozymes from other sources[36].

With sequence alignments and phylogenetic studies it was found that *Rv* laccase has high homology with other plant laccase isozymes (up to 62% in the case of *Acer pseudoplatanus* laccase)[36]. In comparison with other organisms, *Rv* laccase has 24% similarity with *Coprinus cinereus* laccase and 22% with *Trametes versicolor* laccase[36]. Of all these examples, only *Tv* laccase has a known three-dimensional structure. The low homology between *Rv* and *Tv* laccase might be due to their different origins, since one is found in a plant and the other in fungi, which translates into their different biological roles[36]: while plant laccases are involved in lignifications processes, fungal laccases remove toxic phenols from the medium[28].
Furthermore, this study also revealed that the structure of *Rv* laccase was predicted to have 28.7% of β-sheet content, 67.0% loops and random structures and only 4.3% of α-helix content[36].

Phylogenetic studies based on sequence alignments of several laccases from different origins have also shown that the copper-binding domains remain highly conserved[32].
Sequence alignments of more than 100 plant and fungal laccases resulted in the identification of sequences that uniquely characterize laccases as a distinctive group of enzymes from the multi-copper family[32]. These studies also revealed a sequence of 12 amino-acids that serve as copper ligands[32]. Figure 1.7 shows the sequence of amino acids in *Rv* laccase that are involved in copper binding[36]. The sequence encompasses ten histidines (H), one cysteine (C) and one methionine (M). This arrangement was found in other laccases with the exception of the T1 copper axial ligand being either leucine or phenylalanine instead of methionine[32,34,36]. This conservation in structure is intimately linked to the copper oxidation and O_2 reduction mechanism characteristic of these enzymes[32].

56 LTI**H**W**H**GVKQ
99 GTLWW**H**A**H**SDWT
433 **H**PM**H**L**H**GFNL
490 GVWFL**HCH**FER**H**TTEG**M**A

Figure 1.7. Segments from the amino acid sequence in *Rv* laccase primary structure (Genbank: AB062449) involved in copper binding[36]. The numbers refer to the position in the total sequence of the first amino acid at each sequence represented. The amino acids that directly bind to copper are in bold: ten histidines (H), one cysteine (C) and one methionine (M).

1.3.1.1. Laccase active site

With magnetic circular dichroism (MCD) and X-rays absorption spectroscopy, it was possible to conclude that T2 and T3 coppers function as a trinuclear copper cluster in respect to exogenous ligand interaction and interaction with dioxygen. T2 copper is coordinated by two histidines and water as ligands, while the two T3 coppers are each coordinated by three histidines and both bind to a hydroxide molecule (Figure 1.8). T2 copper has been found to be required in the reduction of oxygen and is involved in the stabilization of the peroxide intermediate[37].

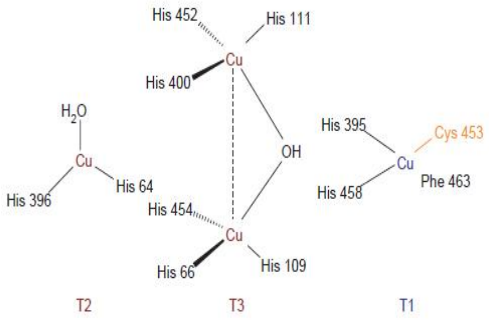

Figure 1.8. Model of the catalytic cluster of the laccase from *Trametes versicolor* made of four copper atoms, one type I (T1), one type II (T2) and two type III (T3)[29].

In the presence of a reducing substrate, T1 copper is the primary electron acceptor, the first to be reduced, and remains oxidised while the electron is transferred to the trinuclear copper cluster[38]. The reduction of the T1 centre was found to be the rate-limiting step of the reactions that occur in the active site of laccases.

Reaction with oxygen, which serves as terminal electron acceptor, is thought to occur in two two-electron steps. The peroxide intermediate facilitates the second two electron reduction from the T1 and T2 sites. At that point, peroxide is coordinated to the reduced T2 site while the T3 site acts as a two electron acceptor[37].

Water seems to be an interchangeable ligand at the T2 site, because it has been reported that some level of enzyme inhibition occurs at high pH values with the formation of a T2-OH^- complex that does not allow the reduction of the T3 site[37].

It is clear that the reactions in the active site yields a reactive cation radical while reducing one molecule of oxygen to two molecules of water, leaving the coppers oxidised[29]:

This reaction is not straight forward, since it is necessary to obtain four electrons to reduce one oxygen molecule to two molecules of water. It is speculated that laccase stores electrons from several substrate oxidation reactions until it is able to reduce molecular oxygen[38].

The radical that is generated in the enzymatic reaction is unstable and quickly undergoes an alternate reaction, either forming a quinone or a polymer[28].

Preferential laccase substrates are generally phenols, *ortho*- and *para*-diphenols[39], aromatic or aliphatic amines and some are the same substrates as used by tyrosinases[28].

In 1999, Huang *et al.*[33] proposed a mechanism for the active site reaction of *Rv* laccase by studying the oxygen-centered radical by UV-Visible spectroscopy, EPR spectroscopy, coupled with stopped-flow and SQUID measurements (Figure 1.9).

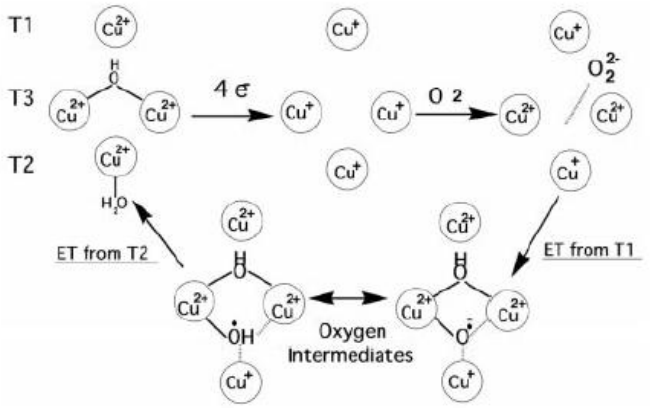

Figure 1.9. Proposed reaction mechanism of dioxygen reduction to water by laccase[33].

The mechanism proposed clarified what was already thought to happen at laccase active sites, and the necessity to obtain four electrons to reduce one oxygen molecule to two molecules of water. In the intermediate state, T1 and T3 coppers are oxidised while both T3 coppers are bridged by a hydroxide or oxide ion. The proton sources to form water from the hydroxide ion are usually the substrate, bulk water or certain amino acids near the active center[33]. Furthermore, the intermediate radicals appeared to be in equilibrium with H^+ depending on the pH. One of the oxygen atoms is converted to the bridging hydroxide and another to the radical species bound to the trinuclear centre. The reaction ends when the final electron is transferred to the intermediate radical to form hydroxide ion or the interchangeable water molecule bound to T2 copper[33].

1.3.2. Laccase applications

The ability to oxidise phenol derivatives makes these enzymes useful in the efforts of decontamination of industrial wastewaters[40]. In addition, the polymeric polyphenolic derivates of their activity are usually insoluble and can easily be removed[29].

Removal of phenols is also a component required for beverages such as wine and certain juices. Still, in this kind of procedure, it is essential for laccases to be immobilized, and able to be removed at the end of the process since laccases are not approved as food additive[29].

The substrate range for laccases can be extended to non-phenolic molecules by the use of a mediator. As a result, laccases with low redox potentials can participate in several mediated systems with high oxidation capacity[28].

These enzymes are also heavily present in textile, dye and printing industries, mainly in the process of decolourisation of dyes, or in paper industries for delignification of woody fibres or in bleaching processes[29,39].

Laccases, heterologous expressed in *S. cerevisiae*, are also used in the production of fuel ethanol[41]. They are also present in the cosmetic industry. Laccases have been used to

substitute harsh chemicals in hair dyes in a way that dye precursors are oxidised by laccase to achieve the colouring agent required[32].

In medicine, these enzymes are also starting to make an appearance in the treatment of various conditions[28].

The field of organic chemistry has also been interested in seeking the benefits of these enzymes, particularly in the area of biocatalysts[29] in order to develop new synthetic applications. It is clear that laccases constitute a green and safe option against the chemicals that are usually implemented in some processes.

Electrobiochemistry allowed laccases to be employed in the design of biosensors for waste water decontamination, or to be used in food industry and to build biofuel cells.

The biotechnology field has looked with interest to the immobilization of laccases on solid supports as an efficient way to improve stability and the ability to recycle the enzyme. There are several immobilization techniques already in use for laccase, such as entrapment by physical interactions, encapsulation into a porous solid matrix, adsorption into a support by ionic forces, covalent binding to a support and self-immobilization with cross-linked laccase aggregates[39]. Immobilization allows recycling the enzyme and making their application process more profitable.

One of the methods currently under investigation is the possibility of laccase immobilization in gold nanoparticles[39], the formation of bionanoconjugates that enhance the enzyme features[42] or using laccase in the synthesis of gold nanoparticles[43].

1.3.3. Rhus vernicifera laccase

The first laccase to be discovered was found in the Japanese lacquer tree *Rhus vernicifera (Rv)*, and it is the one studied in the present dissertation. This enzyme was first described by Dr. Yoshida, in the nineteenth century, and heavily studied ever since. Detection and purification of this protein is a difficult process because the crude plant extracts contain a large quantity of different oxidative enzymes with broad substrate specificities[44]. *Rv* laccase is often purified from the tree's tissue extracts, generally in the form of an acetone powder with heavy content in contaminants[45,46].

Its main function is to oxidise the phenolic subunits present in lignin, although it can also perform the oxidation of other phenol compounds. *Rv* laccase is a monomer and has a molecular mass of approximately 100 kDa determined by SDS-polyacrylamide gel electrophoresis[47].

As seen in section 1.3.1, *Rv* laccase T1 copper has a redox potential of +0.43 V, and it defines the catalytic efficiency of this enzyme[38]. In comparison with the redox potential of other laccases, *Rv* laccase is considered to have a low redox potential (Table 1.1). Nitta *et al.*[36] suggested that the presence of a methionine residue, involved in the binding of T1 copper, might be one of the causes for *Rv* laccase low redox potential.

As discussed in more detail in section 1.3.1, the three-dimensional structure is not yet available for *Rv* laccase, mostly for the incapacity to obtain pure enzyme. The only primary structure accessible is of a isozyme of this protein[36]. It is predicted that the active site is conserved and mostly similar to other laccases which structure is already known[36]. From the already existing X-ray three-dimensional structures of laccases, *Rv* laccase has the best homology with *Trametes versicolor* laccase (22%)[36].

1.3.4. Kinetic studies with *Rhus vernicifera* laccase

In the catalytic reaction of *Rv* laccase with the majority of substrates the formation of a radical intermediate occurs. This unstable radical is then rapidly converted to product. Additionally, several studies indicated that the optimal pH of catalytic activity for this laccase is dependent on the substrate used[46,48].

In order to understand the kinetic performance of *Rv* laccase and its susceptibility to changes in the media, its Michaelis-Menten behaviour was investigated.

$$V0 = \frac{Vmax[S]}{KM + [S]} \qquad [1]$$

In the Michaelis-Menten equation (Equation 1), V_0 stands for the initial rate of the reaction in the presence of a known concentration of substrate ([S]). V_{Max}, also associated with the turnover number k_{cat}, reveals the number of substrate molecules converted into product by the enzyme in a unit time when the enzyme is fully saturated with substrate[49]. K_M indicates the concentration of substrate at which half of the active sites are full, and provides the measure of substrate concentration required for significant catalysis to occur. It also measures the strength of the enzyme-substrate complex, being a measure of the affinity of the enzyme towards the substrate. If K_M is low it indicates that the affinity is high[49,50]. This specific parameter depends on the substrate and on the reaction conditions such as pH, temperature and ionic strength[49].

This kind of kinetic study generates a plot with *V_0 vs [S]* where, by fitting equation 1 to the experimental data, the Michaelis-Menten parameters can be obtained (Figure 1.10).

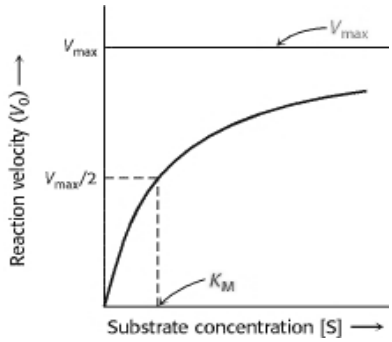

Figure 1.10. Plot of the reaction rate (V_0) as a function of the substrate concentration [S] for an enzyme that obeys Michaelis-Menten kinetics.

Other parameters that can also be obtained include k_{cat}, that is related to the enzyme turnover number when the concentration of active sites is known, and the ratio k_{cat}/K_M that shows the catalytic efficiency of the reaction[50].

One of the synthetic substrates for *Rv* laccase is 3,5-dimethoxy-4-Hydroxybenzaldazine, or commonly known as syringaldazine (SYR) (Figure 1.11). It is usually the preferential substrate used in kinetic studies and detection of this enzyme, since it is the only substrate that is considered to be oxidised only by laccase.

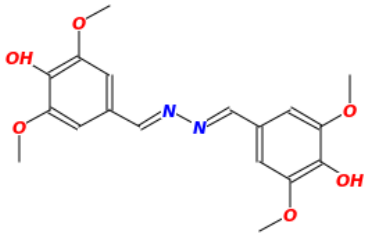

Figure 1.11. Structure of 3,5-dimethoxy-4-Hydroxybenzaldazine, syringaldzine (SYR)[51].

Syringaldazine is a pale yellow crystalline compound synthesized from syringaldehyde and hydrazine hydrochloride[52]. It is a photo-sensitive molecule, and is also sensitive to the media where it is dissolved. To prevent degradation, SYR is usually dissolved in an alcohol solution, preferably methanol, and stored in glass away from light sources.

In the presence of *Rv* laccase SYR is oxidised to a pink coloured product by following the reaction in Figure 1.12a. This reaction is essentially characterized by the two-electron-two-proton transfer performed by laccase. The product is tetramethoxy azobismethylene quinone (TMAMQ) and has an absorption maximum at 530 nm[53] (Figure 1.12b).

The catalysis occurs in the alcohol groups in the aromatic rings and is promoted by the presence of oxygen molecules that are later reduced to molecules of water.

Under appropriate conditions, TMAMQ is not prone to polymerization. The reaction product can be formed at all pH conditions, but decomposes some time after formation if the pH is not in the 3 – 7 range[52].

SYR is also sensitive to the presence of chloride, and this characteristic has been used for the colorimetric determination of chloride in water[54]. On the other hand, laccase-generated TMAMQ has been used to measure the antioxidant activity of a large variety of antioxidants in both food industry and human health[55].

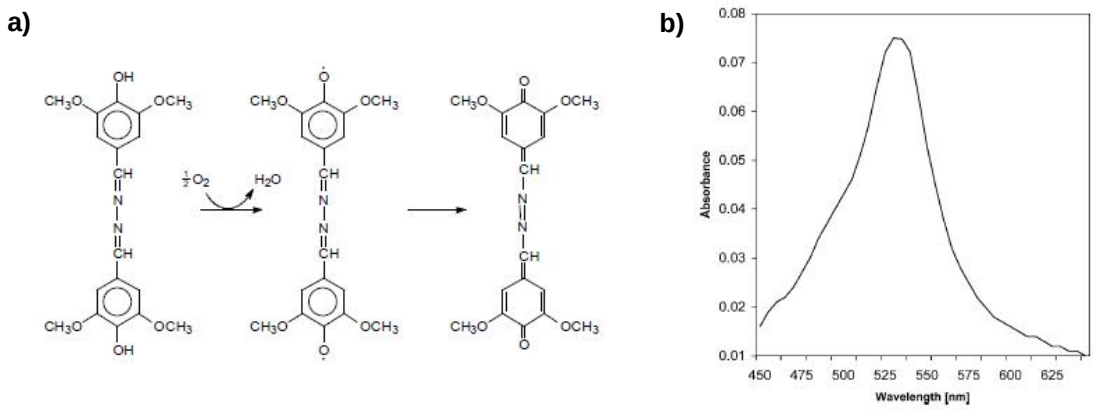

Figure 1.12. a) Schematic representation of the oxidation reaction of syringaldazine in the presence of laccase that results in the formation of water and a quinone (TMAMQ); **b)** Visible spectrum of the quinone (TMAMQ) produced from the oxidation of SYR by laccase with maximum absorbance at 530 nm[56].

1.4. Dynamic Light Scattering (DLS) and Zeta Potential

In an attempt to study the interactions between nanoparticles and proteins in the formation of bionanoconjugates, several methods can be implemented. One of the most reliable ways to study these interactions is by light scattering.

Dynamic light scattering (DLS) is an analytical tool that takes advantage of the proprieties of colloidal solutions, in particular of gold nanoparticles. AuNPs are capable of scattering light at, or near, their surface plasmon resonance (SPR) wavelength, thus offering an approach to measure their size, stability and interaction with biomolecules in solution[57]. Light-scattering cross-section of AuNPs with 60 nm in diameter is 200-300 times stronger than a polystyrene bead of the same size. It is also 4-5 orders of magnitude stronger than of a strong fluorescence dye[57]. Consequently, AuNPs have been used as a light scattering enhancer[57].

The DLS technique allows measuring the increase in particle size in solution, due to aggregation, when an antigen or target DNA binds to antibody or DNA-conjugated AuNPs[57]. Hence DLS is an excellent technique to study the interactions between conjugated AuNPs and target analytes[57].

DLS also allows measuring the size of some biomolecules, for example globular proteins, free in solution[58]. It also is able to indicate conformational changes and denaturation[58].

This technique is based on the Brownian movement of particles in a liquid environment and it is directly related to their size. Large particles have a slow Brownian movement, while small particles can move much faster in solution[59] (Figure 1.13).

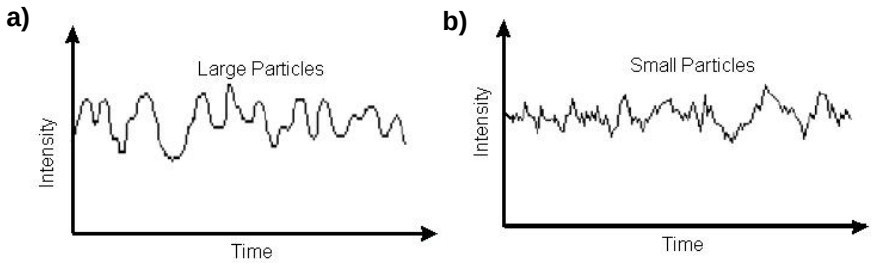

Figure 1.13. Typical intensity fluctuations: **a)** for large particles; **b)** for small particles[59].

Nowadays it is possible to measure the spectrum of frequencies in the intensity fluctuations caused by the Brownian motions rapidly over a period of time[59].

The velocity of this movement is defined by the translational diffusion coefficient that is present in the calculation of the particle size through the Stokes-Einstein equation (Equation 2)[59].

$$d\,(H) = \frac{kT}{3\pi\eta D} \qquad [2]$$

In this equation, *d (H)* refers to the hydrodynamic diameter of the particle, *D* is the translational diffusion coefficient, *k* the Boltzman constant, *T* the temperature and *η* the viscosity.

The translational diffusion coefficient depends not only on the size of the particle core, but also on surface structure, concentration, and type of ions in the medium[59].
The hydrodynamic diameter obtained with this technique is the diameter of a sphere that has the same translational diffusion coefficient as the particle being measured[59].

Another way to evaluate biomolecular binding to colloidal surfaces is by studying zeta (ζ) potential, which is a physical property of particles in solution.
The net charge at a particle's surface affects the ionic distribution that surrounds the interfacial region, which results in an increased concentration of counter ions close to the surface[60]. This feature creates an electrical double layer around each particle. In the inner region (Stern layer), the ions are strongly bound, whereas in the outer layer the ions are less firmly bound and more diffuse. When the particle moves, the ions within the boundary of the diffuse layer move with it, but the ions outside that boundary do not. This boundary is often called slipping plane[60] (Figure 1.14a). The potential in this boundary is known as the zeta potential[60].
By measuring the repulsion or attraction between the particles the stability of the system can be predicted. Particles with very positive or very negative zeta potentials tend to repel each other, while zeta potentials close to neutrality suggest that the particles have the tendency to aggregate[60,61].
This technique takes advantage of the velocity in which the particles travel in solution, the electrophoretic mobility[60]. The particles move due to an electric field imposed in the sample by a system of electrodes. Depending on the charge of the particles, they will migrate towards the electrode of opposite charge with a certain velocity (Figure 1.14b). This velocity is influenced by

the strength of the electric field, the zeta potential, the dielectric constant and viscosity of the medium[60].

The electrophoretic mobility is measured by the intensity of light scattered. The rate of the fluctuations in the intensity signal is proportional to the velocity of the particles[60].

Consequently, by converting the electrophoretic mobility with theoretical considerations, it is possible to know the zeta potential of the particles of a certain colloidal system[61].

The factors that have a major influence in zeta potential are pH and ionic strength[61].

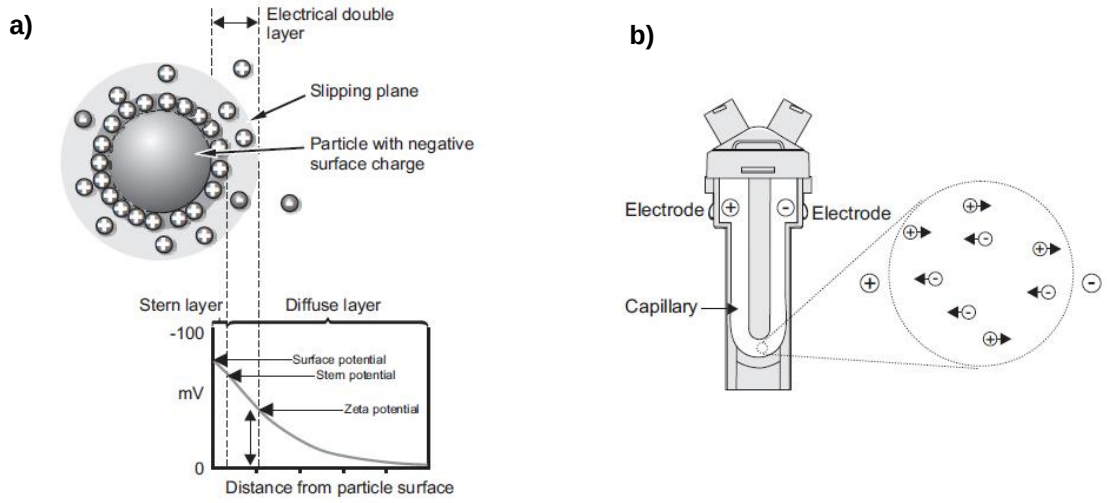

Figure 1.14. a) Schematic representation of the ionic double layer surrounding a particle; **b)** Schematic representation of a zeta potential measuring cell representing the electrophoretic mobility of the charged particles in the electric field[60].

1.5. Computational techniques

In life sciences it is important to identify the structures of macromolecules, such as proteins or DNA, and understand how they undergo conformational changes that make possible for them to function as signalling molecules, transporters, catalysts, sensors, and interact with other molecules[62]. A variety of molecular simulations has been created so far, and will continue to be with the aid of informatics, in order to answer the majority of these questions. So far, computational techniques have been able to predict the conformational changes, dynamics, folding and ligand binding of certain proteins with high accuracy[62]. Drug design has also been one of the major focuses when using computational tools in favour of scientific investigation. The past decades have seen an extraordinary advance in these techniques, as software became more reliable and scientifically accurate, mimicking biological systems with impressive resolution.

There is also the fact that biological data is produced at a high rate these days, and it encompasses the necessity to create databases to store and organize that data. Scientific data also needs to be available to the community worldwide, avoiding redundancy and helping in scientific research[63]. Databases like *NCBI*[64], *SWISS-PROT* or *GenBank* have been

indispensable for protein and genetic researches, just as the *Protein Data Bank* (PDB)[65] has been essential to store three-dimensional structures of macromolecules[63]. To process this data, it is necessary to use appropriate software.

1.5.1. Electrostatic surfaces of proteins

Electrostatic interactions are one of the most important factors when studying the function of biological molecules, and it plays a major role in protein related research[66]. Currently, a variety of computational methods and algorithms are available to aid in studying proteins and their interactions with other molecules. These methods include molecular dynamics simulations, Brownian dynamics simulations, protein pKa calculations, protein-design algorithms and protein-drug or protein-protein docking algorithms[66]. All of them require three-dimensional structures of proteins to analyse the protein characteristics, such as catalytic activity, folding pathway, stability, solubility and ligand/drug binding specificity[66]. However, the full capacity of these methods will only be reached when the electrostatic energies and forces in and around proteins are able to be calculated with accuracy[66]. This goal has been proven difficult to achieve. The electrostatic phenomena in biomolecular systems are complex, and there is the need to consider the interactions between a large number of solvent and solute atoms[66]. Proteins also present many charged groups and the variation in the amino acids pKa values complicates the calculations of charge distribution even more[66]. In addition, the heterogeneous dielectric proprieties of the protein interior also add to the complexity of the calculations[66].
In spite of all these difficulties, the algorithms currently available have been successful in predicting the electrostatic effects in proteins[66].
The study of electrostatic surface of a specific protein is one of the interests of the present dissertation, as well as to understand the possible interactions with other known structures. For that effect the *H*++[67] software, that is able to calculate protonation states of amino acids based on classical continuum electrostatics, basic statistical mechanics and on the pH environment[67], can be used in conjugation with the software *Chemera*[68] to obtain a reasonable approximation to the real electrostatic surface of a protein.

In terms of computational tools, it is always important to keep in mind that the software, mostly the ones that recreate situations that have not been observed experimentally, are based in statistic calculations that attempt to obtain the best approximation to reality. In reality, macromolecules are dependent on a diversity of variables and microenvironments that can influence the system in study and are yet difficult to reproduce by the tools available.

Chapter II: Experimental Procedures

2.1. Instrumentation

Weight measurements of solids were made using an analytic scale *Radwag As 220/C/2* (0.001 ± 0.0001 g) and a semi-analytic scale *Sartorius BP610* (0.1 ± 0.01 g).

All pH measurements for solutions and buffers were performed with a *Crimson pH Meter Basic 20+.*
Spectrophotometric studies for laccase activity were performed using a *Unicam Uv/Vis Spectrophotometer Uv2* connected to a heat control instrument from *Bioblock Scientific*. Experimental data was collected using the rating method of software VisionPro 4.1 and a Uv cuvette macro of 2.5 mL from *Plastibrand*.

Other Spectrophotometric studies, including all kinetic studies, were made using the *Varian Cary 50 Bio Uv-Visible* spectrophotometer and the *Cary WinUv* software using the applications of Scanning Kinetics, Simple Reads, Concentration and Scan. These studies were performed with a 1.5 mL Uv quartz cell semi-micro with black walls, 10 mm, purchased from *Zuzi*.

Electrophoretic studies were made with all necessary instrumentation provided from *Biorad* and a *Biorad PowerPac Basic* electric source.

All necessary centrifugations were achieved using an *Eppendorf Centrifuge 5810 R*, using either the eppendorfs or the tube rotor as necessary.

Agitation and heating procedures were made with the aid of an *Agimatic-N* motor heater from *PSelecta*.

Dynamic Light Scattering and Zeta potential measurements were carried out using the instrument *Zetasizer Nano Zs* with a He-Ne laser (633 nm) and fixed dispersion angle of 173º, and *Zetasizer 6.34* software from *Malvern Instruments*. Folded capillary cells from *Zetasized Nanoseries* were used for zeta measurements, while 1.5 mL Uv cuvettes from *Plastibrand* were used for DLS. These studies were made at Instituto de Tecnologia Química e Biológica (ITQB) in Lisbon.

2.2. Reactants and solvents

In the experimental work performed for the present dissertation, all glass material for AuNP synthesis was cleaned with *Aqua Regia* solutions (nitric acid/hydrochloric acid 1:3 v/v), while the remaining glass and plastic material was cleaned with Milli-Q water (18 mΩ of resistivity).
AuNP synthesis was performed with a gold (III) chloride solution (30% wt in dilute HCl, 99.99% pure, Sigma), sodium citrate (99.9% pure, Sigma), and Milli-Q water.
The MUA ligand used to functionalize AuNPs was purchased from Sigma (98% pure), while the pentapeptide CALNN was purchased from CASLO Laboratory ApS, Technical University of Denmark.

Potassium phosphate buffers were prepared with potassium phosphate dibasic salt (Riedel-de Haen), potassium phosphate monobasic salt (Riedel-de Haen), potassium hydroxide (Pronalab), and sodium chloride (Sigma). Other buffers required for electrophoresis experiments were prepared with trizma base (Fluka, 99% pure) and glycine (Sigma, 99.7% pure). Polyacrylmide electrophoresis also required solutions prepared with methanol (Sigma, 99.8% pure), acetic acid (Sigma, p.a.) and brilliant blue R (Sigma).

PAGE gels were prepared with acrylamide/bis solution 35.5:1 (Biorad, 26%), TEMED (Biorad) and sodium Sodium Dodecyl Sulfate (Lauryl SDS) (Panreac).

Agarose gels were prepared from agarose powder (Invitrogen Ultrapure™ Agarose).

Protein standards for SDS-PAGE nzycolour protein marker II (high and low range) and standards of low range were purchased from NzyTech.

Cross-linker agent solutions were prepared with ethyl(dimethylaminopropyl) carbodiimide (EDC) (Sigma) and N-Hydroxysuccinimide (NHS) (Fluka, 97% pure).

DMSO was purchased from Sigma.

Laccase from *Rhus vernicifera* was purchased as a crude acetone powder from Sigma (≥50 U/mg solid). Syringaldazine, as substrate for laccase used in enzymatic experiments, was purchased from Sigma and a stock solution was prepared by dissolving the powder in methanol (Sigma, 99.8% pure).

2.3. Methods

2.3.1. Synthesis of gold nanoparticles

Gold nanoparticles (AuNPs) were synthesised in the laboratory following Turkevich *et al*.[7] method with some modifications. Briefly, in a round-bottom flask, 200 mL of Milli-Q water were heated to 100 ºC with 175 µL of the gold (III) solution until it reached a reflux state (after approximately one hour). In that stage, 50 mL of a 1% sodium citrate solution were rapidly added to the heated solution. After 15 minutes, the solution changed colour from yellow to grey and finally reached the deep red colour characteristic of spherical AuNPs. Since sodium citrate was used as the reducing agent in this synthesis, the final dimensions of the particles were directly dependant on the citrate concentration.

After the synthesis, the nanoparticles stabilized with citrate were able to be functionalized with the ligands MUA and CALNN of negative charge.

2.3.2. Characterization of gold nanoparticles

Each batch of gold nanoparticles synthesised was characterized by UV-Visible spectrophotometry in order to evaluate the quality of the synthesis by analysing the characteristic surface plasmon resonance band (SPR), and to determine the concentration of

the gold nanoparticles. The concentration of the solutions was determined by the Haiss *et al*[69], method in which the diameter of the particles is measured by the absorbance ratio at 450 nm and the absorbance at the SPR (Equation 3).

$$d = \frac{A\ SPR}{A\ 450\ nm} \quad [3]$$

The concentration was then calculated with the help of a calibration curve, which related the diameter of nanoparticles with the extinction coefficient (ε), and with the Lambert-Beer equation (Equation 4).

$$c = \frac{A\ 450\ nm}{\varepsilon\ 450\ nm} \quad [4]$$

2.3.3. Functionalization of gold nanoparticles

The ligands used for functionalization were mercaptoundecanoic acid (MUA) and the pentapeptide CALNN (Cysteine, Alanine, Leucine, Asparagine, Asparagine). Both are negative ligands due to the fact that at neutral pH conditions the $^{-}$OH group of the carboxyl can be deprotonated and the remaining electrons are in resonance between the two oxygen atoms, creating a negative dipole thus conferring an overall negative charge to the functionalized AuNPs.

AuNP-MUA solutions were prepared in the concentration ratio of 1:5000 using 10 mM stock solution of MUA in ethanol, and AuNP-CALNN solutions were prepared with the ratio of 1:1000 from 5 mM stock solution of CALNN.

2.3.4. Stability of gold nanoparticles

2.3.4.1. Stability of gold nanoparticles with buffer concentration

Solutions of 1 nM AuNP-MUA and AuNP-CALNN were prepared for 1 mL final volume with increasing concentrations of potassium phosphate buffer (10, 20, 30, 40, 50, 60, 70, 80, 90, 100 mM) at pH 7.5, to study the colloidal stability of AuNPs. UV-Visible spectrum of each solution was obtained from 270 to 700 nm.

2.3.4.2. Stability of gold nanoparticles with pH

Solutions of 1 nM AuNP-CALNN were prepared for 1 mL final volume with 30 mM potassium phosphate buffer with increasing pH (6, 6.5, 7, 7.5, 8, 8.5) to study the colloidal stability of AuNPs with pH variation. UV-Visible spectrum of each solution was obtained from 270 to 700 nm.

2.3.4.3. Stability of gold nanoparticles with methanol

Solutions of 1 nM AuNP-CALNN were prepared for 1 mL final volume with 30 mM potassium phosphate buffer at pH 7.5 and increasing percentages of methanol (0.5, 1, 2, 3, 4, 5 %). The aim was to study the stability of AuNPs with methanol which is the solvent used to dissolve and stabilize the enzyme substrate. UV-Visible spectrum of each solution was obtained from 270 to 700 nm.

2.3.5. Studies with *Rhus vernicifera* laccase

2.3.5.1. Laccase preparation

Laccase from *Rhus vernicifera* (EC 1.10.3.2) was purchased from Sigma and prepared with a method adapted from a previous study carried out by Catarina Loureiro at Faculdade de Ciências da Universidade do Porto[70].

Rhus vernicifera laccase was a powder difficult to dissolve in buffer and was reported to contain high amounts of insoluble material. The following method was the best combination found to yield a good amount of active enzyme in a clear solution.

The necessary quantity of laccase was weighed and dissolved in potassium phosphate buffer using a vortex for 10 minutes to help dissolve the powder.

The first attempt to improve laccase solubility included the addition of 10% DMSO to the enzyme solutions. It was proven that this method was not successful in improving solubility and keeping enzymatic activity. Consequently, the use of DMSO was discarded.

After adding the powder to the buffer, the solution was centrifuged at 8000 rpm for 20 minutes to form a pellet that contained insoluble material. In spite of this procedure, not all insoluble material formed a pellet, therefore the supernatant was filtered with an acrodisc syringe filter with HT Tuffryn membrane, 0.45 µm, 25 mm, non sterile (1 pk = 75 ca) purchased from Sigma. The resultant clear solution was stored in aliquots at -20 ºC that maintained activity for several weeks.

2.3.5.2. Determination of laccase activity

Laccase activity was determined by following the standardized enzymatic assay provided by Sigma[71], where syringaldazine was used as substrate and activity was measured at 30 ºC (Appendix I). The active enzyme in solution was calculated using equation 5.

$$Units/mL\ enzyme = \frac{[\Delta 530\ nm/\min(sample) - A520\ nm/\min(blank)] * df}{(0.001) * (0.5)} \quad [5]$$

In the previous equation, df stands for dilution factor.

2.3.5.3. Determination of total protein concentration

The total content of protein in laccase solutions was determined by the BCA protein assay method. The calibration curve was built with a bovine serum albumin (BSA) standard (1mg/mL, Sigma) by adding increasing concentrations (0 – 24 μg) to solutions of 1 mL of Bicinchoninic acid (BCA) and copper (II) solution mixture (Sigma).

This is a colorimetric assay where copper (II) ions react with some amino acids (majorly cysteine, tyrosine and typtophan), in an alkaline medium, forming a blue chelation complex. Afterwards, BCA quelates the reduced copper (I), resulting in a purple coloured complex. The absorbance measured at 562 nm for this complex can be directly related to protein concentration using a standard curve for comparison[72].

100 μL of laccase solution was added to 1 mL of BCA mixture to determine protein concentration and the absorbance was measured at 562 nm.

The concentration of the samples was determined with the help of a calibration curve produced with bovine serum albumin (BSA) standard (1mg/mL). The calibration curve from one of the concentration determinations can be seen in appendix IV, Figure 5.2.

2.3.5.4. Laccase purity

Since laccase solutions were diluted and the characteristic copper bands were not visible in a UV-Visible spectrophotometric measurement, a batch of laccase solution was concentrated using a *Microsep™ Advance* centrifugal device with a 30 kDa pore membrane from *PALL Corporation*. The solution was centrifuged at 5000 rpm for 5 minutes to yield 750 μL solution with the concentration of 1 mg/mL (determined by the BCA protein assay method). The spectrum of the oxidized form of this laccase sample was measured between 200 and 700 nm, and the spectrum of the reduced form was measured by adding a small amount of sodium hydrosulfite (85%, Sigma) to the same sample. Purity of the oxidized laccase sample was determined by the $A_{614\ nm}$ / $A_{280\ nm}$ ratio[21].

2.3.5.5. Dynamic Light Scattering (DLS) studies of laccase

A laccase solution with 36 µg/mL (total protein concentration by BCA assay) and PBS (phosphate buffer saline) containing 0.5 M NaCl, was prepared to the final volume of 1 mL to be measured by the DLS technique. The sample was measured with 180 seconds of stabilization, 3 cycles of 100 measurements each, in the protein reading mode at 25ºC.

2.3.6. PolyAcrylamide Gel Electrophoresis (PAGE)

2.3.6.1. SDS-PAGE

Laccase samples used in this experiment were prepared by ultrafiltration-ultracentrifugation methods, in order to obtain concentrated laccase samples to be observed in the gels. The sample with 1 mg/mL of total protein was obtained by ultrafiltration of laccase solutions in a Microsep^{TM} Advance centrifugal device that included a membrane with 30 kDa pore (PALL Corporation).

Another approach encompassed the ultrafiltration of laccase solutions in a centrifugal device that included a membrane with 100 kDa pore (Millipore), at 5000 g during 2 minutes for 6 times, each time washing the laccase solution retained in the membrane with PBS (Appendix II). The solution that passed through the membrane pores of this centrifugal device was recovered and ultrafiltrated in a device that contained a membrane with 10 kDa pores. This experiment was carried out at 5000 g for 10 minutes, and the solution retained in the membrane was also washed with the same PBS solution. The concentration of protein in these samples was measured with the BCA assay and their laccase activity was measured following the activity assay from Sigma.

Several denaturing PAGE were performed to evaluate the presence of laccase, as well as the molecular weight and purity of the concentrated laccase solutions. The first polyacrilamide gel was prepared with a concentration of 10% in polyacrylamide and 15 µL of the 1 mg/mL solution were loaded into a well while another well contained 4 µL of *NZYColour Protein Marker II*.
Other gels were also prepared with 10% polyacrylamide concentration and samples with and without β-mercaptoethanol were loaded into the wells. For these gels, a low range protein standard from Nzytech was used.
All electrophoresis were performed in running buffer solution pH 8.3 (Appendix II) at 180 V for 45 minutes. After running, the gels were stained with a 0.5% coomassie blue solution for half an hour, followed by a destaining solution (Appendix II) overnight.

The bands in the gel of Figure 3.7a were analysed with the software ImageJ[73]. This software analysed the colour intensity and contrast of the black and white gel image and generated lane

profile plots. The area of the peaks of interest was measured with the 'wand' tool of the software. The area of the bands was then represented in percentage[74].

2.3.6.2. Native-PAGE

Native PAGE was carried out to evaluate both the activity and purity of the concentrated laccase solution. Native gels with 10 and 8% concentration in polyacrilamide were prepared. Samples of 20 µL from the 1 mg/mL solution without β-mercaptoethanol were loaded into the wells. In order to evaluate the ideal conditions for this electrophoresis, the gel was performed in non-denaturing running buffer at different voltages, 75, 100 and 180 V for 3 hours. Once the electrophoresis was finished, the gel was cut in two equal parts: One half was stained with 0.5% coomassie blue and later immersed in destaining solution (Appendix II) to reveal the total protein content, while the other half was immersed in substrate solution 1 mM syringaldazine to reveal the areas that contained active laccase, as shown in Figure 2.1.

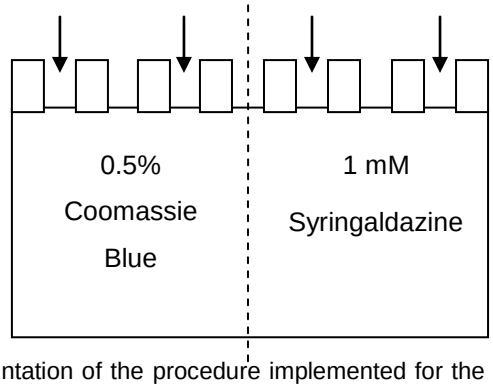

Figure 2.1. Schematic representation of the procedure implemented for the native-PAGE electrophoresis with arrows representing the wells where laccase samples were loaded. Half of the gel was stained with 0.5% coomassie blue and the other half with 1 mM syringaldazine.

2.3.7. Studies with syringaldazine substrate

2.3.7.1. Preparation of syringaldazine

Solutions of 1 mM syringaldazine (Sigma) were prepared in methanol (99.8 %, Sigma) and dissolved for 3 hours in a combination of stirring with the aid of a magnet and of an ultrasound bath. The solutions were stored in a brown glass flask covered with aluminium paper at 4 ºC.

2.3.7.2. Concentration studies of syringaldazine

Solutions of syringaldazine with increasing concentrations (10, 20, 30, 40, 50, 60 µM) were prepared in 30 mM phosphate buffer at pH 7.5. UV-Visible spectrum of each solution was taken between 270 and 600 nm. A plot was built with the absorbance at 355 nm for all concentrations tested.

2.3.7.3. pH dependence of syringaldazine

Solutions with 1 mL final volume were prepared with 20 µM syringaldazine and 30 mM potassium phosphate buffer at increasing pH from 6 to 8.5 to determine the absorbance dependence of this substrate with pH variation. UV-Visible spectrum of the solutions was taken between 270 and 600 nm.

2.3.8. Conjugation studies

2.3.8.1. Preparation of bionanoconjugates

Conjugates between 1 nM AuNP-CALNN and laccase were prepared with Milli-Q water and 30 mM potassium phosphate buffer in the pH range from 6 to 8.5. Previously of being used, the solutions were incubated overnight at 4ºC.

Solutions where laccase was covalently bound to AuNP-CALNN were prepared with a mixture of 2.8 mM EDC and 1.2 mM NHS cross-linking agent solution. The solutions were incubated at room temperature for 2 hours before use.

2.3.8.2. Zeta potential

In this study the BNCs with 1 nM AUNP-MUA and AuNP-CALNN were prepared with Milli-Q water, 30 mM phosphate buffer at pH 7.5 and increasing concentration of *Rv* laccase solution: 0.54, 1.08, 2.70, 5.41, 8.11, 10.8, 16.23, 21.64 µg/mL (determined by BCA assay). The solutions were incubated overnight at 4ºC.

Zeta-potential measurements of these solutions were performed in the following day with a stabilization time of 180 seconds and 3 readings of 100 measurements each at 25ºC. 1 nM AuNP-MUA and AUNP-CALNN without laccase were used as control. The values presented are the average and standard deviation of the 3 measurements performed. The experimental data obtained was fitted with the help of *MsExcel and OriginPro 8* software using the Langmuir isotermic equation.

2.3.8.3. Agarose gel electrophoresis

Agarose gels were prepared by dissolving 0.22 g of agarose (*Ultrapure™*, *Invitrogen)* in 45 mL of TAE buffer pH 8, with the final concentration of 0.5% in agarose.

BNCs were prepared with 1 nM AuNP-CALNN with and without the cross-link agent EDC/NHS linking the particles and laccase at pH 7.5. Protein concentration added to the particles were 0.54, 1.08, 2.70, 5.41, 8.11, 10.8, 21.64 µg/mL measured by BCA assay.
All BNCs solutions were centrifuged at 14000 rpm for 1 hour. The supernatant was discarded and 3 µL of glycerol was added to 30 µL of pellet. The final mixture was inserted in the wells of the gel. Several horizontal electrophoresis were performed, all used TAE as running buffer pH 8, and were performed at 75, 100, 150 and 180 V for 30 minutes.
The elestrophoretic mobility (µ) was calculated by measuring, in centimetres, the distance of the bands to the well and according to Equation 6:

$$\mu = \frac{v}{E} \qquad [6]$$

In this equation, µ stands for the electrophoretic mobility (cm^2/V.s), v is the rate of migration (cm/s) and E is the strength of the electric field (V/cm).

2.3.9. Kinetic Studies

2.3.9.1. Kinetic studies of free laccase and of laccase in the bionanoconjugates

Studies with protein concentration in 1 nM AuNP-CALNN were performed by the preparation of BNCs in 30 mM phosphate buffer at pH 7.5 with and without cross-linking agent and increasing concentrations of protein (0.54 µg/mL, 1.08 µg/mL, 2.70 µg/mL, 5.41 µg/mL, 8.11 µg/mL, 10.8 µg/mL, 21.64 µg/mL). The solutions were incubated overnight at 4ºC. Previously to activity measurements, the solutions were centrifuged at 14000 rpm for 1 hour. The supernatants were saved, while the pellets were re-suspended in 30 mM phosphate buffer and Milli-Q water. Laccase activity in each sample was measured by adding 20 µM syringaldazine, to the samples. Activity over time was measured by the increase of absorbance due to product formation at 530 nm. For comparison, solutions of free laccase and BNCs not centrifuged were also measured in the same conditions.
Kinetic studies to obtain Michaelis-Menten profiles were carried out with BNCs with 1 nM AuNP-CALNN, 30 U/mL of active laccase in Milli-Q water and 30 mM phosphate buffer in the pH range from 6 to 8.5. The BNCs were prepared and tested in duplicates. Additionally, solutions with free laccase were prepared under the same conditions to act as comparison to the BNCs. As before, these solutions were incubated overnight at 4 ºC.

The reactions of substrate consumption and formation of product were followed for each sample. Syringaldazine was used in the concentration range 0 to 40 µM. The reactions were followed by taking UV-Visible spectra each 30 seconds for at least 3 minutes. Syringaldazine consumption at pH 6, 6.5, 7 and 7.5 was followed by the decrease in absorbance at 350 nm. At pH 8 the consumption was followed at 365 nm, while at pH 8.5 the decrease in absorbance was followed at 400 nm. In the case of product formation, for all pH conditions tested, the reactions were followed by the increase of absorbance at 530 nm. The initial rates (V_0) of both reactions were plotted in a Michaelis-Menten plot. To obtain kinetic parameters and standard errors, the experimental data was fitted with the Hill function (n=1) using *Origin Pro 8* software.

2.3.10. Structural analysis by molecular modelling

The three-dimensional X-ray structure of *Trametes versicolor* (PDB: 1GYC[34]) laccase was used to generate electrostatic surfaces depending on pH conditions.

For this analysis, two software tools were used: “H++” and “Chemera”. The online software “H++” allows to calculate the protonation states of amino acids based on classical continuum electrostatics, basic statistical mechanics and on the pH of the environment.[67] Chemera is a software developed by Professor Ludwig Kripphal that allows generation of an image of the three-dimensional structure of proteins, and aids in calculating the electrostatic surface.
The software H++ online software[67] computed the pKa of ionisable groups in the amino acids for pH values of 6, 6.5, 7, 7.5, 8, 8.5. The software generated a file with charges that was uploaded to Chemera[68] along with the original structure. Chemera was able to assign the newly calculated charges to the original structure and generate a Poisson-Boltzmann grid[66,75]. The conditions used to generate the grids were the standard values already in the software and the buffer conditions used in the kinetic experiments of this dissertation. To simplify the structure, the grid was built with a field of 0.01 eV and without the z axis. The resultant structure was coloured according to the charges of the amino acids and images of the structure were taken from various angles.

Chapter III: Results and discussion

3.1. Synthesis and characterization of gold nanoparticles

The colloidal solutions of AuNPs used in the experimental work of this dissertation were synthesized by following the Turkevich[7] method of gold reduction by citrate. In general, these solutions maintain their optimal stability for a little over one month. So during the time span of this work it was necessary to perform several syntheses in order to have fresh and stable particles available to use. This method was found to be extremely reproducible.

All syntheses were successful and yielded red coloured solutions with stable particles according to their UV-Visible spectrum. After the end of each synthesis the UV-Visible spectrum of a diluted sample was taken. They showed the characteristic plasmonic profile, which indicated the presence of AuNPs, and had the absorption maximum at approximately 520 nm, as expected for these solutions. The spectrum taken from one of the synthesis can be seen in Figure 3.1.

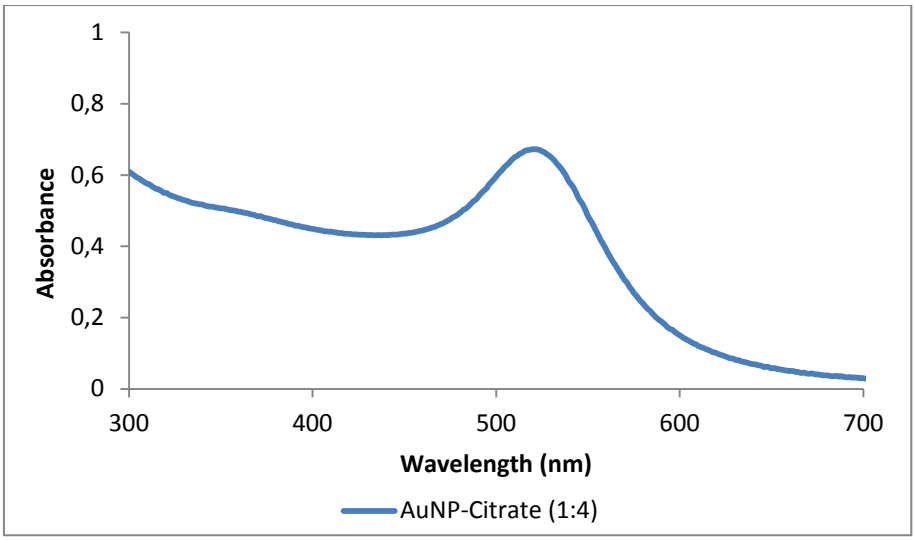

Figure 3.1. UV-Visible spectrum of one AuNPs solution obtained from the Turkevich citrate reduction method with 1:4 dilution, showing the typical absorption maximum at 520 nm.

The concentration of the solutions was determined by the Haiss *et al*[69], method as described in "2.3.2. Characterization of gold nanoparticles". The colloidal solutions were obtained with particles with an estimated size of approximately 12 nm and concentration around 15 nM. These values are within the size and concentration expected for this synthesis. Since all batches revealed similar values, it also demonstrated the consistency of the Turkevich[7] method for successive AuNP synthesis.

Light scattering techniques were also implemented to characterize these AuNPs stabilized with citrate. Zeta-potential evaluation showed that these particles had a superficial charge of -19.4 mV ± 1.05, with very small distribution in size as it can be seen by the very narrow peaks obtained in the measurements (Appendix III, Figure 5.1). This value is somewhat less negative than often described in previous studies[76]. This might be due to the fact that this experiment was only possible to be executed several weeks after the synthesis was made. By this time, the

particles might be more aggregated than right after the synthesis, which might have contributed to a less negative potential.

3.2. Functionalization of gold nanoparticles

AuNP-Citrate particles are usually very stable in solution. However, in order to increase their stability and to be able to resist changes in the media, as well as to create a more appropriate environment for biomolecular conjugation, AuNPs had to undergo a change in the functionalization. It was a simple process and envisioned the change of ligand at the surface of the AuNPs. Citrate is a small molecule and can rapidly suffer chemical changes at unfavourable conditions, usually when the pH of the media is below 5, or with the variation of ionic strength[77]. This results in the loss of the charges at the surface of the particles, that otherwise allow them to repel each other and remain stable in solution. The loss of repelling forces leads to aggregation. To overcome this effect, the citrate coating of AuNPs was changed into more stable ligands.

The ligands chosen were mercaptoundecanoic acid (MUA) and the pentapeptide CALNN (Cysteine, Alanine, Leucine, Asparagine, Asparagine). Both are thiolated negative ligands with higher affinity for gold than citrate. These ligands, different in structure, were chosen to evaluate which would bring more stability and increased features to the BNCs systems.

After functionalization, its success was evaluated by UV-Visible spectroscopy. The spectra of AuNP-MUA and AuNP-CALNN at the concentration of 1 nM in water were obtained and compared with the spectrum of 1 nM AuNP-Citrate to evaluate the changes that occurred at the surface of the particles. Figure 3.2 a) and b) shows the spectra of AuNP samples with both ligands functionalized from the same AuNP-Citrate batch.

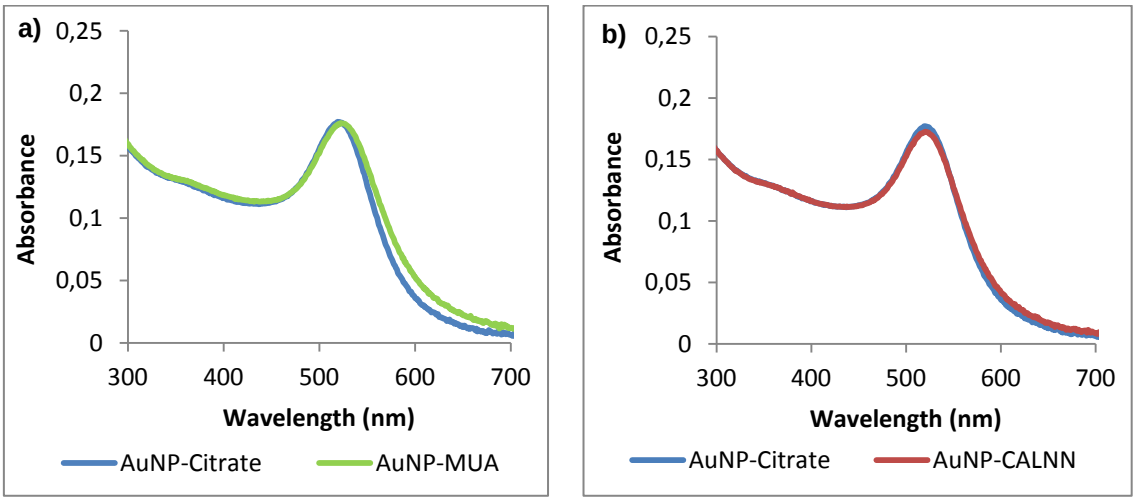

Figure 3.2. a) UV-Visible spectra of 1 nM AuNP-Citrate (—) and 1 nM AuNP-MUA (—); **b)** UV-Visible spectra of 1 nM AuNP-Citrate (—) and 1 nM AuNP-CALNN (—).

Table 3.1. Maximum wavelength values from the spectra of AuNP-Citrate, AuNP-MUA and AuNP-CALNN.

Ligand	Maximum wavelength (nm)
Citrate	519.0
MUA	522.9
CALNN	520.9

With the change of the surface from a small molecule to ligands slightly larger and covalently bound to the particles, the resonance of the AuNPs surface electrons also changed. This effect was translated into the spectra of AuNP-MUA and AuNP-CALNN suffering shifts in the plasmonic towards slightly higher wavelengths (Table 3.1).

The shifts, of 3.9 nm for AUNP-MUA and 1.9 nm for AuNP-CALNN, were consistent with the shift value (around 2 nm) previously described by Hussain *et al*[13]*.,* in AuNP-ligand studies by UV-Visible spectroscopy. These studies consisted in investigating the stability of AuNP-CALNN in comparison with AuNP-Citrate. What was found was that not only the SPR shifted 2 nm when citrate was exchanged to CALNN, but CALNN protected AuNPs from aggregation in conditions where AuNP-Citrate where not stable.

Consequently, with the results obtained here, it was possible to observe that the functionalization was successfully achieved.

3.3. Stability studies of CALNN-functionalized gold nanoparticles

One of the problems that colloidal solutions have is the possibility of particle destabilization, or aggregation, which can occur when the characteristics of the media are changed. This event can occur even when the particles are functionalized to achieve higher levels of stability. The following studies were carried out only with AuNP-CALNN because the particles functionalized with MUA were found to be less stable in further studies with the enzyme used in this experimental work.

3.3.1. Stability with buffer concentration

The aim of this study was to observe the behaviour of AuNP-CALNN with changes in buffer concentration and find a suitable concentration in which the particles were stable. The pH of 1 nM AuNP-CALNN solutions was fixed at 7.5 with potassium phosphate buffer, while the concentration of the latter increased from 10 to 100 mM. The effects on the SPR were observed by UV-Visible spectroscopy (Figure 3.3).

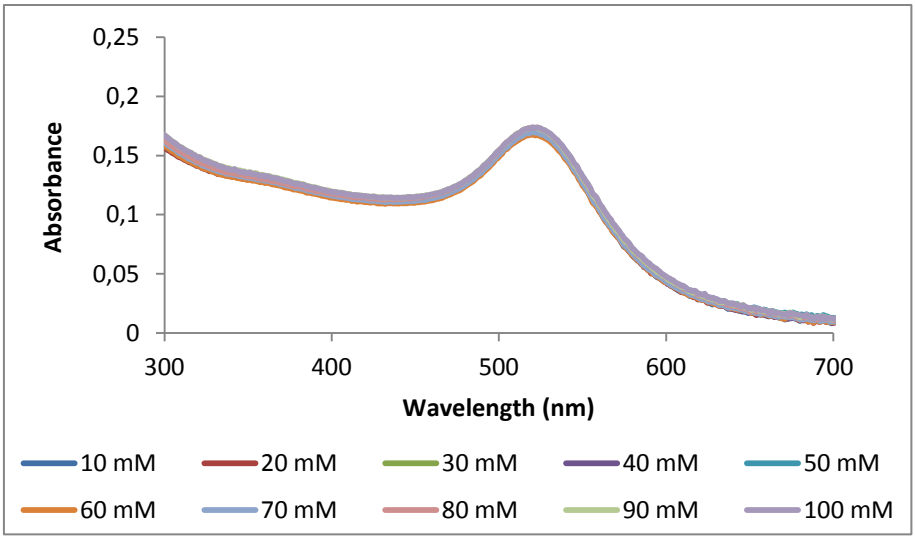

Figure 3.3. UV-Visible spectra of the stability studies with 1 nM AuNP-CALNN solutions by increasing the potassium phosphate buffer concentration from 10 to 100 mM at pH 7.5.

The UV-Visible spectra of all solutions indicated no major shift in the SPR, or the increase in absorbance around 600 nm and higher, as it would be evident if aggregation had occurred. The maximum absorption remained around 522 nm as expected after functionalization and the solutions continued with the typical red colour. No aggregation occurred in all concentrations tested. This result seemed to indicate that, up to 100 mM of potassium phosphate buffer, the concentration of positive ions in the media was not high enough to cause effects in the terminal amino acids of CALNN, which could lead to stability loss.

Any of the buffer concentrations could be used in further studies, but due to the fact that the present dissertation aimed to obtain results comparable to previous studies, the concentration chosen to use in the remaining studies was 30 mM of potassium phosphate buffer.

3.3.2. Stability with pH

Another important characteristic to observe is how the pH of the media also influenced the stability of 1 nM AuNP-CALNN in solution. In this case, the concentration of phosphate buffer was fixed at 30 mM, while the pH increased from 6 to 8.5. The reason why this specific pH range was chosen was inherent to the following enzyme activity studies that would be performed within this range. Additionally, it also aimed to keep the study in the range of a single buffer system. One of the pKa of phosphate is 7.22, and to be able to function properly, the pH of buffer solutions need to be within the value of pKa ± 1. Reaching pH 6 and 8.5 was already stretching the capacity of the buffer, but still able to be used. Once again, the effects of pH in AuNP-CALNN were studied by UV-Visible spectroscopy (Figure 3.4).

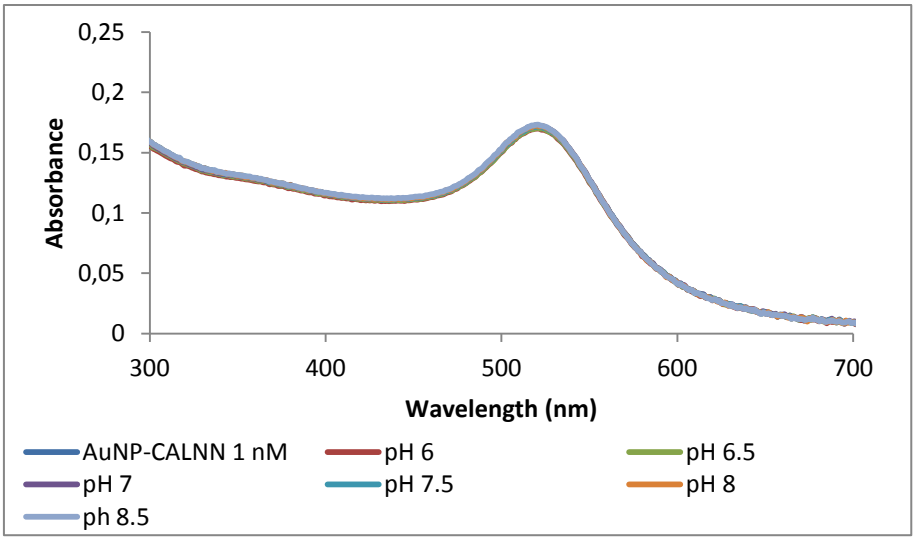

Figure 3.4. UV-Visible spectra of the stability studies with 1 nM AuNP-CALNN solutions by increasing the 30 mM potassium phosphate buffer pH from 6 to 8.5.

The spectra of all samples showed that the SPR did not suffer major shifts towards higher wavelengths, and the absorption maximum was still around 522 nm for all of them. This suggested that within this pH range no massive protonation events occurred in the terminal amino acids of the ligand. AuNP-CALNN particles were stable through all changes in pH, securing the fact that aggregation due to pH change would not be a problem in the studies ahead. Previous experiments described that AuNP-CALNN solutions only lose their stability below pH 4 as the terminal carboxylic group pKa is 4[13].

3.3.3. Stability with methanol

Apart from changes in buffer concentration or pH, the other parameter introduced in the enzymatic studies of this work, and that might interfere with AuNP-CALNN stability as well, was methanol. This potential effect comes from the fact that the substrate used, syringaldazine, is highly insoluble in aqueous media and to increase its solubilisation and stability it was dissolved in 99% methanol. Methanol, being a polar molecule, could influence the stability of AuNPs. 1 nM AuNP-CALNN was studied in the presence of the same percentages of methanol, 0 to 5%, used in the enzymatic studies with syringaldazine. The effects of methanol were observed by UV-Visible spectroscopy (Figure 3.5).

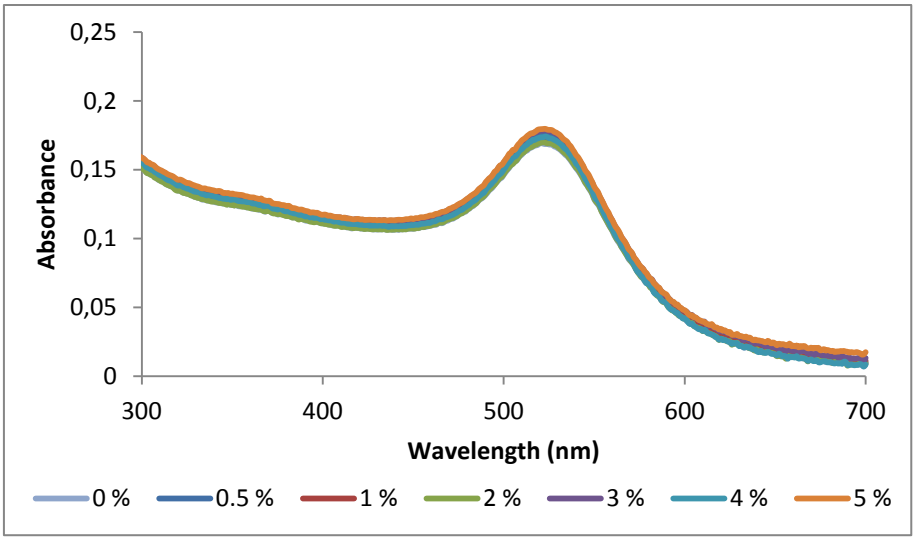

Figure 3.5. UV-Visible spectra of the stability studies with 1 nM AuNP-CALNN solutions by increasing the percentage of methanol in solution from 0 to 5%.

From the spectroscopic data obtained, it was possible to observe that even at 5% methanol, no aggregation was apparent, for the absorption maximum remained around 521.9 nm. With this data, it was apparent that at least up to 5% of methanol, the particles were stable in solution and possible aggregation in further studies would not be due to the presence of this solvent.

3.4. Studies with *Rhus vernicifera* laccase

Laccase from the lacquer tree *Rhus vernicifera* was prepared following a procedure that envisioned the solubilisation of the majority of the crude acetone powder commercialized by Sigma. This particular powder was extremely insoluble and was also reported to contain contaminants. The first approach to increase the powder solubility, and help in the solubility of the enzyme in the aqueous media, was to add 10% of DMSO to the laccase preparation. It has been reported that most studies on enzymes use 10% or less of DMSO to prevent denaturation and activity loss[78]. In fact, when more than 10% was added, the solutions showed foam formation, which could be an indication of protein denaturation. Laccase activity of samples with and without 10% DMSO were measured following the Sigma assay, and the total protein concentration was measured by BCA assay. The results showed that not only the solutions with DMSO presented less active laccase, but there was no improvement in the amount of protein dissolved. Since these results seemed to point in the direction that DMSO reduced laccase activity, this procedure was discarded from the preparation of laccase samples.

With the process that combined vortex action, centrifugation at 8000 rpm and filtration with a membrane, it was possible to obtain clear solutions of the enzyme in phosphate buffer to be used in the remaining experiments.

3.4.1. Determination of total protein content

Since the samples prepared from laccase acetone powder (such as the one produced by Sigma) are described to contain more than just laccase[45], protein quantification was important in order to keep track of the quality of the samples. To address this issue, the protein content was determined with the BCA protein assay.

This procedure was applied to all laccase solutions, and with the method used to dissolve the powder, the samples prepared had a concentration of approximately 70 µg/mL of total protein.

3.4.2. Laccase purity

Another important matter to address was the purity of the laccase samples prepared and the extent of contamination by other proteins. Purity of copper-containing proteins is usually determined by the ratio A_{280nm}/A_{614nm}. It evaluates the amount of protein (due to aromatic amino acids absorbance at 280 nm) relative to the absorbance of the T1 copper at 614 nm from the CysS → Cu^{2+} transition[33,79].

The samples used for kinetic studies were somewhat diluted in protein content, and it was spectroscopically difficult to observe the absorbance contribution of some of the copper atoms, mainly of T1 copper. The strategy implemented was to concentrate several laccase samples until the concentration was high enough to observe a significant absorbance in the copper-absorbing regions in the UV-Visible spectrum. Then, the spectrum of a 1 mg/mL (in total amount of protein by BCA assay) sample diluted 2.5 times was obtained (Figure 3.6, blue line).

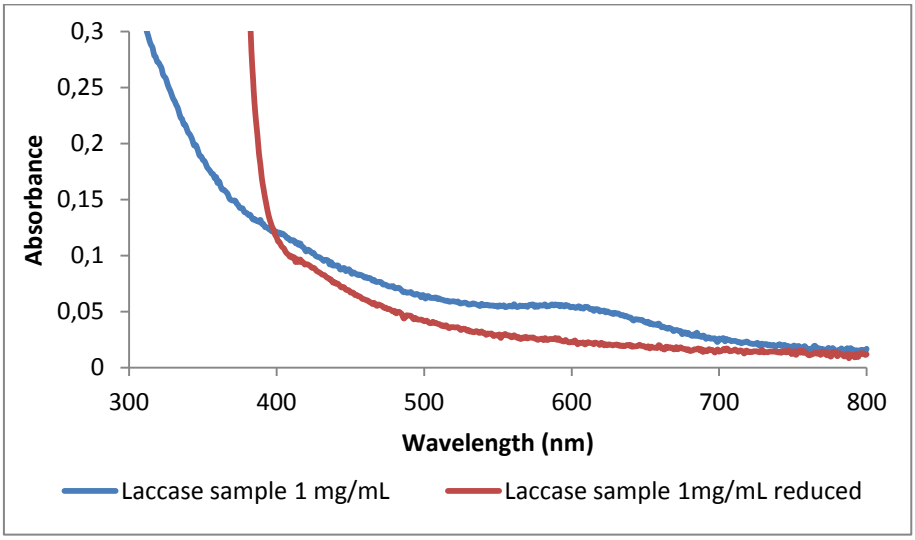

Figure 3.6. UV-Visible spectrum of a laccase sample with the total protein concentration of 1mg/mL (—) diluted 2.5 times, and the spectrum of same sample after reduction with sodium hydrosulfite (—), both zoomed in the region of T1 copper absorbance.

The spectrum of the sample showed a band around the expected area of absorbance of T1 copper (ε = 5000 M^{-1} cm^{-1} [80]).

To understand if this band was in fact related to a copper ion, a small amount of sodium hydrosulfite was dissolved in the same sample and the reduced spectrum was obtained. A decrease of absorbance in the 600 nm region was observed, which was most likely due to the reduction of the T1 Cu^{2+} to Cu^{+} (Figure 3.6, red line). In addition, the A_{280nm}/A_{614nm} ratio was 17.37, a value slightly higher than the one predicted for pure laccase samples (16.2[33,79]), which indicated the presence of contaminants.

3.5. Structural characterization of free laccase

3.5.1. SDS-PAGE

Denaturanting SDS-polyacrylamide gel electrophoresis was used to assess protein purity in laccase solutions, the presence of contaminants, as well as their molecular weights. The laccase samples used in this method were concentrated by ultrafiltration from the original samples prepared from the powder stocks as previously described. The resulting solution was of 1 mg/mL in total protein as determined by BCA assay and laccase activity was 4,399 U/mL.

Following concentration, two laccase samples were loaded in 10 % polyacrilamide gels. One sample contained sample buffer with β-mercaptoethanol (Figure 3.7a), while the other did not (Figure 3.7b).

The reason why one sample was treated with β-mercaptoethanol was because this compound disrupts disulfide bonds that connect protein subunits and leads to a separation by their subunits. In this case, it was used to rule out the presence of potential subunits in *Rv* laccase, and address if it is a monomer as described. Samples without β-mercaptoethanol served as control.

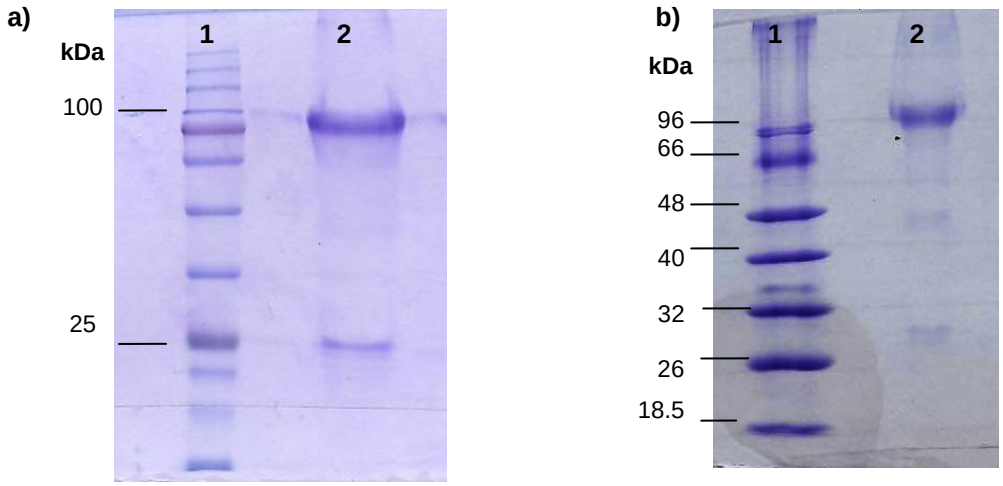

Figure 3.7. a) 10 % SDS-PAGE gel: lane 1 – high range protein standards; lane 2 – 15 µL of the 1 mg/mL solution treated with β-mercaptoethanol; **b)** 10 % SDS-PAGE gel: lane 1 – low range protein standards, lane 2 – 15 µL of the 1 mg/mL solution without β-mercaptoethanol.

The gel in Figure 3.7a, revealed two bands in the laccase sample, with different molecular weights and colour intensity. With the relative mobility of each standard it was possible to build a calibration curve and calculate the relative molecular weight of each sample bands (Appendix V, Figure 5.4).

The calibration curve indicated that the top band in this gel has approximately 84 kDa. The fact that this band appeared slightly below the 100 kDa standard might be due to the high amount of protein that migrated to that area. In fact, the small amounts of sample that overflowed to adjacent wells showed small bands in the same line as the 100 kDa standard. The lower band appeared at the approximate relative mobility as the 25 kDa standard.

Due to the use of β-mercaptoethanol it was not yet clear if this low weight band was a subunit of *Rv* laccase.

Due to low resolution in the higher molecular weight bands of the standard used in Figure 3.7a, a low molecular weight standard was used in the next electrophoretic studies.

The sample without β-mercaptoethanol (Figure 3.7b), showed one band with molecular weight above the 96 kDa protein standard, as well as a band with a relative mobility above the 26 kDa protein standard.

It was possible to deduce that the first band seemed to belong to *Rv* laccase, since it appeared close to the 100 kDa molecular weight reported for this protein by other SDS-PAGE studies[47].

The fact that the same profile was obtained with and without β-mercaptoethanol indicated that the lower molecular weight band was not a laccase subunit. This result supported the conclusion that *Rv* laccase is a monomer as previously described[47].

It was still possible that the band with lower molecular weight was a proteolysis product of the enzyme or simply a contamination. The next course of action was to try to separate the proteins that originated the bands in the gels.

The following strategy took into consideration the molecular weight of both bands and the material available in the laboratory. New solutions of laccase were prepared and concentrated through ultrafiltration following the scheme in Figure 3.8.

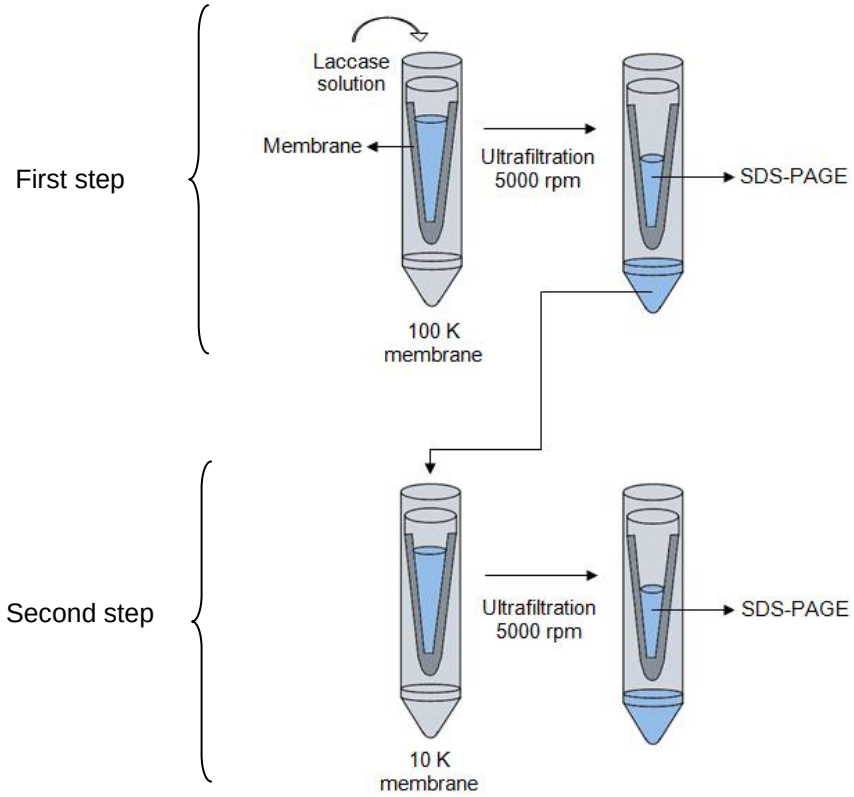

Figure 3.8. Schematic representation of the ultrafiltration process with the ultrafiltration devices of 100 kDa and 10 kDa size pore membranes.

In the first step a laccase solution was ultrafiltrated in a centrifugal unit that had a membrane with a pore size of 100 kDa. A SDS-PAGE was performed with samples from the solution that remained in this membrane, without and with β-mercaptoethanol (Figure 3.9a, lane 2 and 3).

In the second step, the solution filtered through the pores of the 100 kDa membrane and remained in the bottom of the unit was transferred to a centrifugal device with a 10 kDa membrane for another ultrafiltration process. A SDS-PAGE was performed with samples from the solution that remained in this membrane, without and with β-mercaptoethanol (Figure 3.9a, lane 4 and Figure 3.9b, lane 2).

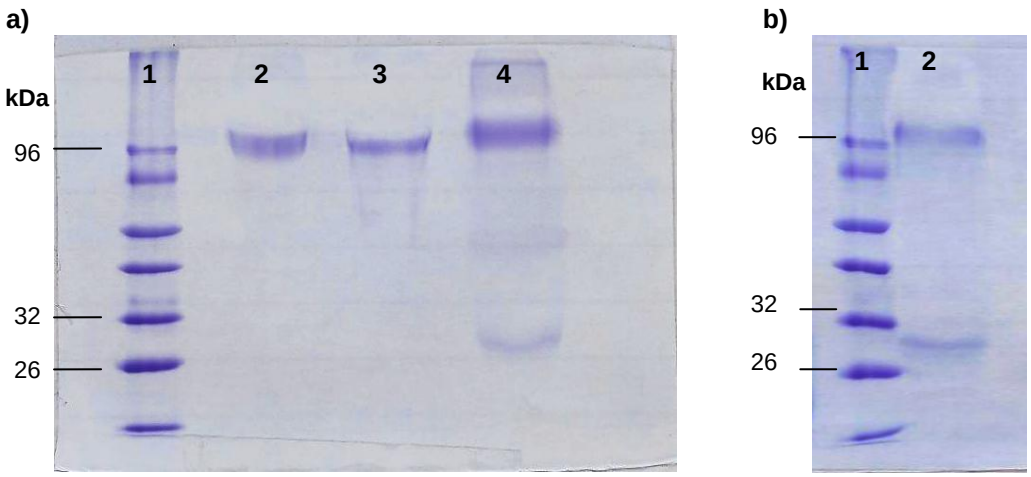

Figure 3.9. a) 10 % SDS-PAGE gel: lane 1 – low range protein standards; lane 2 – 15 µL of the solution concentrated with the 100 kDa membrane not treated with β-mercaptoethanol; lane 3 – 15 µL of the solution treated with β-mercaptoethanol; lane 4 – 15 µL of the solution concentrated in the 10 kDa membrane not treated with β-mercaptoethanol; b) 10 % SDS-PAGE gel lane 1 – low range protein standards, lane 2 – 15 µL of the solution concentrated with the 10 kDa membrane treated with β-mercaptoethanol.

In Figure 3.9a, the samples in lane 2 and 3 were from the solution concentrated with the 100 kDa membrane. Lane 2 did not contain β-mercaptoethanol while lane 3 sample did. The gel showed that for both samples only a single band appeared with higher molecular weight than the 96 kDa protein standard. This band appeared to be from *Rv* laccase.

Lane 4 (Figure 3.9a) was loaded with a sample from the solution concentrated in the 10 kDa membrane without β-mercaptoethanol treatment. Lane 2 of the second gel (Figure 3.9b) shows a sample from the same membrane treated with β-mercaptoethanol.
In both lanes, a band with molecular weight higher than 96 kDa could be observed. It appeared that some amount of this protein passed through the pores of the 100 kDa membrane and was transferred to the 10 kDa membrane. This might have been due to the cut-off of the membrane being close to the molecular weight of laccase. This band was most likely *Rv* laccase as well.
The samples from the 10 kDa membrane also showed a second band of molecular weight higher than the 26 kDa standard protein.

The total amount of protein in each solution was determined with the BCA assay, and the active concentration of laccase in them was also determined. The specific activity of the solution from the 100 kDa membrane was 4.07 U/µg. On the other hand, the specific activity of the solution from the 10 kDa was 2.28 U/µg (Appendix IV, Figure 5.3). This data showed that there was more active laccase in the solution from the 100 kDa membrane than in the one from the 10 kDa membrane.

With this experiment, it was possible to understand that *Rv* laccase presented itself as a monomer with a molecular weight of approximately 100 kDa as predicted[47].
The low molecular weight band was probably not a proteolysis product of laccase. If it were a proteolysis product the remaining of that product would have appeared as well and there would

be another band at approximately 75 kDa (weight difference of the 100 kDa band and the band above 26 kDa).

The lower specific activity in the solution of the 10 kDa membrane and the treatment with and without β-mercaptoethanol of all samples indicated that the low molecular weight band observed was not a *Rv* laccase subunit and might have been a contaminant. Other researches also reported a low molecular weight band of the same approximate weight as found here[81]. This band might belong to other glycoproteins that have also been described to be found in solutions produced from acetone powder of lacquer tree sap[46,81].

This low molecular weight band seemed to only represent a small portion of the total protein observed in the gel. For a more accurate comparison, the area of colour intensity of each band in lane 2 of Figure 3.7a was measured with the help of the ImageJ[73] software as explained in section 2.3.6.1. The software produced a plot with the colour intensity of the bands in the gel and calculated the area of the bands of interest. This low molecular weight band represented 13.71% of the total protein present in the gel.

3.5.2. Native-PAGE

Native-PAGE is a very powerful technique to study proteins with enzymatic activity, and in this case could be useful to characterize *Rv* laccase in native conditions. This technique was carried out in the same manner as SDS-PAGE, with the difference that all denaturant agents, such as SDS and β-mercaptoethanol, were not used. Therefore, proteins retained their structure and activity. During this electrophoresis, migration did not depend exclusively on the molecular weight of the protein but also on shape and charge[82]. The interesting feature of this technique is that it can be informative of both total amount of protein and activity as well, being a qualitative method of studying proteins in their native state.

So far, there are not many native-PAGE experiments done for *Rv* laccase, so the behaviour of this enzyme in native conditions is not fully understood. The conditions used to perform the SDS-PAGE were taken as a starting point to perform the native gel. A few parameters were changed afterwards in order to obtain a gel with good resolution. Three values for the electric field applied were used: 75, 100 and 180 V. The gel that showed better resolution was performed at 180 V for 3 hours (Figure 3.10). Other native gels are presented in appendix VI, Figure 5.5.

In the gel of Figure 3.10, four samples of the laccase solution with 1 mg/mL were loaded into four separated wells. After the electrophoresis finished, the gel was cut in half. Half of the gel was stained to reveal the total amount of protein with coomassie blue (Figure 3.10a). The other half of the gel was immersed into a syringaldazine solution to stain for activity (Figure 3.10b).

a) 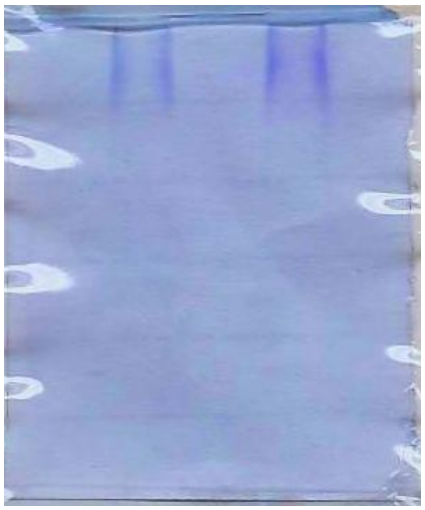 **b)** 

Figure 3.10. a) Native-PAGE gel with two wells loaded with 15 µL of a 1 mg/mL laccase solution stained for total amount of protein with coomassie blue; **b)** Native-PAGE gel with two wells loaded with 15 µL of a 1 mg/mL laccase solution stained for activity with 1 mM syringaldazine. Gel run at 180 V for 3 hours at pH 8.3.

After developing each half of the gel with two different techniques, it was possible to observe that only a single band appeared in each lane. Furthermore, not only the protein did not move significantly along the gel, but also the single bands were poorly defined. This behaviour was previously reported in other native-PAGE experiment for this enzyme[83].

When the second gel was exposed to substrate, the characteristic pink colour of the quinone from syringaldazine oxidation with laccase was revealed within seconds of the gel being submersed in the solution. This effect did not last long, because the product does not remain permanently in the gel but disperses into the solution and eventually disappears.

Comparing the two gels, it was easy to identify that the smear pathway of the only band was common for both gels. If superimposed, it showed that the laccase present in the sample had enzymatic activity when in contact with syringaldazine. Nevertheless, the resolution in these gels was not the best.

3.5.3. Dynamic light scattering of laccase

The dynamic light scattering technique was also implemented to characterize the size of *Rv* laccase. This method is sensitive to the Brownian motions, the motion of particles in solution. Large particles have a slow Brownian movement, while small particles can move much faster in solution[59]. By measuring the velocity of this movement it is possible to calculate the hydrodynamic diameter of the particles, making DLS a powerful technique to calculate the size of proteins with great accuracy.

The laccase sample tested had a total protein concentration of 36 µg/mL and contained PBS with 50 mM NaCl in order to maintain the protein stable. This buffer with high concentration of

ions could prevent the protein molecules from forming large aggregates and stabilized the sample during the experiment.

The sample was measured three times and each time it showed single and narrow peaks that illustrated a small distribution of sizes in the sample (Figure 3.11). Size information was obtained from the relative intensity of light scattered by the particles in solution[60]. However, the intensity distribution was not a single well defined peak. The intensity results were converted into number of particles in solution to obtain a better correlation of the particle size of the populations. The number distribution shows the number of particles in solution with a certain size and is usually used to estimate the relative amounts of multi size peaks samples[84,85]. In this manner it was possible to evaluate the percentage of particles in solution that would have a diameter that could correspond to laccase.

The measurements revealed that the average diameter of particles in this sample were 5.65 ± 0.83 nm, which is in agreement with the 5 nm in diameter reported for laccases[86,87].

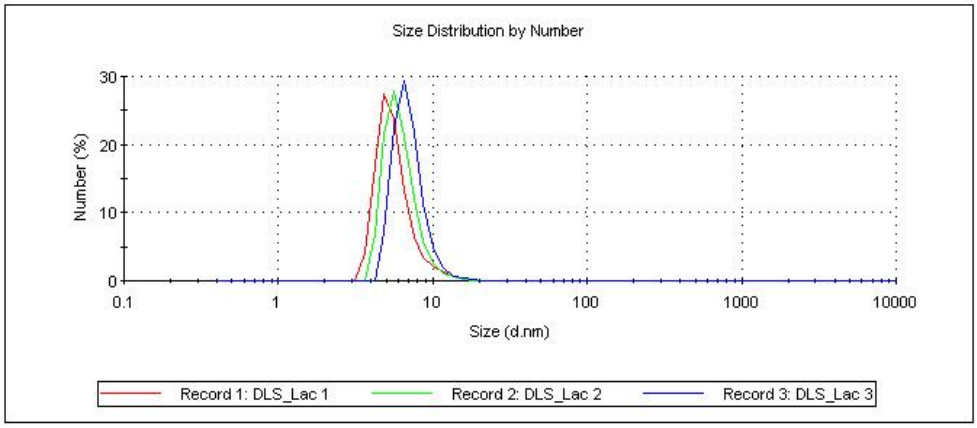

Figure 3.11. Graphical representation of the size distribution from three measurements of *Rv* laccase by number acquired using the dynamic light scattering technique.

3.6. Characterization of laccase in bionanoconjugates

The aim of the experimental work of this dissertation was to produce bionanoconjugates with AuNPs covered with *Rv* laccase and study the behaviour of the enzyme when conjugated with a nanometric surface. The first course of action was to study the enzyme connection with nanoparticles and obtain the amount of protein necessary to cover the surface of AuNPs functionalized with two different ligands. With this aim, two techniques were implemented. One was zeta-potential measurements that took advantage of the mobility of BNCs in solution to address if adsorption of protein to AuNP surface occurred. The other technique, which can be seen as a support to data obtained by zeta-potential, was agarose gel electrophoresis.

3.6.1. Zeta potential

Zeta potential relies on the electrophoretic mobility of charged particles in aqueous media. AuNPs alone have a defined superficial charge that will change as proteins conjugate to the surface through opposite charged residues. The result is that, if conjugation occurs, AuNPs become less charged and their electrophoretic mobility in solution is altered. The difference in superficial charge between the particles alone and the BNCs as the protein concentration increases at AuNPs surface is an indirect measure of protein coverage.

In order to study conjugation between *Rv* laccase with AuNP-MUA and AuNP-CALNN, zeta potential experiments were performed. The aim was to observe how the charges in the negative AuNPs changes as increasing amounts of the contents of laccase solutions adsorbed to their surface. The experiments with both kinds of AuNPs were done following the same method fixing the concentration of AuNPs at 1 nM and varying the concentration of laccase solution from 0 to 21.64 µg/mL.

Zeta potential experiments for BNC-MUA are represented in Figure 3.12.

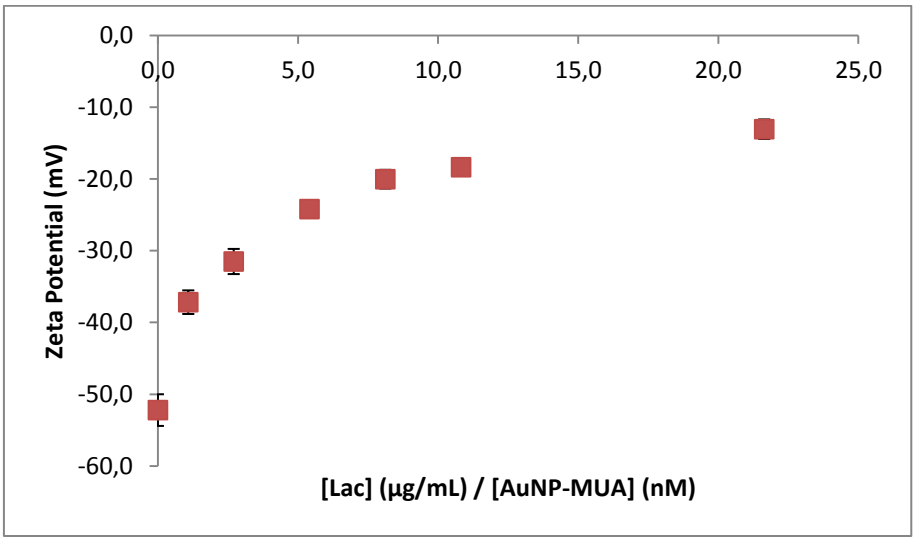

Figure 3.12. Graphical representation of the average zeta potential values and their standard deviation obtained for 1 nM AuNP-MUA with increasing concentrations of laccase adsorbed to the surface a pH 7.5.

AuNP-MUA particles alone appeared with negative surface charge of -52.22 ± 2.20 mV. This value is close to the value published for AuNP-Citrate[76].

As the quantity of *Rv* laccase increased in the samples, the zeta potential value increased to less negative values until it reached a saturation point in which the charge did not change with the addition of more protein. These results are compatible with several zeta potential experiments made with other enzymes[76]. The superficial charge of AuNPs decreased as the amount of protein adsorbs to the surface until reaching the total coverage.

However, at the time when these measurements were performed the solutions appeared slightly less red coloured than it was expected. To evaluate the stability conditions of the BNCs, all samples were measured by UV-Visible spectroscopy as well (Figure 3.13).

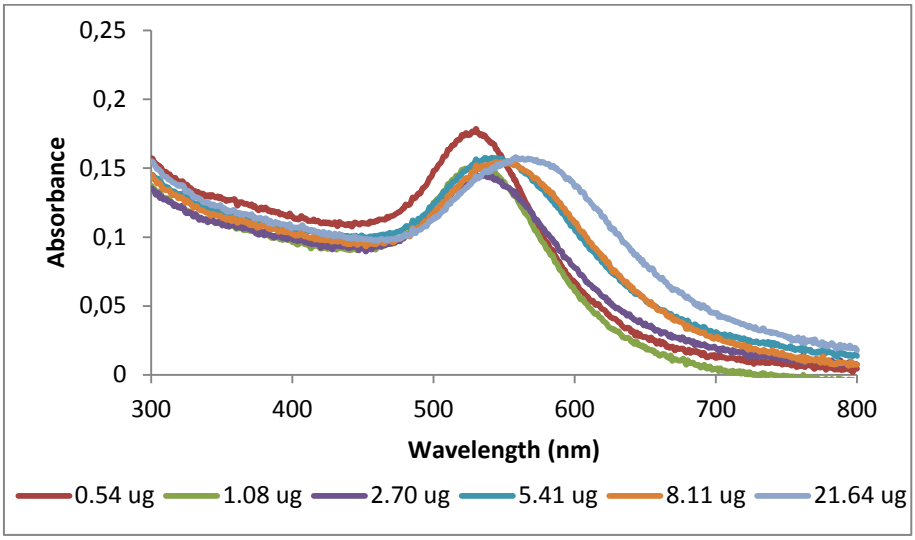

Figure 3.13. UV-Visible spectra of BNC-MUA samples with increasing concentrations of laccase used in zeta potential experiments.

What the UV-Visible spectra revealed was unexpected. The spectrum of the sample with less laccase, red line, appeared with the same shape and maximum absorption wavelength expected for 1 nM AuNP-MUA. As the amount of protein increased in the solutions, the plasmonic decreased in absorbance and shifted to higher wavelengths. This behaviour is characteristic of aggregated AuNPs solutions. It was expected that the negative ligand charge could be cancelled by the positive residues of the protein when forming stable bionanoconjugates. Other reactions might have occurred with this enzyme, or even with the possible contaminants present in the solution, that forced aggregation of the particles.
With these results, MUA was discarded from the subsequent experiments, because it did not provide stable bionanoconjugates.

The same procedure was done to BNCs with the pentapeptide ligand. Increasing amounts of protein were added to 1 nM AuNP-CALNN and the zeta potential change was studied (Figure 3.14).

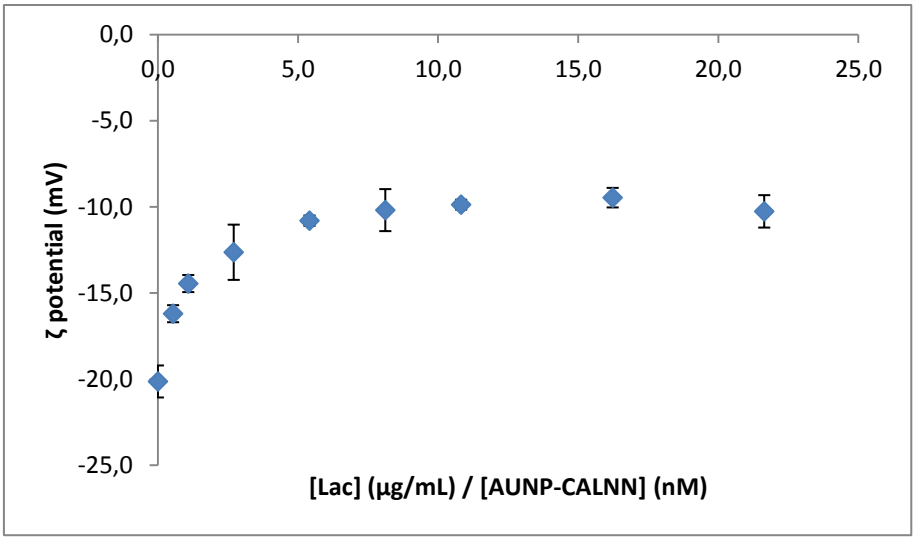

Figure 3.14. Graphical representation of the average zeta potential values and their standard deviation obtained for 1 nM AuNP-CALNN with increasing concentrations of laccase adsorbed to the surface at pH 7.5.

The zeta potential value obtained for AuNP-CALNN was -20.13 ± 0.93 mV, which was found to be a less negative value in comparison to the one reported for AuNP-CALNN (-47.7±0.3 mV)[24]. This outcome could be related to the fact that this experiment was carried out a few weeks after the synthesis of the particles. Some level of aggregation might have already occurred to the particles in the meantime, as they were not as negative as they should be right after the synthesis.

As laccase concentration increased on the surface of the particles, the charge on their surface increased and became less negative. This increase in zeta potential value went on until the protein concentration reached a saturation point, after which the potential remained stable around -10 mV. The variation in zeta potential was calculated and the experimental points were fitted with a Langmuir-type equation[24,76] (Equation 7).

$$\Delta\zeta = \frac{\Delta\zeta max.kL.R}{1+ kL.R} \qquad [7]$$

Δζ is the difference between the zeta (ζ) potential value of the particles with protein and the particles alone, Δζmax the maximum value obtained, kL the Langmuir adsorption constant and R the [Protein]/[AuNP] ratio.

The Δζ experimental points fitted with the Langmuir equation is presented in Figure 3.15.

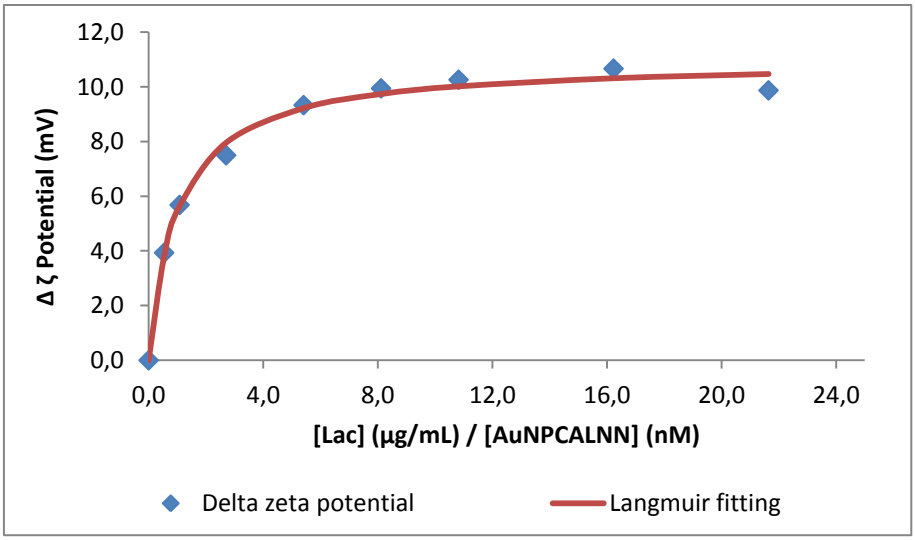

Figure 3.15. Graphical representation of the zeta potential variation values obtained for 1 nM AuNP-CALNN with increasing concentrations of laccase adsorbed to the surface at pH 7.5.

As it can be observed by the Δζ experimental points, the fitting with Langmuir equation follows the profile expected in these experiments. The fitting results and errors are represented in Table 3.2.

Table 3.2. Values obtained from the fitting of Langmuir equation to the experimental zeta potential data of AuNP-CALNN and BNCs.

	Value	Error
Δζmax (mV)	10.96	0.22
kL	0.98	0.102

From AuNP-CALNN to BNC with the maximum amount of protein tested, the charge in the surface varied 10.96 mV. In the early stages of protein addition, the zeta potential value increased rapidly and reached a stable value early in the experiment.

Saturation of the surface started around 8.1 µg of protein and the superficial charge did not change appreciably for higher laccase concentrations.

In these experimental conditions, the adsorption constant kL had a value of 0.98. It translates into the tendency for *Rv* laccase to bind to the AuNP-CALNN surface.

To compare the kL value obtained with the ones published by other authors, it was necessary to calculate the concentration ratio [Protein]/[AuNP] in nM. To that aim it would be necessary to assume that all protein content in the solution was laccase. SDS-PAGE studies (section 3.5.1) revealed that there was contamination in the commercial laccase used, but for comparison purposes only the protein content was assumed to be only laccase. The fitting to the data with R = [Protein]/[AuNP] (nM) can be seen in Figure 5.6, appendix VIII. The results were 10.97 ± 0.22 mV for Δζmax and 0.10 ± 0.01 for kL. The adsorption constant kL in these calculations was higher than the values published from similar studies with other proteins (Table 3.3)[24,76].

Table 3.3. kL parameters obtained from the Langmuir isotherm fitting of zeta potential data with concentration ratios in nM for the conjugation of different proteins and AuNPs.

[Protein]/[AuNPs] (nM)	kL
Laccase-AuNP-CALNN	0.105 ± 0.011
Heart Cytochrome c-AuNP-Cit[76]	0.025 ± 0.010
Tyrosinase-AuNP-CALNN[24]	0.050 ± 0.005

This experiment has to be regarded as describing an equilibrium. Since the enzyme was only adsorbed to the particles' surface by electrostatic interactions, there was still free laccase in solution. Additionally, there was also the possibility that contaminants in the laccase solution can adsorb to AuNPs surface as well.

With the intention of evaluating the stability of the BNCs used in this experiment, UV-Visible spectra were taken of the samples used for zeta potential experiments (Figure 3.16).

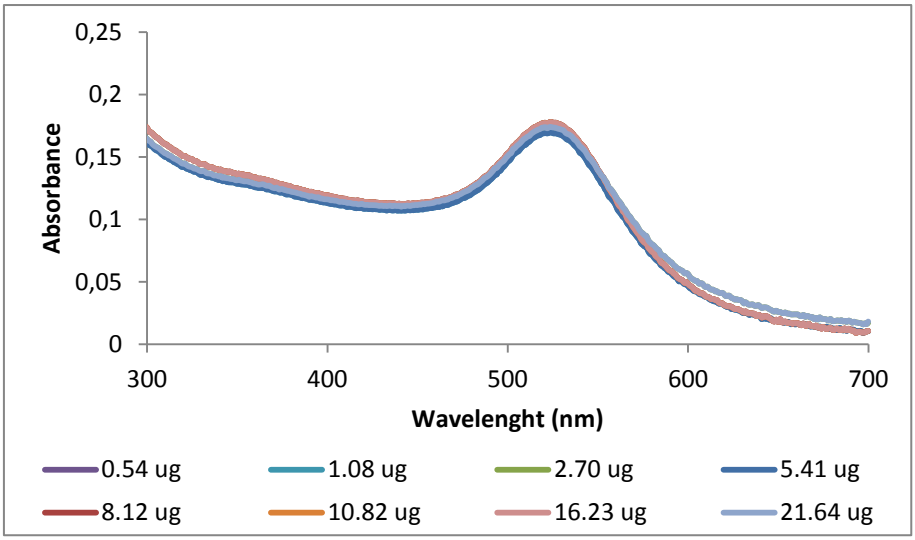

Figure 3.16. UV-Visible spectra of BNC-CALNN samples with increasing concentrations of laccase used in zeta potential experiments.

The UV-Visible spectra of all solutions showed the characteristic plasmonic profile with absorption maximum around 522 nm, and revealed that there was no aggregation.
Therefore, the BNCs remained stable in solution throughout zeta potential experiments, and the data achieved was not influenced by aggregation, but was a consequence of conjugation.

From this experimental data, it seemed that the maximum surface area of AuNP-CALNN was covered after the addition of approximately 8 µg, in total protein content of the *Rv* laccase solution. This was perceived as the optimal ratio of particle coverage. The active enzyme present in the *Rv* laccase solution was measured and the optimal ratio obtained can be translated into 30 U/mL of laccase activity. This was the fixed value used in the subsequent kinetic experiments.

The reason why the ligand CALNN was found to be more stable than MUA in bionanoconjugates preparation with this specific enzyme might be related to their inherent chemistry rather than their ability to bind to positive charges in laccase. CALNN is a small peptide and has a more complex chemistry in the terminal amino acids. Also, it is of the same composition as the protein. CALNN might have allowed a more "biofriendly" environment for conjugation to occur. In addition, a study presented later in this dissertation revealed that the superficial charges of a similar laccase do not encompass large localized charged regions such as proteins like cytochrome c[76]. Negative and positive regions seem evenly distributed throughout the protein, which might allow for several binding points between AuNPs and laccase.

3.6.2. Agarose gel electrophoresis

Agarose gel electrophoresis has been widely applied in research, not only to separate biomolecules, but recently it has also been used to separate particles according to their shape and size[88]. Separation of AuNPs can be achieved in this process, but it has also been shown to successfully separate BNCs. When solid, agarose gel is a thick and porous matrix where, much like polyacrilamide, molecules migrate by the action of an applied electric field[82]. Since the gel has a white colour it is possible to visualize the migration of conjugates made with AuNPs because of their red colour. The electrophoretic mobility is determined by the shape of the particles as well as by their superficial change.

In the present case, AuNPs were negatively charged and migrated towards the positively charged electrode. The superficial charges of the AuNPs surface changed by the addition of protein, becoming less negative as more protein adsorbed.

BNCs with AuNP-CALNN were produced in order to evaluate the formation of conjugation and to support the data obtained by zeta potential experiments. An increasing amount of *Rv* laccase solution was added to 1 nM AuNP-CALNN. To aid in the visualisation of the bands in the gel, the BNCs solutions were concentrated by centrifugation until they formed a sediment. Those sediments, containing the concentrated conjugates, were re-suspended and loaded into the wells of a 0.5% agarose gel. The agarose gel was run at 180 V for 30 minutes (Figure 3.17).

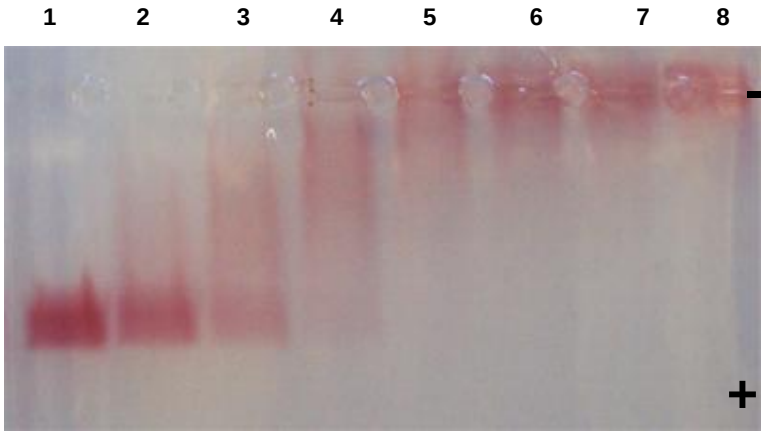

Lane	[Lac] (µg/mL)
1	0
2	0.54
3	1.08
4	2.7
5	5.41
6	8.11
7	10.8
8	21.64

Figure 3.17. Image of a portion from the 0.5% agarose gel of BNC-CALNN with 1 nM AuNP-CALNN and increasing amounts of *Rv* laccase. The table on the right shows the concentration of laccase in each lane. Gel performed at 180 V for 30 minutes at pH 8.

The image of the gel revealed that in lane 1 AuNP-CALNN alone migrated throughout the gel in a well-defined band, and there was not a wide size dispersion in these particles.
When laccase was added in the minimum amount tested, lane 2, the majority of the particles still migrated uniformly, but a slight smear could already be observed.
As the concentration of protein increased the particles did not migrate equally in the gel or created defined bands. Instead they were dispersed in the lane and smears with progressively less mobility could be seen from lanes 4 to 7. In lane 8 the BNCs seemed to not have migrated at all.

Previous studies in this area[77] showed that BNCs, with other proteins or antibodies, migrate uniformly in the gel and create well defined bands like the ones seen in lane 2. What was expected in this case was to observe defined bands that migrated slightly less as the amount of protein increased.

This test showed was that there was a difference between the migration of AuNP-CALNN and the remaining BNCs, which seemed to migrate less as more protein was added to the solutions. The smears seemed to account for differences in the charges of the particles, possibly due to some having protein adsorbed and others not. In light of these results, it seemed that the protein was not adsorbing properly to the particles' surface.

The next course of action was to covalently bind the protein to the surface of the particles to see if better results were obtained. To that effect, the covalent bond was provided by the cross-linking agent EDC/NHS. This agent has the ability to bind acidic functional groups to primary amines present in a protein, making the connection between laccase and AuNP-CALNN. The BNCs used in this experiment were prepared in the same manner as the previous ones but were incubated for 2 hours at room temperature. Afterwards, the same procedure as before was carried out. For comparison, four gels were performed with four different voltages, 75, 100, 150 and 180 V.

The agarose gels were carried out 75, 100 and 150 V (Appendix VIII), showed the same migration profile with smears as the gel made with BNCs without cross-linker. As the concentration of protein increased in the samples, smears appeared in the gel.
The results obtained in the agarose electrophoresis made at 180 V seemed to be the one with better results (Figure 3.18). This gel, opposed to the others, showed that the bands in lane 2 and 3 appeared more defined and with fewer smears.

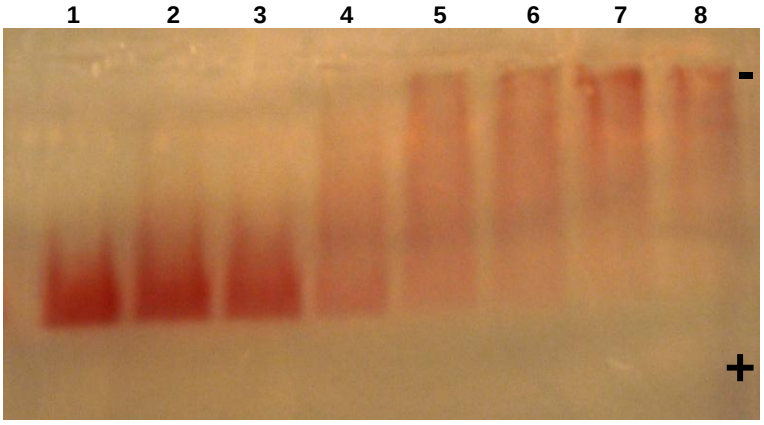

Lane	[Lac] (µg/mL)
1	0
2	0.54
3	1.08
4	2.7
5	5.41
6	8.11
7	10.8
8	21.64

Figure 3.18. Image of a 0.5% agarose gel of BNC-CALNN with 1 nM AuNP-CALNN and increasing amounts of *Rv* laccase cross-linked to AuNPs. The table on the right shows the concentration of laccase in each lane. Gel performed at 180 V for 30 minutes at pH 8.

Since the voltage was higher than in the previous experiments, it was expected for the migration velocity to increase in a way that it could possibly not allow the formation of smears along the gel.

In lane 1, AuNP-CALNN migrated with a well-defined band. As stated previously, lane 2 and 3 presented defined bands, although with just slight smears. From lane 4 and higher, rather than behaving as the more diluted samples, presented smears along the gel. However the end of the smears seemed to point out in the direction that as the concentration of the protein in the BNCs increased, BNCs migrated slightly less. Calculations of the electrophoretic mobility, from the distance the bands travelled in the gel, revealed that from lane 1 to lane 6 there was a difference of -7.34E-5 $cm^2/V.s$ (Appendix VIII, Figure 5.10). The electrophoretic mobility of lanes 7 and 8 could not be measured because the end of the smears was not as pronounced as the remaining bands.

The smear effect reflects differences in the BNCs charge. The particles seemed to have different amounts of proteins bound, possibly some having protein and others not, even with a covalent bond between AuNP-CALNN and laccase.

One of the influential factors might have been the preparation of the pellets. The method of centrifugation could have been too aggressive, leading to detachment of the protein from the AuNPs surface.

In the case of BNCs with laccase adsorbed electrostatically, some of the protein might have remained in the supernatant. This idea was proven correct when syringaldazine was added to the supernatant recovered from these BNCs. The characteristic pink colour of the quinone product formed in the presence of laccase was observed after a few minutes in the majority of the tubes. This qualitative test allowed observing that not all laccase remained adsorbed to AuNP-CALNN after centrifugation. As the quantity of protein increased, so did the quantity that remained in the supernatant (Figure 3.19).

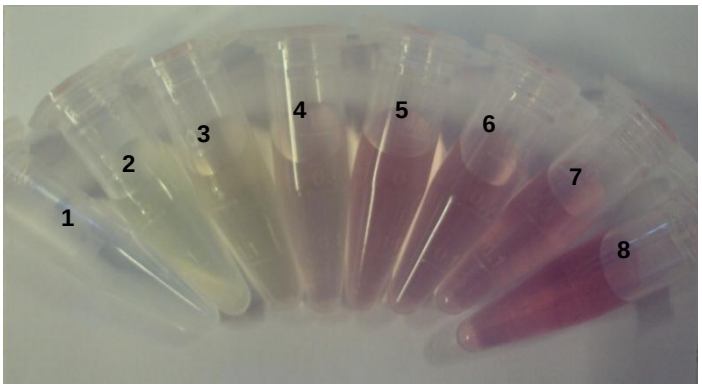

Tube	[Lac] (µg/mL)
1	0
2	0.54
3	1.08
4	2.7
5	5.41
6	8.11
7	10.8
8	21.64

Figure 3.19. Image of the supernatants recovered from the samples used in an agarose gel electrophoresis in Figure 3.17 where BNCs were made with *Rv* laccase adsorbed electrostatically to 1 nM AuNP-CALNN. The table on the right shows the laccase concentration that was initially used to prepare the BNCs.

In the case of AuNP-CALNN cross-linked with this laccase, there was the possibility that they might require longer incubation time. Another possibility was that native *Rv* laccase might be sensitive to electric fields, since smears of this protein also appeared in native-PAGE.

These results revealed that agarose gel electrophoresis was not the best technique to study the conjugation phenomenon that occurred between AuNP-CALNN and *Rv* laccase in the conditions it was performed.

3.7. Kinetic studies

In order to characterize laccase activity when conjugated with AuNPs, and evaluate their performance, several kinetic studies were carried out. The first course of action was to study the behaviour of the substrate in the conditions used in these studies. With that insight it would be possible to plan a suitable kinetic strategy for the BNCs that would enable observing how AuNPs influence the activity of laccase.

3.7.1. Studies with syringaldazine

Syringaldazine (SYR) has been regarded as the best suitable substrate to be used for laccase identification. It is an organic symmetric molecule with alcohol groups in the extremity of aromatic rings, which are the preferential action spots for laccases to oxidise into a coloured quinone product of easy detection (Figure 3.20). To improve SYR solubility and prevent degradation it was necessary to dissolve it in methanol as advised by the selling company.

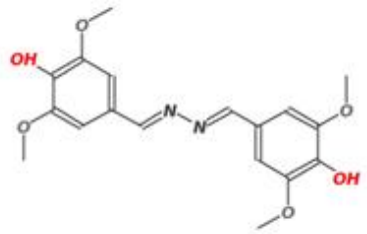

Figure 3.20. Structure of 3,5-dimethoxy-4-Hydroxybenzaldazine, syringaldazine (SYR)[51] with alcohol groups coloured in red.

The first step was to evaluate the UV-Visible spectrum of SYR solutions and observe where the maximum absorbance of the compound appeared (Figure 3.21).

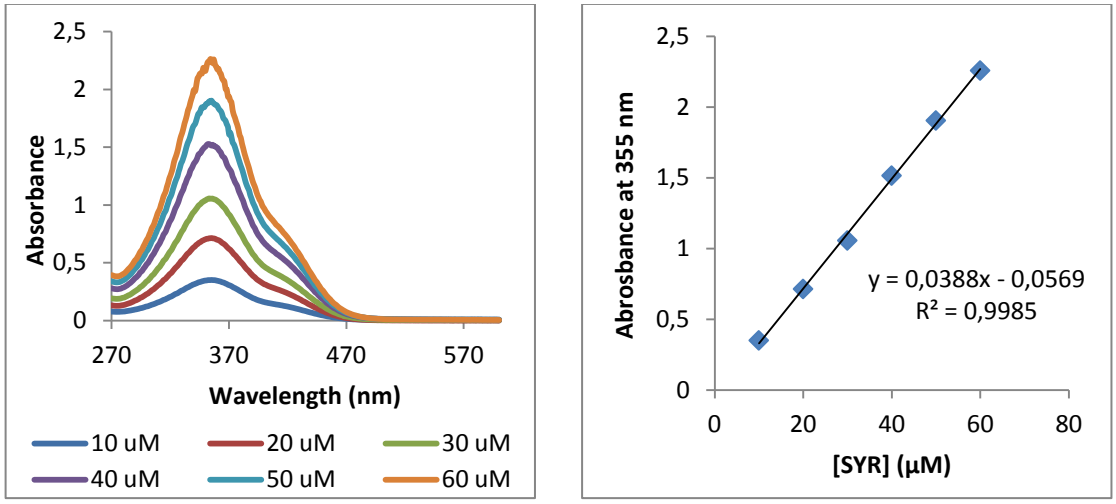

Figure 3.21. a) UV-Visible spectra of syringaldazine samples in 30 mM phosphate buffer pH 7.5 in the concentration range of 10 to 60 µM; **b)** Absorbance at 355 nm in function of syringaldazine concentration.

The spectrum of each sample at pH 7.5 (Figure 3.21a), showed pronounced absorption bands in the 270 – 470 nm spectral region. The maximum absorbance of the bands was 355 nm, a value consistent with the substrate's yellow colour. This value was found to be in agreement with the maximum absorbance value reported by previous studies[53]. This is also the region of significant SYR consumption by laccase. There was a linear increase in absorbance at this wavelength as the concentration of substrate increased (Figure 3.21b). The molar absorptivity

(ε) obtained from this plot was 38.8 mM^{-1} cm^{-1}. Above 40 µM of syringaldazine, the spectra started to show interference, which suggested that the concentration was too high for absorbance to be measured accurately. These results indicated that a concentration range between 0 and 40 µM would be the best to use in the kinetic experiments without falling out of the spectrophotometer's measuring range.

In these conditions, another band was also observed in the 400 nm region. In pH conditions investigated by other authors (pH 6.5), syringaldazine was reported to have a single band around 352 nm[89]. It is possible that the complex chemistry of the molecule could be influenced by changes in the media.

Several studies reported that in solution, SYR stability can be heavily influenced by pH variation and the presence of chloride ion[90]. All buffers used in the experiments contained potassium phosphate, so the influence of chloride was ruled out. Thus, the only major influence in the SYR spectrum could come from pH changes. Since pH variation was an essential part of the kinetic studies for laccase, it was also necessary to study the behaviour of SYR at the different pH envisioned to be applied.

The influence in the pH range from 6 to 8.5 in 10 µM syringaldazine was observed by UV-Visible spectroscopy (Figure 3.22).

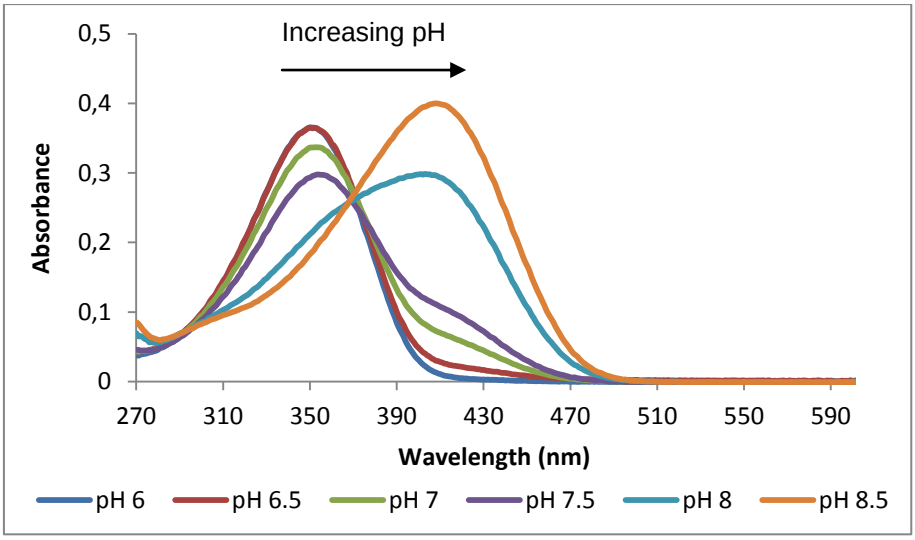

Figure 3.22. UV-Visible spectra of 10 µM syringaldazine samples in the pH range from 6 to 8.5.

As expected for this type of dyes with protonable groups, pH had a large influence on the UV-Visible spectrum of SYR.

At pH 6 (dark blue line in the spectrum of (Figure 3.22), the spectrum appeared as a single band with the maximum absorption at 350 nm. The spectrum of SYR at pH 6.5 appeared overlapped with the one of pH 6. There was still a single absorption band at this pH although the absorption around 400 nm increased slightly. The single band suggested that the stable form of syringaldazine was present around pH 6 and 6.5.

As the pH increased to 7 (green line in the spectrum of Figure 3.22), three events could be observed: the maximum absorbance shifted to 353 nm, the absorbance at the maximum decreased in comparison with the previous samples, and the absorbance at 400 nm increased even more.
With pH 7.5 (purple line in the spectrum of Figure 3.22), the absorbance decreased again. The maximum absorbance for this band was at 354 nm and once more, the absorbance around 400 nm increased.
It was at pH 8 (light blue line in the spectrum of Figure 3.22), that the spectrum changed completely. The band from the 350 nm region decreased significantly while the second band, in the 400 nm region, became the one with maximum absorption as pH increased. This change was even more dramatic at pH 8.5 where the maximum absorption was around 400 nm.

None of the spectra showed bands in the 530 nm region. This is the region where the product of the reaction between SYR and laccase appears. Thus the UV-visible spectrum of SYR as a substrate does not contribute to absorbance in the product region.
With these results, it was easy to observe that pH has a great influence in the chemistry of SYR, and as the pH changed so did the maximum absorption regions. In addition, research on SYR revealed that the ionisable OH groups have a pKa of 8.8[91].
This ability of the substrate to be influenced by changes in pH in this manner must be accounted when planning the enzymatic kinetics experiments.

The next step was to observe if changes in pH had the same influence in the absorption of the quinone product formed when SYR was in the presence of laccase. The catalytic oxidation reaction of SYR by laccase leads to a pink product tetramethoxy azobismethylene quinone (TMAMQ) with the reported maximum absorbance at 530 nm (Figure 3.23).

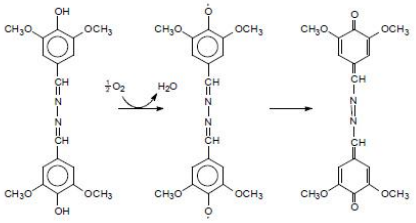

Figure 3.23. Schematic representation of the oxidation reaction of syringaldazine in the presence of laccase that results in the formation of water and a quinone (TMAMQ)

In this experiment, a fixed concentration of SYR was added to *Rv* laccase in the pH range 6-8.5. The UV-Visible spectrum of each sample was taken after 10 minutes of reaction (Figure 3.24).

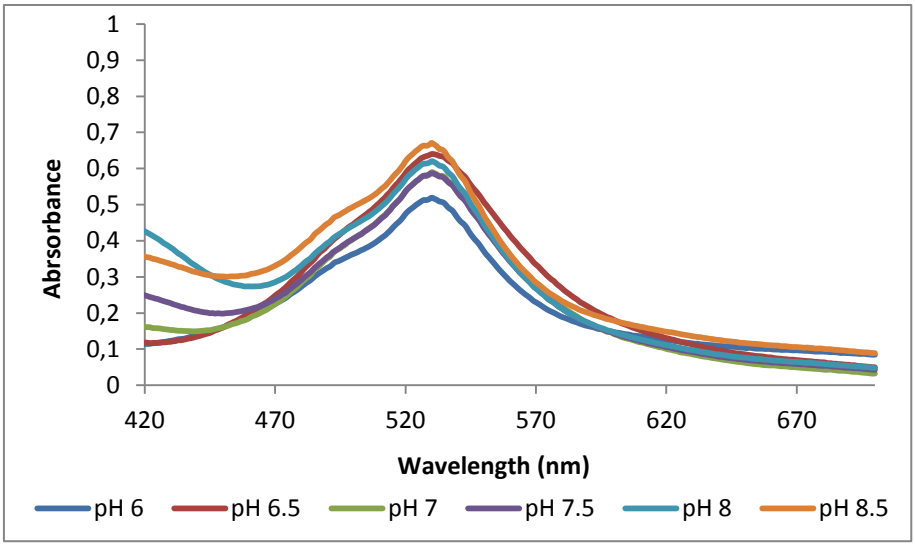

Figure 3.24. UV-Visible spectra of syringaldazine samples incubated with 30 U/mL of *Rv* laccase in the pH range from 6 to 8.5. Spectra taken after 10 minutes of reaction.

The spectra showed a significant increase of absorbance in the 470 – 600 region after 10 minutes reaction. The absorbance maximum of the bands was found at 530 nm, correspondent to the quinone product of this reaction. The spectra also showed a typical shoulder at 495 nm as previously described[54].

The product maximum absorbance remained stable at 530 nm in the pH range tested.

Since the main focus of this dissertation was to study the behaviour of *Rv* laccase when conjugated with AuNPs, it was necessary to study their UV-Visible absorption, in order to address the best way to conduct the posterior enzymatic experiments. The spectrum of syringaldazine incubated with *Rv* laccase was superimposed with the spectrum of 1 nM AuNP-CALNN solution (Figure 3.25).

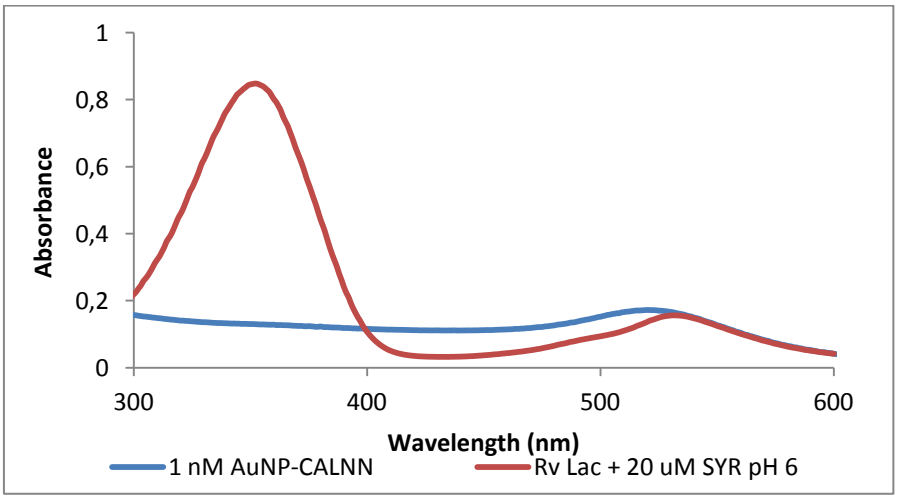

Figure 3.25. UV-Visible spectrum after five minutes of the reaction between 20 µM syringaldazine incubated at pH 6 with 30 U/mL of *Rv* laccase (—); and the spectrum of 1 nM AuNP-CALNN (—).

The aim of the previous comparison was to address the influence that the absorption bands of SYR and its product would possibly produce when laccase was conjugated with AuNP-CALNN. In the spectra of Figure 3.25, the absorption band of SYR appeared in a region where the absorption of AuNP-CALNN is low. Therefore, the influence of the particles on the absorbance of SYR was small. The region where AuNPs were of more influence was in their maximum absorbance, at the SPR band (ca. 520 nm).

Since the concentration of AuNP-CALNN in the BNCs was fixed at 1 nM, the maximum absorption was found to be approximately 0.2 around 522 nm. In addition, the maximum absorbance of the quinone product of the laccase reaction always appeared at 530 nm, independently of the pH. The absorbance of the product could suffer some influence from the AuNPs SPR band. Experiments had to be performed in a way that the influence of AuNP-CALNN in the absorption was minimized. This was achieved by using the mixture of phosphate buffer, Mili-Q water, *Rv* laccase and AuNP-CALNN without substrate as a blank.

The activity of laccase for SYR consumption and quinone production were measured at different wavelengths. Table 3.4 shows the wavelengths used to monitor both reactions in the pH range 6 to 8.5. This was found to be the best solution to work with the pH influence and still be able to observe catalytic activity (Table 3.4).

Table 3.4. Wavelength values in nanometers used to follow the reactions of syringaldazine consumption by laccase and the formation of the quinone in the pH range from 6 to 8.5.

pH	Wavelength (nm)	Wavelength (nm)
6	350	530
6.5	350	530
7	350	530
7.5	350	530
8	365	530
8.5	400	530

Additionally, it is necessary to keep in mind that product [P] formation assays are preferred. Measuring the appearance of product is usually more accurate in enzymology studies. In fact, detecting small changes in [P] (when [P]=0) is easier and less error-prone than detecting small changes in [S][92].

3.7.2. Kinetic studies of enzyme concentration in bionanoconjugates

Following the unexpected results obtained in the agarose gel electrophoresis, it was necessary to understand if, after the ultrafiltration procedure, there was still enzyme conjugated with the particles. The qualitative activity test shown in Figure 3.19, suggested that there was laccase

present in the supernatant. It was still necessary to quantify how much of the total enzyme added to the BNCs remained in the supernatant and how much was conjugated to the particles. With that objective, new solutions of BNCs, with the same range of laccase concentration used in the agarose gels were prepared. One batch of BNCs was prepared to enable electrostatic adsorption of laccase to 1 nM AuNP-CALNN to occur. Another batch was prepared with chemical bond between laccase and the particles provided by the cross-link agent EDC/NHS. These BNCs went through the same process required to obtain the pellets used in agarose electrophoresis. Afterwards, the clear supernatants were separated from the pellets, and pellets were re-suspended to the original volume. Laccase activity, in each solution of supernatant and pellet, was measured with a fixed concentration of syringaldazine. The formation of product was measured by the increase of absorbance at 530 nm and the activity was calculated with the initial rates.

The results for both kinds of BNCs were similar. However, since BNCs with cross-linking agent were later discarded from the kinetic studies, the activity records shown in this section are from laccase electrostatically adsorbed to AuNP-CALNN (Figure 3.26).

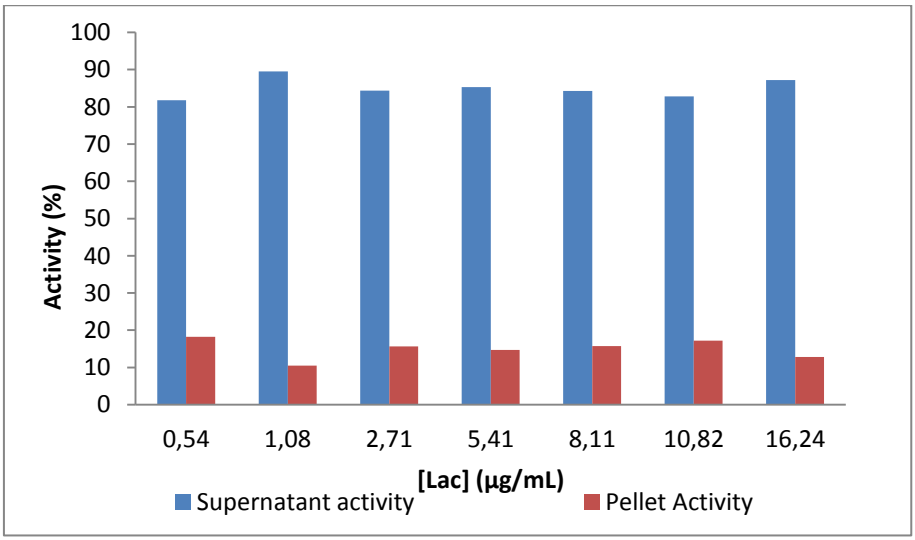

Figure 3.26. Activity data in percentage from pellet (■) and supernatant (■) solutions obtained from ultrafiltration BNC solutions with 1 nM AuNP-CALNN and increasing concentrations of *Rv* laccase.

Figure 3.26 showed that in all samples there was activity both in the supernatant and in the pellet. An average 85.01 ± 2.63 % of laccase activity was found in the supernatant.

The average percentage of laccase with activity that remained in the pellet was 14.99 ± 2.67 %. It is a low percentage, but still indicated that there was a small portion of active laccase that was able to successfully adsorb to the surface of the particles and resist the centrifugation process.

These results suggested that, although the majority of laccase was present in the supernatant, some amount still remained conjugated with AuNP-CALNN.

Laccase activity of BNCs not submitted to centrifugation was measured and compared with the sum of activity from supernatants and their pellets from the previous experiment (Figure 3.27).

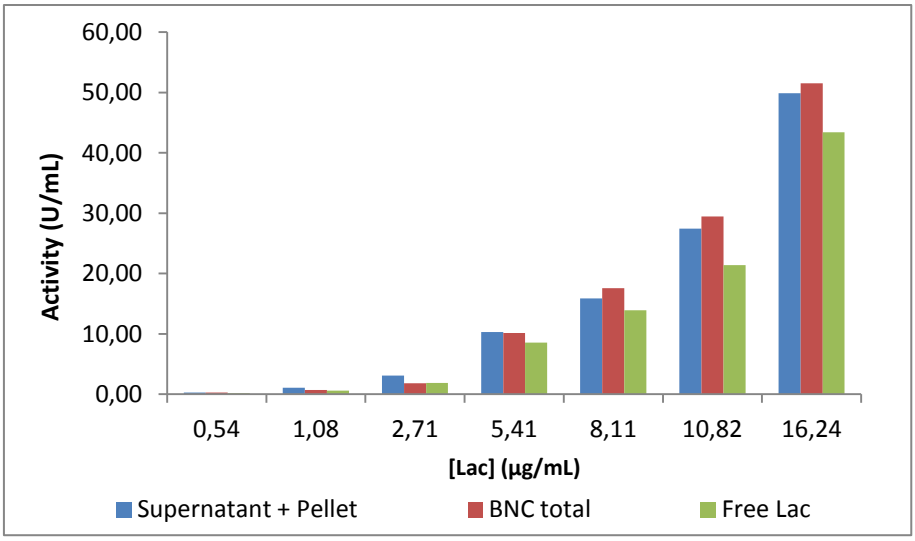

Figure 3.27. Comparison between the activity data from the sum of activity in supernatant and pellet (■), total BNCs (■) and free laccase (■).

Laccase activity in the complete BNCs was similar to the sum of activity in supernatant and pellet. This result seemed to indicate that there was no significant loss of enzyme activity during ultrafiltration. The activity of the BNCs not submitted to the centrifugation process was compared with free laccase in the same conditions. The plot in Figure 3.28 shows the difference of activity of BNCs in comparison to free laccase.

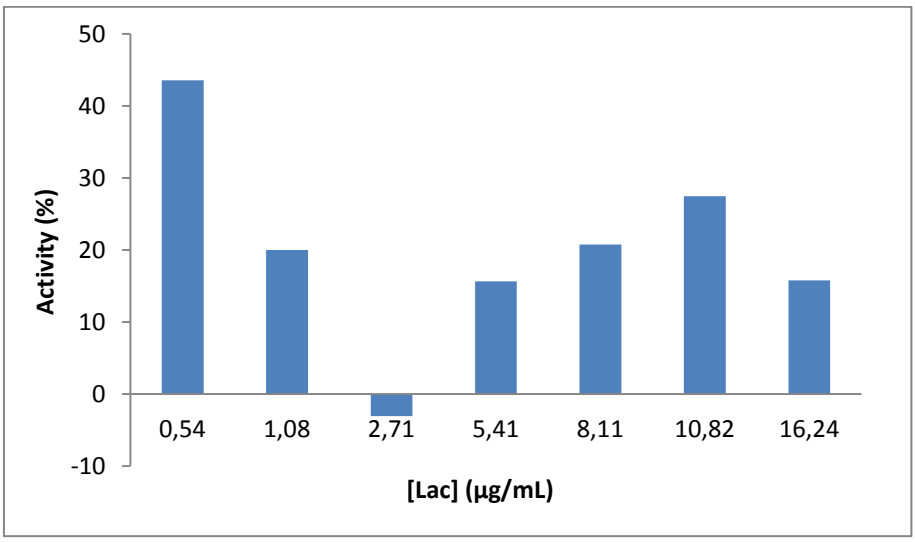

Figure 3.28. Increase of laccase activity in percentage from BNCs in comparison to the activity of free laccase.

By comparing the activity of free laccase in the same conditions as BNCs, it was possible to observe that laccase had higher activity when conjugated with AuNP-CALNN than when free in solution. Only in the case of 2.71 µg/mL of laccase there was a slight reduction in laccase activity in the BNCs.

These results were highly encouraging since AuNP-CALNN seemed to improve laccase activity, which is one of the goals in the construction of enzymatic biosensors with gold nanoparticles.
The previous experiments demonstrated that the centrifugation process led to the appearance of a high quantity of non-conjugated laccase in the supernatants. Yet, there was still a small portion of enzyme that was able to resist the centrifugal force and remain conjugated.

3.7.3. Kinetic studies with pH variation

The strategy implemented to study the kinetic behaviour of free laccase and laccase conjugated with AuNP-CALNN was based on the knowledge acquired from the previous experiments. In order to follow both the consumption of SYR and the production of the quinone product, it was necessary to work in a substrate concentration range that allowed following both reactions and staying within the detection limit of the spectrophotometer. The active enzyme was fixed at 30 U/mL while the substrate concentration varied from 0 to 40 µM to obtain Michaelis-Menten kinetic curves. The buffer concentration was fixed at 30 mM potassium phosphate buffer with pH varying from 6 to 8.5 at room temperature.

To obtain the initial rates of substrate consumption and product formation, the strategy used was to take continuous UV-Visible spectra in a short period of time while the enzymatic reaction occurred as seen in the example in Figure 3.29.

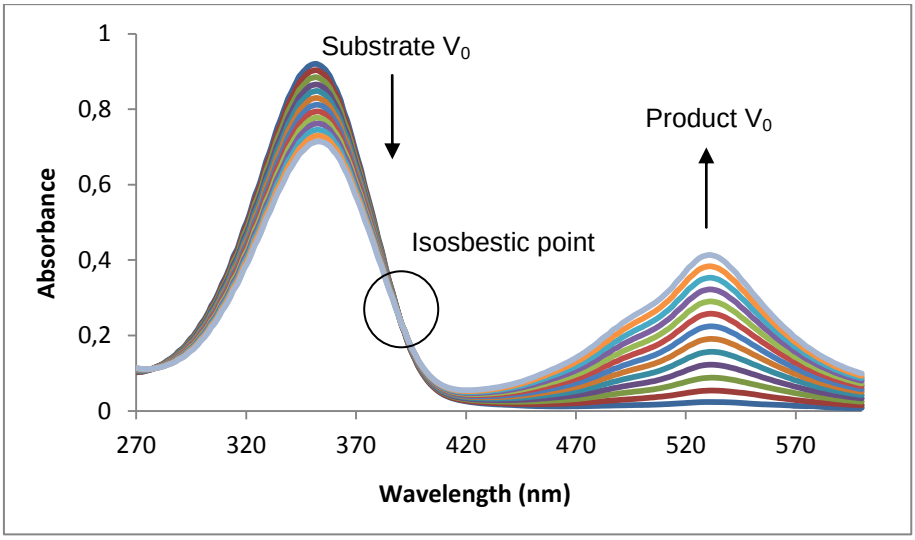

Figure 3.29. UV-Visible spectra of the reaction between 30 U/mL laccase and 20 µM syringaldazine at pH 6. Spectra taken every 30 seconds during 10 minutes between 270 and 600 nm. The black circle shows an isosbestic point.

By taking into consideration the wavelength region between 270 and 600 nm, it was possible to observe both the bands that corresponded to substrate and the bands for product.

At pH 6, shown in the example above, the maximum absorbance of the substrate was found at 350 nm as seen in the previous studies. The absorbance of that band decreased with time as the reaction with laccase progressed due to SYR consumption.
At the same time, the band at 530 nm, typical of the quinone which results from the oxidation of SYR by laccase, showed an increase in absorbance over time.
During this experiment, it was also possible to observe that there was a particular region where all spectra overlapped and created an isosbestic point between the bands of substrate and product (marked in the circle). This region is known as the wavelength where two species have the same molar absorptivity. In the laccase reaction with SYR, this region shifted slightly as pH increased, but was observed more distinctively at approximately 430 nm at pH 7.5. It has been reported that this reaction is performed on a 1:1 ratio[53], where one molecule of substrate is transformed into one of product. The presence of an isosbestic point between both seemed to suggest that there was no formation of an intermediate. However, it is known that laccases produce a SYR radical as an intermediate stage before the formation of the product. The fact that it could not be observed spectroscopically might be due to that radical having a short life time and not being detectable.
The initial rates (V_0), in minutes, were measured by the slope of the decrease in absorbance in the first 2 minutes of enzymatic reaction, in the case of substrate consumption, and the slope of absorbance increase in the case of product formation in the same window of time. As a result of this approach, for the same sample, it was possible to measure both reactions with accuracy.
It was also necessary to take into account the shift in absorbance of the substrate bands created by pH variation. Consequently, it was necessary to follow different absorbance maximums to obtain the initial rates for SYR consumption by laccase as it had been seen in the experiment described in section 3.7.1.

The first kinetic experiment performed was with the purpose of designing an activity profile for free laccase in solution as the pH of the media varied. Like many other enzymes, laccase activity also has the particularity of being pH dependant. This kind of procedure was also important to obtain the optimal pH condition at which the enzymatic activity was higher for SYR, since many publications mention that laccase catalytic activity is also dependant on the substrate used[48].
Since the experiment was only performed with phosphate buffer, which has previously been reported as the preferential buffer for this laccase, 6 to 8.5 was the only pH range possible to test. To obtain the catalytic dependence on an expanded range of pH, it would have been necessary to use buffers such as Acetate, for pH lower than 6, and glycine-NaOH for pH above 8. However, all three buffers have different ionic compositions and would probably influence the enzymatic activity in different ways. For this strategy to be successful all samples, independently of pH, would have to have in their composition all three buffers that would have their contribution in their respective pH ranges. The mixture of these buffers would raise the complexity of the samples and possibly create other variables in the catalytic reaction. In order to keep the experiment as simple as possible, pH was only measured in the range of phosphate

buffer. In these conditions it would still be possible to observe the optimal activity conditions for *Rv* laccase with SYR as substrate. Additionally, the pH dependence of catalytic activity for this enzyme in the presence of SYR was evaluated by the quantity of product that was able to form in the same time period under the different conditions tested. The fact that it was the product formation chosen to be measured in this particular experiment was mainly because the product absorbance band was not disturbed by the change in pH. Therefore it provided a more stable environment to study only the influence of pH in the enzymatic reaction and not the influence of pH in the substrate alone.

To obtain the pH dependant activity, this experiment was carried out with the proposed conditions in the previous kinetic experiments with pH being the only variable. Laccase activity against a fixed concentration of substrate was obtained by measuring product formation at 530 nm (Figure 3.30).

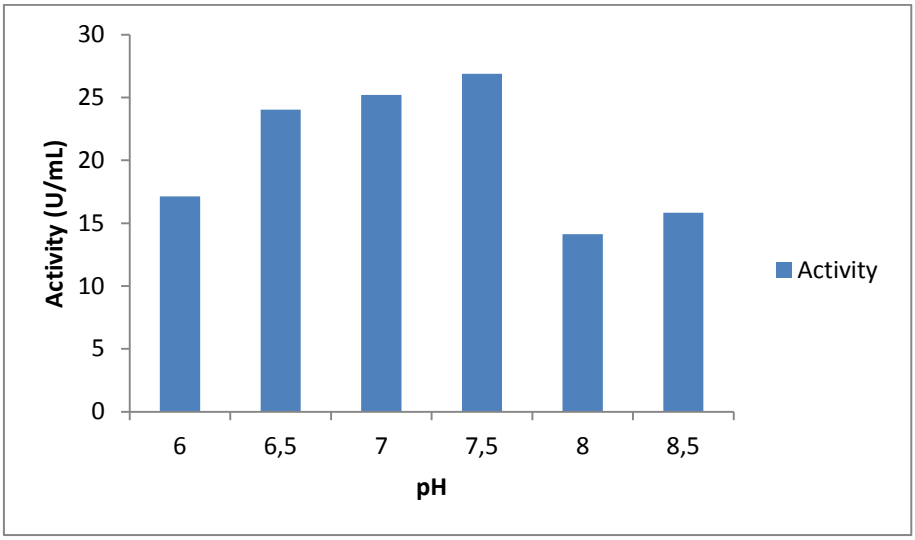

Figure 3.30. Dependence of *Rv* laccase catalytic activity with pH, using 30 U/mL of enzyme, 20 µM syringaldazine and 30 mM phosphate buffer in the pH range from 6 to 8.5.

The experiment in this particular pH range revealed that the pH dependence was a portion of the bell-shaped profile that is usually described for enzymes such as laccase. The activity at pH 6 was low, but it increased as pH increased, with maximum activity found to be at pH 7.5. When pH reached alkaline levels, pH 8 and 8.5, the activity dropped to the same values as observed for pH 6.

Some studies demonstrated that the optimal pH for *Rv* laccase, in the presence of SYR, was around pH 8-8.5[48]. However, this was not observed in this experiment, since pH 8 and 8.5 were the conditions when laccase had the lowest activity. One of the reasons for this occurrence could be due to the fact that alkaline conditions have a large effect on laccases, because of the presence of a higher concentration in hydroxide anions. Hydroxyl anions have been reported to act as an inhibitor of the internal electronic transfer between the T2 and T3 sites leading to lower enzymatic activity in certain types of laccases[48]. The composition of the phosphate buffer used could be responsible for the lower activity at the alkaline conditions tested.

In any case, other studies indicated that plant laccases, such as *Rv* laccase, can also present a pH dependence profile centred in neutral conditions[30].

The next approach was to study the stability of the BNCs produced from *Rv* laccase and AuNP-CALNN. The solutions of the BNCs prepared in the same conditions, and at the various pH conditions that would be tested in the kinetic experiments, were studied by UV-Visible spectroscopy (Figure 3.31).

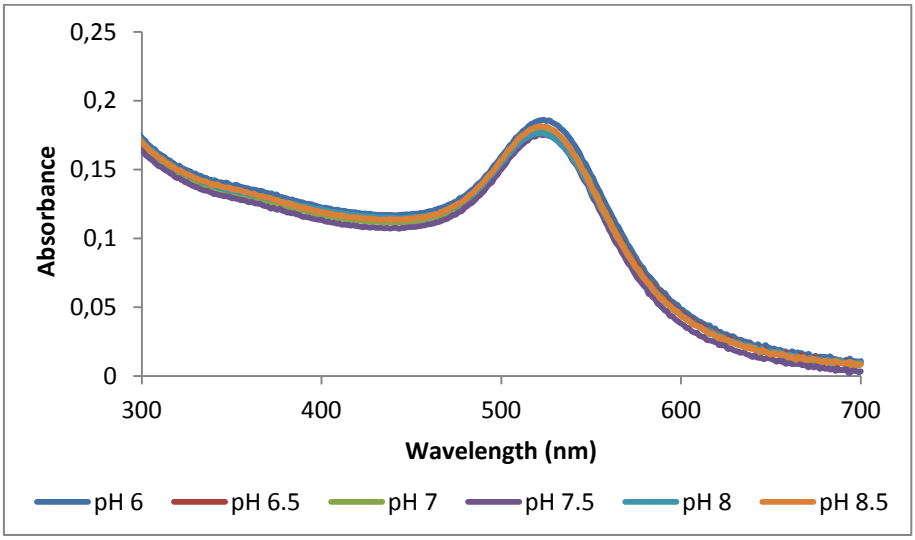

Figure 3.31. UV-Visible spectra of the BNC solutions produced with 30 U/mL *Rv* laccase, 1 nM AuNP-CALNN at 30 mM potassium phosphate buffer in the pH range from 6 to 8.5.

The UV-Visible spectra of all BNCs revealed similar absorbance profiles to the one of 1 nM AUNP-CALNN. In all pH conditions tested, no aggregation was detected, since the plasmonic profile showed maximum absorbance around 523 nm.

These results showed that, in the conditions in which they were prepared and from pH 6 to 8.5, the conjugates remained stable in solution and were not prone to aggregation.

Since these BNCs seemed to be stable in the pH range necessary, the enzymatic studies proceeded with the purpose of obtaining Michaelis-Menten profiles. With this study it was possible to observe the influence of pH in laccase activity in both substrate consumption and product formation reactions. The studies were performed in samples with free laccase and samples with laccase conjugated with AuNP-CALNN.

Kinetic experiments were also performed for BNCs where laccase was covalently bound to AuNP-CALNN through the cross-link agent EDC/NHS. The experimental data and respective errors are represented in Table 5.3 and Table 5.4 in appendix IX. The kinetic values obtained appeared to be unreasonable in comparison with the ones obtained for free laccase and the BNCs with adsorbed laccase. Furthermore, the data revealed high errors for the value of k_M for both substrate consumption and product formation. A hypothesis for these results having high error might be due to interference from the cross-linking agent in the structure of the protein when conjugated with AuNPs. If the protein's structure was altered upon the formation of a

covalent bond between the AuNPs with cross-linking and the protein residues it could have influenced the arrangement of the active site. In addition, problems in protein orientation are one of the known drawbacks of using cross-linking agents[93]. These events might have lead to the inability of covalently bound laccase to efficiently catalyse the enzymatic reaction with syringaldazine. These results were not taken into consideration.

3.7.3.1. Substrate consumption

The first reaction to be evaluated was the consumption of substrate by *Rv* laccase free in solution and in BNCs (Figure 3.32 and Figure 3.33).

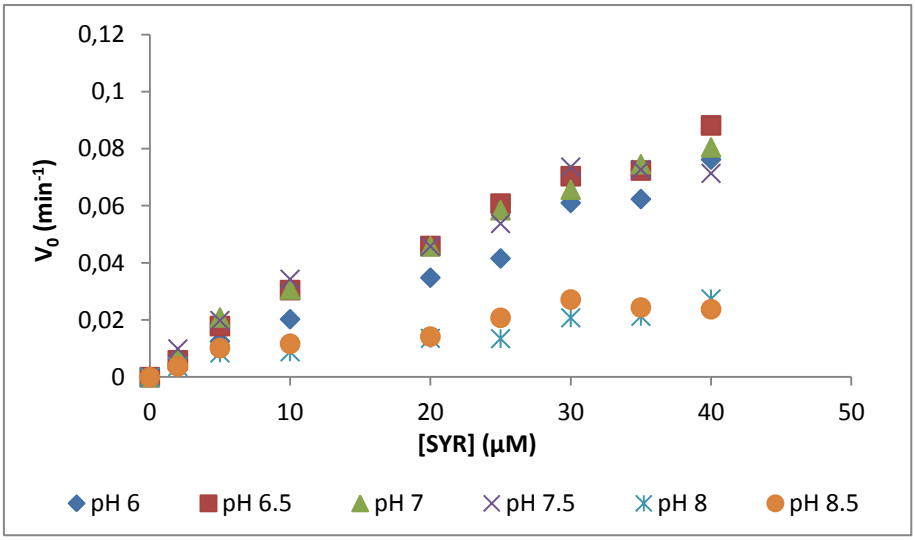

Figure 3.32. Representation of the initial rates (V_0) in function of SYR concentration obtained for substrate consumption reaction by free *Rv* laccase in the pH range of 6 to 8.5.

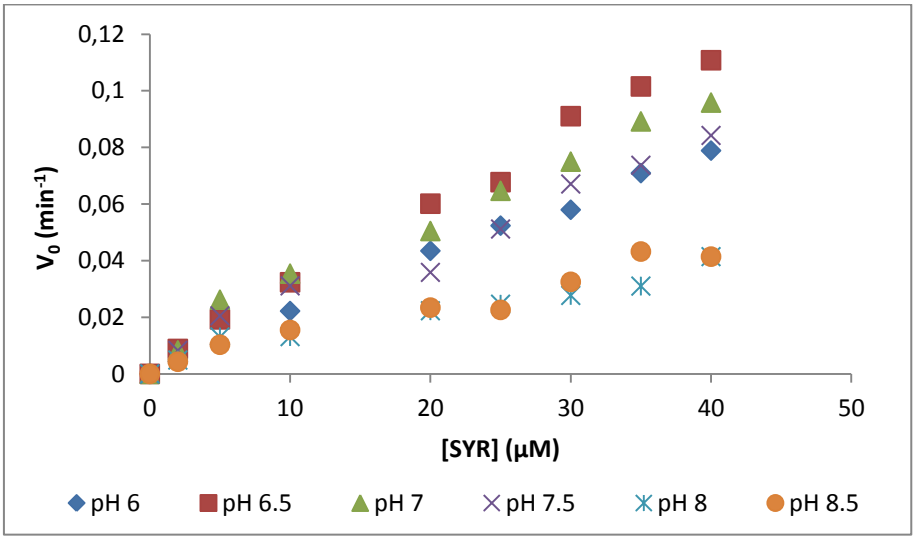

Figure 3.33. Representation of the initial rates (V_0) in function of SYR concentration obtained for substrate consumption reaction by BNCs in the pH range of 6 to 8.5.

The kinetic parameters, V_{max}, K_M, k_{cat} and k_{cat}/K_M, were able to be calculated by fitting the Michaelis-Menten equation (Equation 1, Chapter I) to the experimental data of initial rates (V_0) obtained in the pH range in study. The experimental data was obtained both for free laccase and for BNC, and is represented in Table 3.5 and Table 3.6 respectively.

Table 3.5. Michaelis-Menten parameters obtained for the reaction of SYR consumption of free laccase in pH conditions from 6 to 8.5. The errors were generated by the software Origin from the fitting of the Michaelis-Menten equation.

Lac	**Substrate consumption**					
pH	**V_{Max} (min^{-1})**	**error**	**k_M (µM)**	**error**	**k_{cat} ($min^{-1}.U^{-1}.mL$)**	**k_{cat}/k_M ($min^{-1}.U^{-1}.mL.\mu M^{-1}$)**
6	0.41	0.14	193.17	44.05	1.37E-02	7.07E-05
6.5	0.264	0.077	85.12	34.37	8.80E-03	1.03E-04
7	0.185	0.032	53.25	14.47	6.17E-03	1.16E-04
7.5	0.133	0.027	31.56	12.19	4,43E-03	1.40E-04
8	0.035	0.013	27.06	19.36	1.17E-03	4.31E-05
8.5	0.038	0.009	20.99	11.5	1.27E-03	6.03E-05

Table 3.6. Michaelis-Menten parameters obtained for the reaction of syringaldazine consumption of BNCs in pH conditions from 6 to 8.5. The errors were generated by the software Origin from the fitting of the Michaelis-Menten equation.

BNC	**Substrate consumption**					
pH	**V_{Max} (min^{-1})**	**error**	**k_M (µM)**	**error**	**k_{cat} ($min^{-1}.U^{-1}.mL$)**	**k_{cat}/k_M ($min^{-1}.U^{-1}.mL.\mu M^{-1}$)**
6	0.358	0.108	148.36	103.2	1.19E-02	8.04E-05
6.5	0.41	0.15	113.67	44.05	1,37E-02	1.20E-04
7	0.264	0.09	72.83	36.06	8.80E-03	1.21E-04
7.5	0.294	0.08	107.49	25.82	9.80E-03	9.12E-05
8	0.045	0.007	19.08	6.69	1.50E-03	7.86E-05
8.5	0.11	0.016	69.94	13.57	3.67E-03	5.24E-05

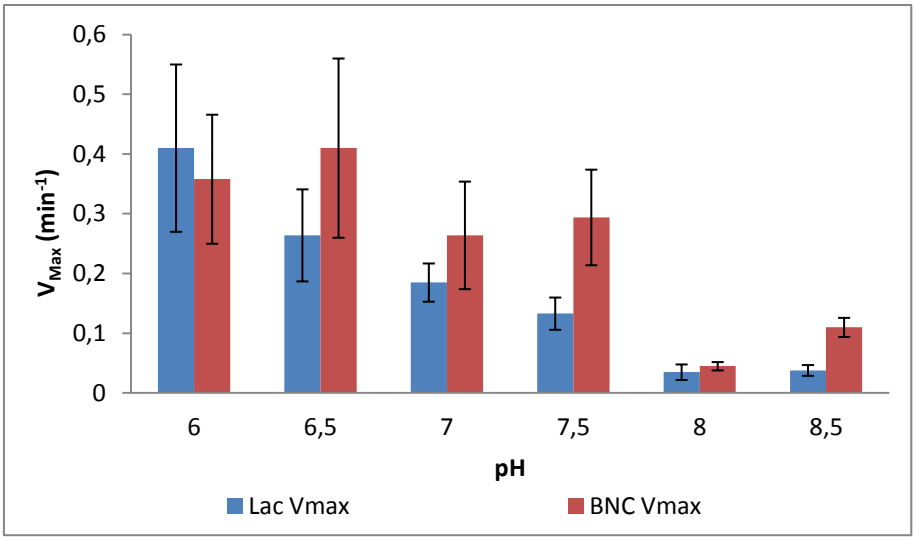

Figure 3.34. Comparison between the V_{max} values obtained for substrate consumption in the case of free laccase (■) and BNCs (■) in pH conditions from 6 to 8.5.

The kinetic data showed that in the case of maximum rate (V_{max}) of substrate consumption (Figure 3.34), it decreased for free laccase as the pH increased. The error values have to be taken in consideration, especially when comparing the V_{max} results obtained for pH 6, 6.5 and 7. Only in the case of pH 7.5 and 8.5 the increase of V_{max} in the BNCs in relation to free laccase can be observed as favourable, since the errors were lower in these cases. For pH 8, the values were similar for free and conjugated laccase.

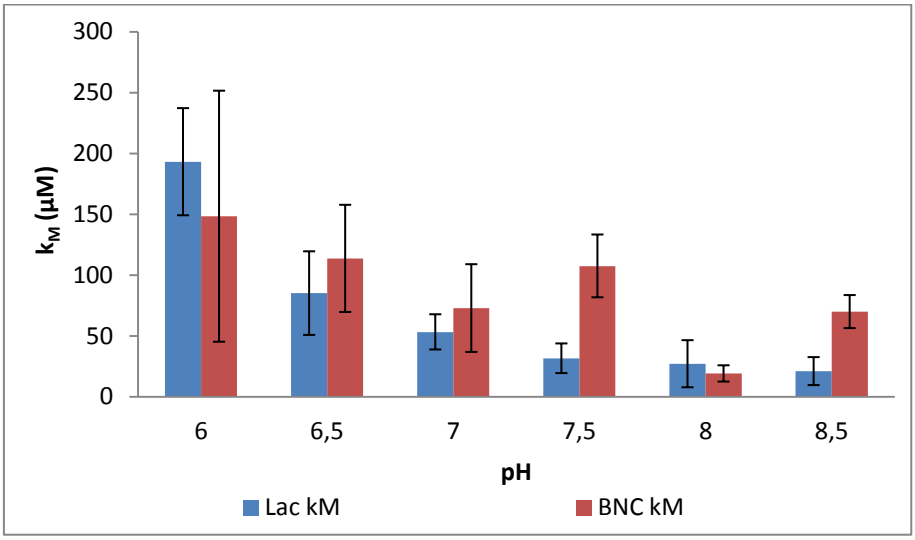

Figure 3.35. Comparison between the K_M values obtained for substrate consumption in the case of free laccase (■) and BNCs (■) in pH conditions from 6 to 8.5.

The parameter K_M (Figure 3.35), which reflects the affinity of the enzyme for the substrate, revealed that it only decreased in BNCs in relation to free laccase for pH 6 and 8. However, the error values at these pHs do not permit to assume that there was in fact an increase in affinity.

From pH 6.5 to 7.5 the BNCs K_M increased, but due to high error, only in the case of 7.5 this increase was significant. At pH 8, K_M in BNCs also increased, suggesting low affinity for the substrate.

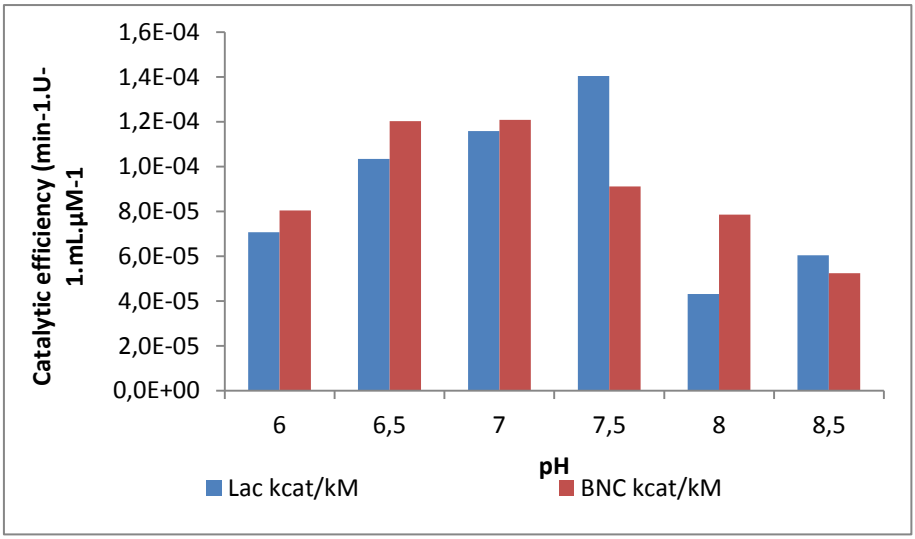

Figure 3.36. Comparison between the catalytic efficiency (k_{cat}/K_M) values obtained for substrate consumption in the case of free laccase (■) and BNCs (■) in pH conditions from 6 to 8.5.

The most relevant parameter for catalysis can be obtained by the ratio between k_{cat}, which is directly influenced by V_{max}, and the affinity for substrate, K_M (Figure 3.36). This ratio indicates the catalytic efficiency of the enzyme for SYR. At pH 6, 6.5, 7, and 8, it was possible to observe that the absolute value of catalytic efficiency increased when laccase was conjugated with AuNPs.

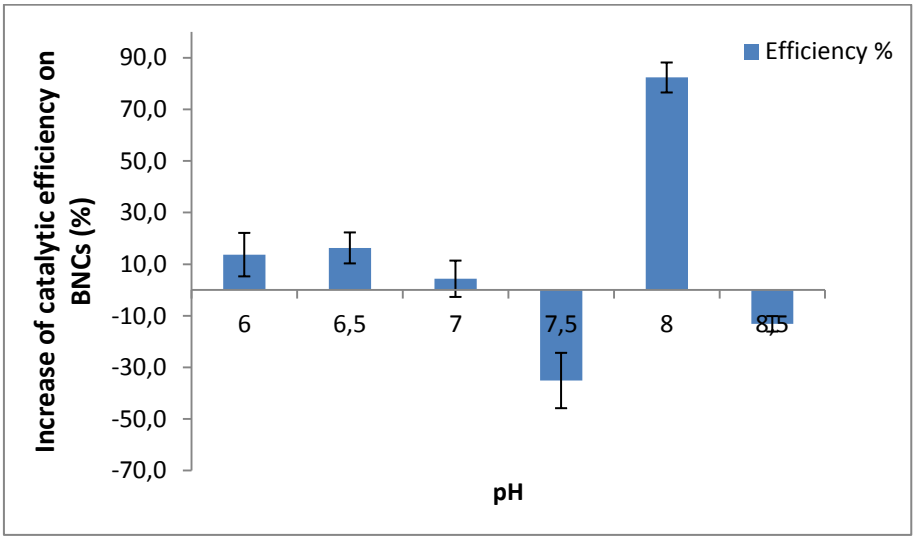

Figure 3.37. Representation of the percentage of catalytic efficiency obtained by BNCs when in comparison with free *Rv* laccase catalytic efficiency.

Figure 3.37 shows the increase of catalytic efficiency for substrate consumption obtained for BNCs. At pH 6, 6.5 there was an increase in efficiency when laccase was conjugated with AuNP-CALNN. At pH 7 there was also an increase but due to high error this data was not reliable. At pH 7.5 laccase efficiency decreased approximately 35%. When pH was 8, the efficiency of the BNCs increased significantly (82.35%). At pH 8.5 there was a decrease of approximately 13% in BNCs efficiency.

3.7.3.2. Product formation

The production of quinone was also followed in the same conditions as previously described, to observe the influence of pH variation in the enzymatic action of laccase. Once more, a Michaelis-Menten profile was obtained by the experimental data for initial rates (V_0) versus SYR concentration in the case of free laccase and BNCs (Figure 3.38 and Figure 3.39).

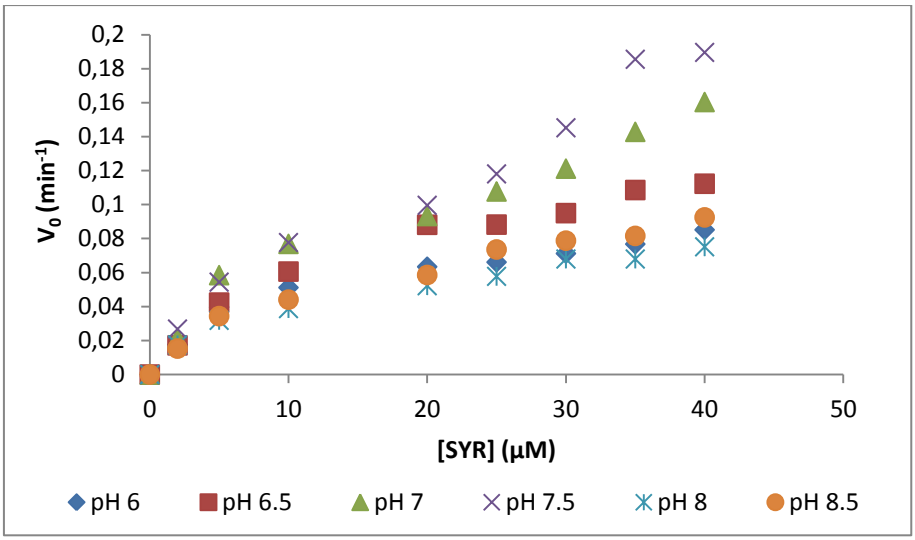

Figure 3.38. Representation of the initial rates (V_0) in function of syringaldazine concentration obtained for the product formation reaction by free *Rv* laccase in the pH range of 6 to 8.5.

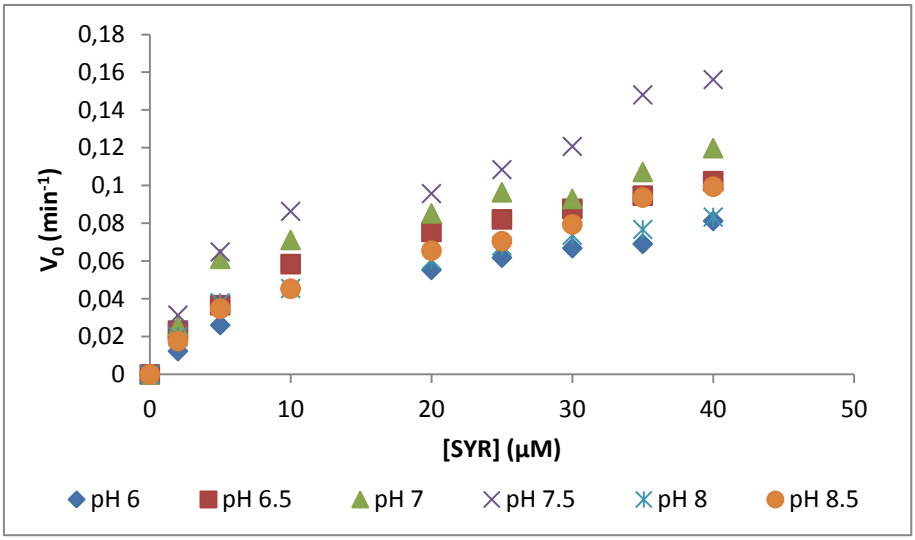

Figure 3.39. Representation of the initial rates (V_0) in function of syringaldazine concentration obtained for the product formation reaction by BNCs in the pH range of 6 to 8.5.

The fitting of the Michaelis-Menten equation to the experimental points allowed obtaining the kinetic parameters for product formation when laccase was free in solution and conjugated with AuNP-CALNN (Table 3.7 and Table 3.8)

Table 3.7. Michaelis-Menten parameters obtained for the reaction of product formation by free *Rv* laccase in pH conditions from 6 to 8.5. The errors were generated by the software Origin from the fitting of the Michaelis-Menten equation.

Lac	**Product formation**					
pH	**V_{max} (min^{-1})**	**error**	**K_M (µM)**	**error**	**k_{cat} ($min^{-1}.U^{-1}.mL$)**	**k_{cat}/K_M ($min^{-1}.U^{-1}.mL.\mu M^{-1}$)**
6	0.094	0.005	8.33	1.66	3.13E-03	3.76E-04
6.5	0.147	0.008	14.06	2.23	4.90E-03	3.49E-04
7	0.22	0.041	20.94	8.71	7.33E-03	3.50E-04
7.5	0.482	0.229	64.28	44.9	1.61E-03	2.50E-04
8	0.091	0.0078	11.79	2.97	3.03E-03	2.57E-04
8.5	0.125	0.013	17.57	4.46	4.17E-03	2.37E-04

Table 3.8. Michaelis-Menten parameters obtained for the reaction of product formation by BNCs in pH conditions from 6 to 8.5. The errors were generated by the software Origin from the fitting of the Michaelis-Menten equation.

BNC	Product formation					
pH	**V_{max} (min^{-1})**	**error**	**K_M (μM)**	**error**	**k_{cat} ($min^{-1}.U^{-1}.mL$)**	**k_{cat}/K_M ($min^{-1}.U^{-1}.mL.\mu M^{-1}$)**
6	0.102	0.008	14.79	3.16	3.40E-03	2.30E-04
6.5	0.126	0.006	11.99	1.82	4.20E-03	3.50E-04
7	0.126	0.009	7.17	1.97	4.20E-03	5.86E-04
7.5	0.182	0.025	12.17	4.87	6.07E-03	4.98E-04
8	0.097	0.006	9.67	1.93	3.23E-03	3.34E-04
8.5	0.142	0.019	20.9	6.36	4.73E-03	2.26E-04

For comparison, the values for each parameter V_{max}, K_M and k_{cat}/K_M were graphically represented for product formation for free laccase and BNCs, in order to access how each parameter was influenced by laccase-AuNP conjugation.

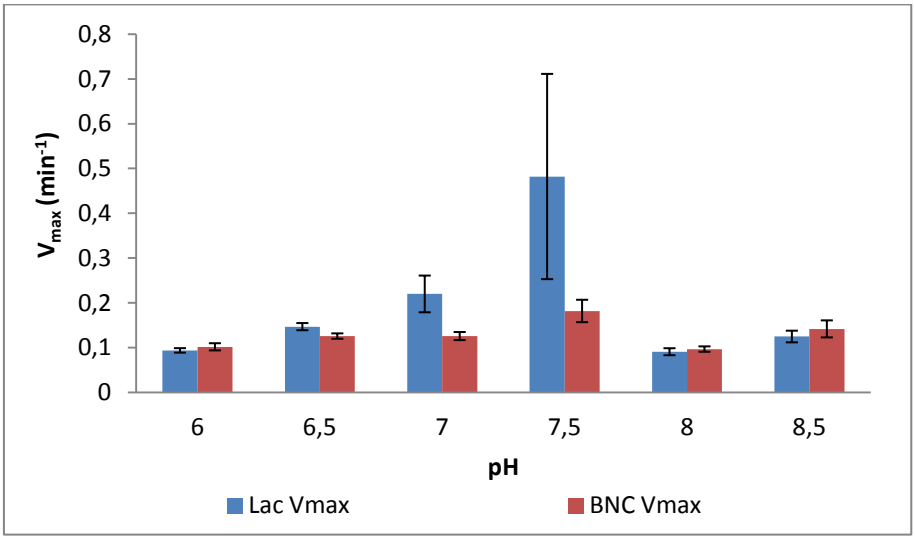

Figure 3.40. Comparison between the V_{max} values obtained for product formation in the case of free laccase (■) and BNCs (■) in pH conditions from 6 to 8.5.

The first noticeable change between the V_{max} values obtained for product formation was that, for pH 6, 6.5 and 7, they were 5-10 times lower than the ones obtained for the reaction where substrate consumption was followed. For example for substrate consumption by free laccase at pH 6, V_{max} reached up to 0.41 min^{-1} while in product formation V_{Max} was 0.094 min^{-1}.
Nonetheless, in the case of this specific reaction of quinone formation, the V_{max} values obtained were very similar and with low error values for both free laccase and BNCs, except in the case of pH 7 and 7.5 where the values obtained for the BNCs were smaller than for the free enzyme.

At pH 6, 6.5, 8 and 8.5 there was not much difference in the velocity of the reaction with BNCs in comparison with free laccase. These results showed that in these conditions AuNP-CALNN did not influence the reaction velocity negatively. Additionally, since k_{cat} is directly related to $V_{max,}$ k_{cat} only decreased significantly at pH 7 and 7.5.

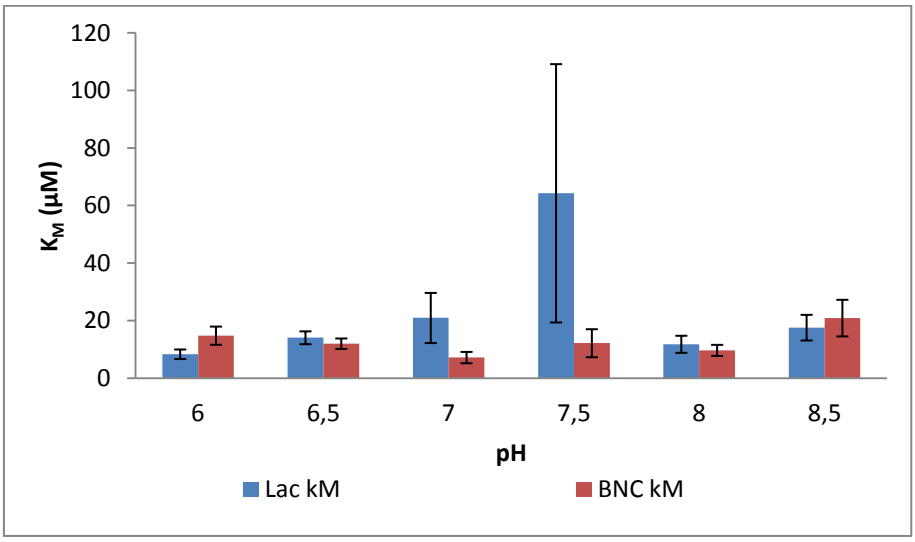

Figure 3.41. Comparison between the K_M values obtained for product formation in the case of free laccase (■) and BNCs (■) in pH conditions from 6 to 8.5.

Comparing K_M values of enzyme affinity obtained for free laccase and BNCs they showed that for BNCs, the K_M value increased approximately 80%, which means that at this pH there was a decrease in affinity in the BNCs. K_M then decreased 65.76% at pH 7 and 81.07% at 7.5. At pH 7.5 the highest error was observed. This decrease in K_M can be translated into an improvement of affinity when laccase was conjugated with AuNPs. The percentages of K_M are shown in Figure 5.11, Appendix IX.

The fact that for the majority of pHs tested, with the exception of pH 6, 7 and 7.5, the enzymatic affinity did not change dramatically showed that AuNPs did not influence the enzyme function in a negative manner. Also, the experimental data fitted the Michaelis-Menten model with low error which supported the consistency of the data obtained and the comparisons made.

In addition, even though the reaction velocity of laccase in these conditions decreased in BNCs, the presence of AuNPs increased the enzymatic affinity.

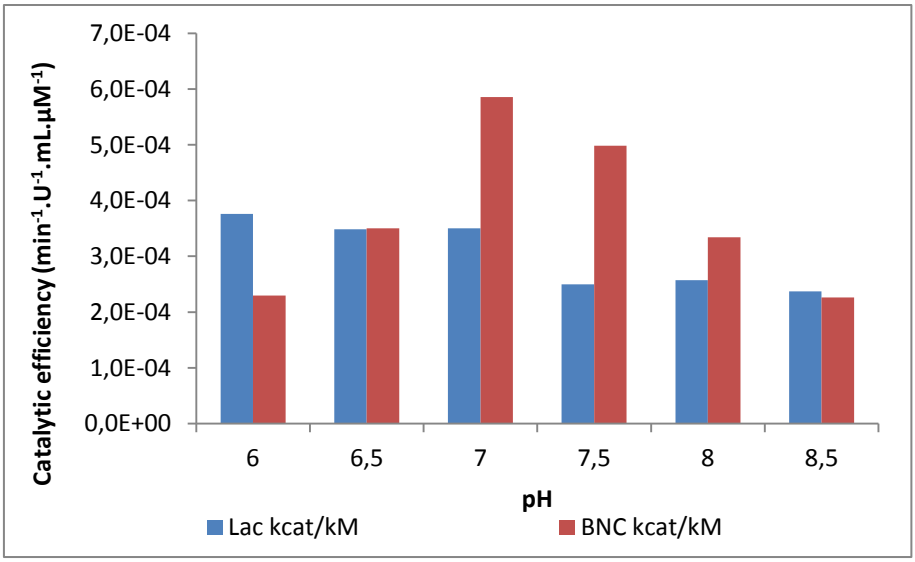

Figure 3.42. Comparison between the catalytic efficiency (k_{cat}/K_M) values obtained for product formation in the case of free laccase (■) and BNCs (■) in pH conditions from 6 to 8.5.

Calculating the ratio between the reaction turnover and the enzymatic affinity, k_{cat}/K_M, it was possible to infer about the influence of AuNPs in the catalytic activity of *Rv* laccase.

The results represented in Figure 3.42 showed that at pH 6 the catalytic activity was higher for free laccase. It seemed that for the more acidic pH on the scale tested, AuNP-CALNN had an unfavourable influence in the enzymatic activity of laccase.

For pH 6.5 and 8.5, the catalytic efficiency did not differ significantly between free laccase and BNCs. It was only at pH 7, 7.5 and pH 8 that differences were revealed. In these conditions, the catalytic activity increased significantly, and demonstrated that AuNPs enhanced laccase activity.

The influence of AuNP-CALNN in the enzymatic efficiency was calculated taking into consideration that the standard value was the one obtained when laccase was free in solution (Figure 3.43).

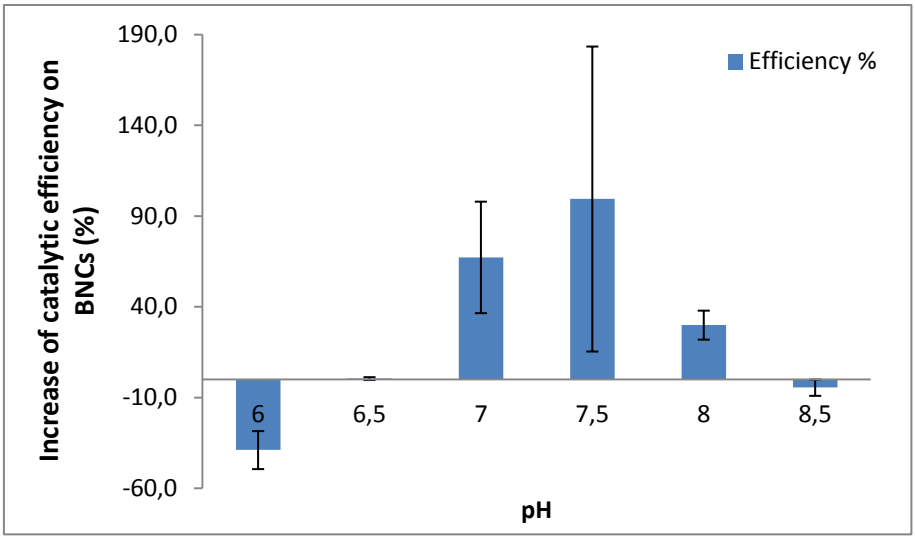

Figure 3.43. Representation of the percentage of catalytic efficiency obtained by BNCs when in comparison with free *Rv* laccase catalytic efficiency.

As shown in Figure 3.43, at pH 6 BNCs had a decrease in catalytic efficiency of approximately 38% of the value obtained for free laccase. On the other hand, for pH 6.5 there was a very small increase (0.51 %), but not enough to be assumed as an enhancement. At pH 7 the increase in efficiency was more than 50%.

In the case of pH 7.5, the increase reached approximately 100%. However, in this case the result needs to take into consideration the high error value associated.

For pH 8, the increase in affinity was less than seen in the previous two conditions, but still remarkable higher than seen for free laccase. This was a very good result taking into consideration that the pH dependence curve (Figure 3.30) showed that this pH was not in the optimal pH zone. Therefore, AuNPs were able to enhance the performance of laccase in this condition.

As explained in section 3.7.1, the advantage of following product formation is that the measurement is more reliable than measuring substrate consumption. Also, there was the additional advantage that the quinone product did not seem to be influenced by the changes of pH like syringaldazine showed by UV-Visible spectroscopy.

3.8. Structural analysis by molecular modelling

3.8.1. Electrostatic surface of laccase and bionanoconjugates interaction

The electrostatic potentials of proteins are known to be one of most important and difficult characteristics to predict by molecular modelling[66]. Still, there is a vast display of algorithms that allow taking into account the different parameters that influence protein charges and predict the electrostatic surface of proteins[66].

To study the formation of electrostatic complexes between proteins and other molecules or structures (such as AuNPs) it is important to predict with accuracy the electrostatic surface of a protein.

One of the parameters that influences the electrostatic potentials, as well as the interaction of proteins and other molecules, is pH[66]. The pH dependence of the surface electrostatic potential of proteins arises from pKa values of ionisable side chains in amino acid [66].

The aim of this study was to predict superficial charges of *Rhus vernicifera* laccase, used in the experimental part of this dissertation, and evaluate its predisposition to form electrostatic BNCs with negatively charged AuNPs. Unfortunately, the three-dimensional structure of this protein is still not available, which makes this study currently not possible. The only three-dimensional structure with full copper content published of a laccase that has some degree of similarity with *Rv* laccase is *Trametes versicolor* laccase. However, the similarity between *Tv* laccase and *Rv* laccase is reported to be 22%[36]. Even with this low percentage of similarity, this is currently the best approximation possible to evaluate the electrostatic surface of laccases for conjugation purposes.

In this study, the charges of amino acids were calculated taking into consideration their pKa and 6 different pH values, namely, at pH 6, 6.5, 7, 7.5, 8 and 8.5, and implemented into *Tv* laccase structure to generate the electrostatic surface. The surfaces are shown in spherical mode and coloured for residues charges as shown in the colour scheme in Figure 3.44. Negative charges are coloured in red, neutral charges are in white and positive charges are coloured in blue. The charge value is represented by the intensity of the colours.

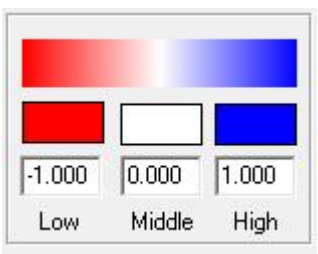

Figure 3.44. Colour scheme representation of residue charges in the protein. Red represents negative charges, white represents neutral charges and blue represents positive charges.

For an easier spatial visualization, the default position that appeared when the structure was uploaded in Chemera was considered to be the “front view” of the structure.

3.8.1.1. Front view

pH 6

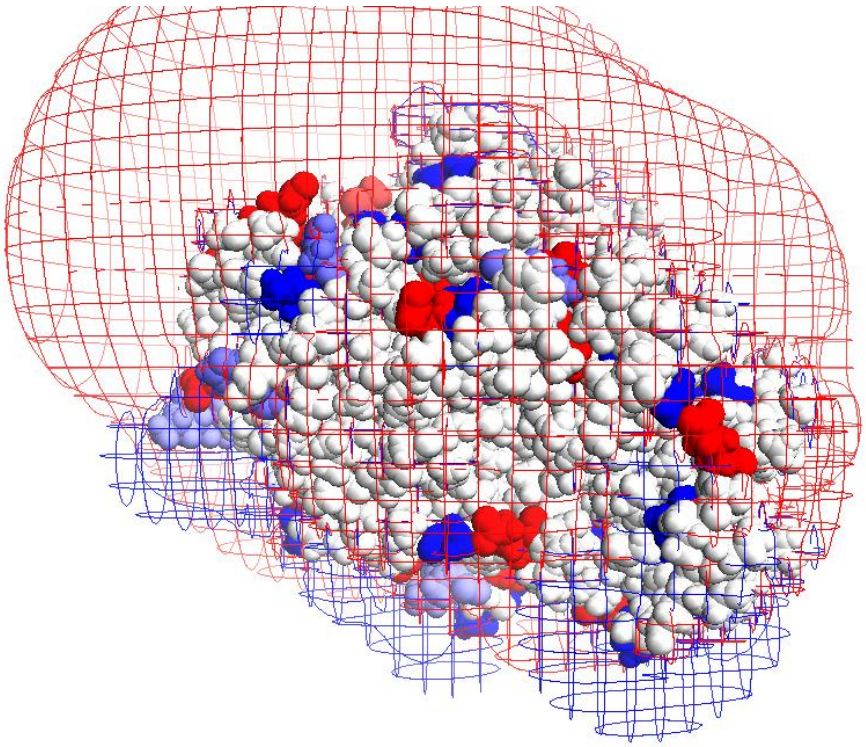

Figure 3.45. Front view of the electrostatic surface of *Tv* laccase at pH 6. Structure represented in spheres Charge colour-code is as explained in Figure 3.44.

Chemera calculated the values of the electrostatic field that surrounded the protein taking into account the charge distribution and media conditions. The grid is influenced by the shape of the protein as well. The grid represents the isopotential surface, negative in red and positive in blue. Additionally, the grid does not represent an area where positive or negative charges are mainly present in the protein.

The grid that was obtained for this laccase showed that for the intensity of the field applied (0.01 eV), the negative area is projected farther away from the surface and occurs mainly in one side of the protein. The positive area of the grid (blue) is closer to the protein’s surface and smaller in comparison with the red grid. This effect might be due to the positive areas being weaker than the negative areas.

Figure 3.45 shows the electrostatic surface and grids generated by Chemera at pH 6.

The charge of the residues in the protein appeared evenly distributed on the surface of the protein and without large defined areas of positive or negative charges. Several residues of negative charge (red) and positive charge (blue) can be seen in this front view.

The regions that are of interest for electrostatic interaction with the negatively-charged AuNPs are of course the positive (blue). If BNCs were to be made with this enzyme, these would be the

areas with which the negatively charged ligand CALNN would preferentially create an electrostatic interaction. At this pH condition and this side of the protein, there were a few possibilities for AuNP-CALNN adsorption.

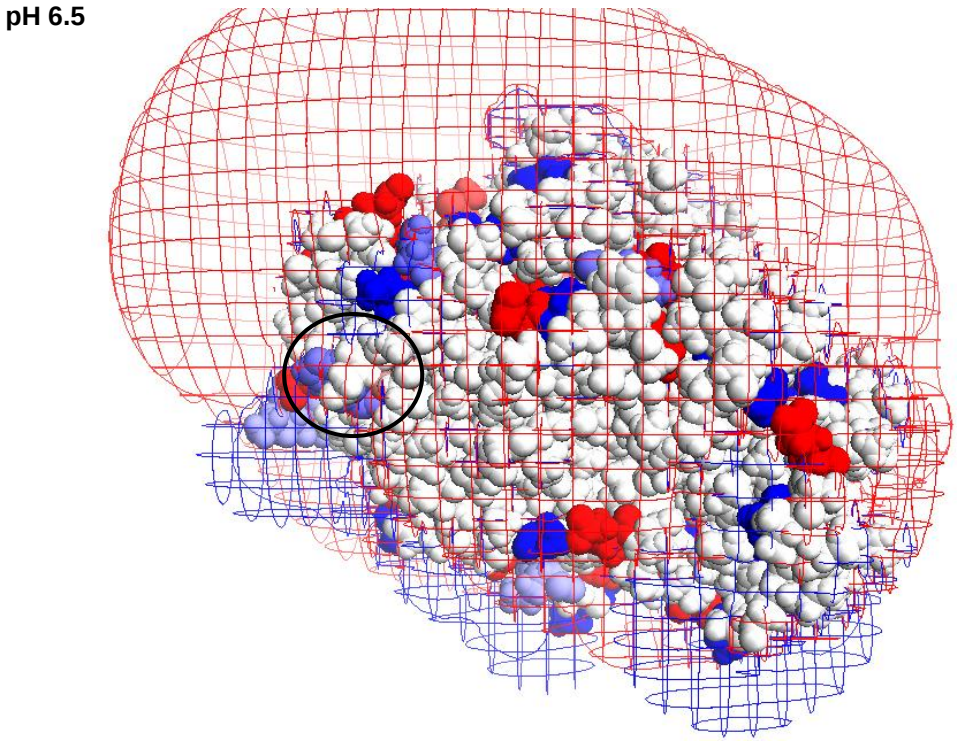

Figure 3.46. Front view of the electrostatic surface of *Tv* laccase at pH 6.5. Charge colour-code is as explained in Figure 3.44. The black circle marks a positive charge region at pH 6.5 that became neutral at pH 7.

pH 7

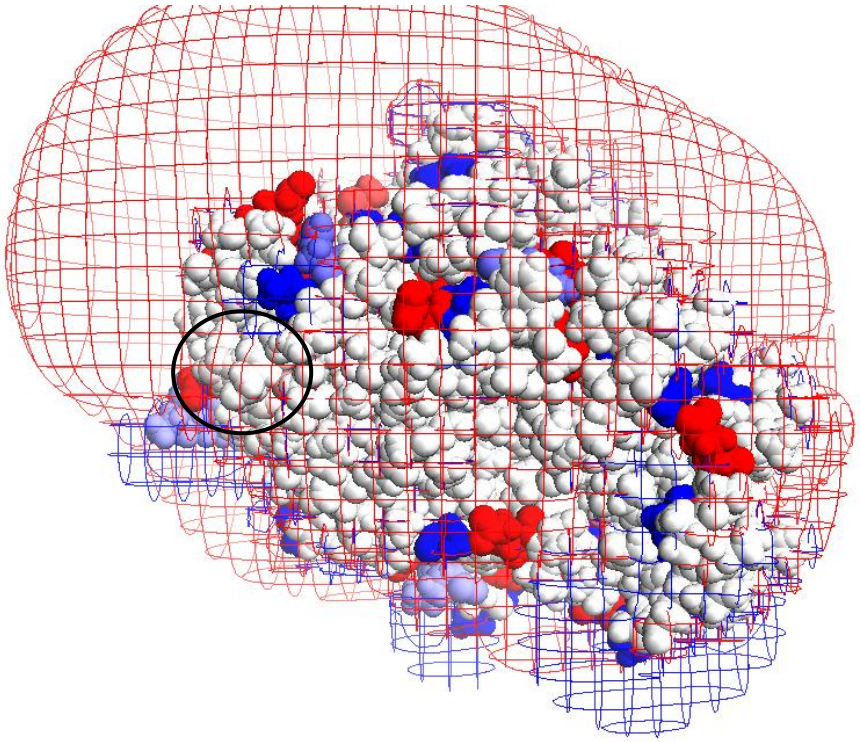

Figure 3.47. Front view of the electrostatic surface of *Tv* laccase at pH 7. Charge colour-code is as explained in Figure 3.44. The black circle marks a positive charge region at pH 6.5 that became neutral at pH 7.

At pH 6.5, Figure 3.46, there were no alterations in the electrostatic pattern of the surface when in comparison with pH 6.

When pH increased to 7, Figure 3.47, the electrostatic surface presented a visual change in the charges. In Figure 3.46 at pH 6.5, a black circle denotes a positive charged area in blue, which was no longer positive but neutral in Figure 3.47 at pH 7. At pH 7 it was also possible to observe that there was a decrease in the blue grid at the left side of the structure that might signify that the positive regions became weaker as pH increased.

pH 7.5

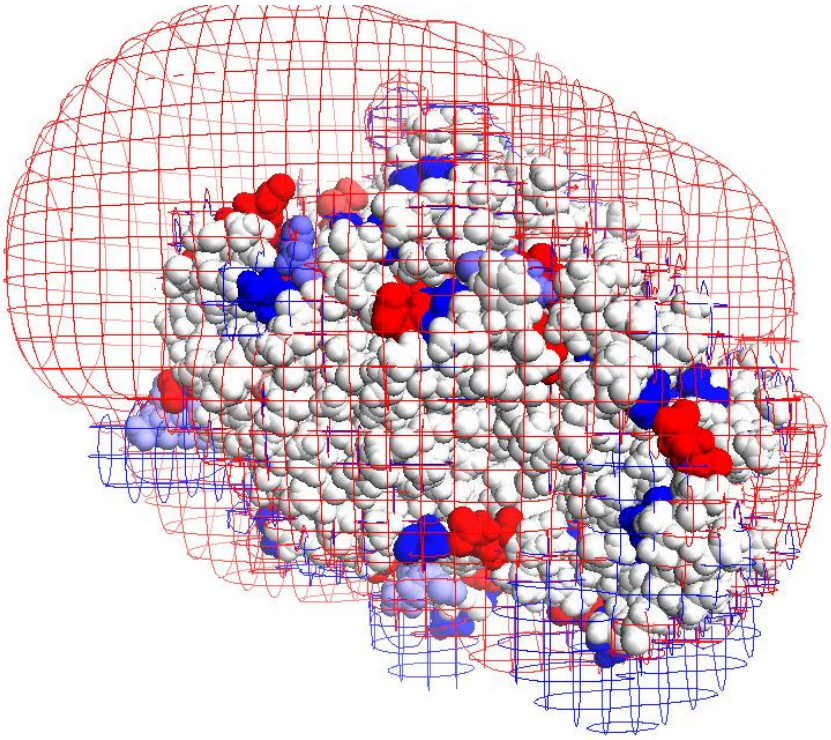

Figure 3.48. Front view of the electrostatic surface of *Tv* laccase at pH 7.5. Charge colour-code is as explained in Figure 3.44**.**

When pH was 7.5, Figure 3.48, the electrostatic surface of the protein did not change from what had been seen at pH 7. The surface remained unaltered as pH changed to 8 and 8.5 (not shown).

3.8.1.2. Lateral view

The lateral view rose from turning the front view of the protein towards left. This view demonstrates a large area of protein that was not able to be seen from the front or back of the protein.

pH 6

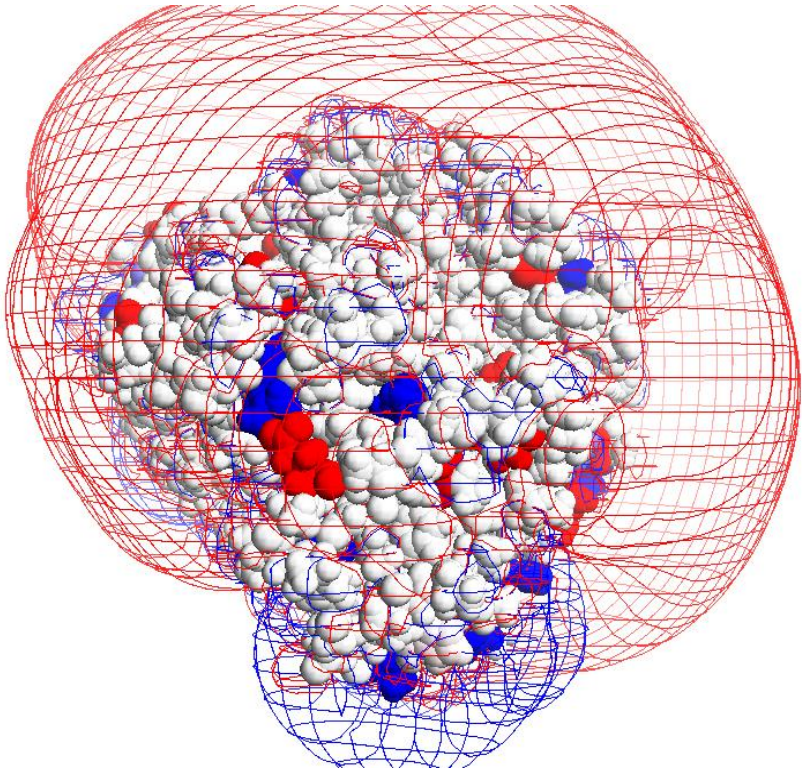

Figure 3.49. Lateral view of the electrostatic surface of *Tv* laccase at pH 6. Charge colour-code is as explained in Figure 3.44**.**

At pH 6 (Figure 3.49), the electrostatic surface of the lateral view showed a similar result to the front view. Positive and negative charges were distributed along the surface.

There were also a few positive areas (blue) that would favour AuNP-CALNN conjugation to form BNCs.

The images of the lateral view at the remaining pH conditions was not show here, because they did not suffer visual changes in the electrostatic surface and remained identical to the structure at pH 6.

3.8.1.3. Back view

The back view is the result of turning the front view of the structure towards left approximately 180 degrees.

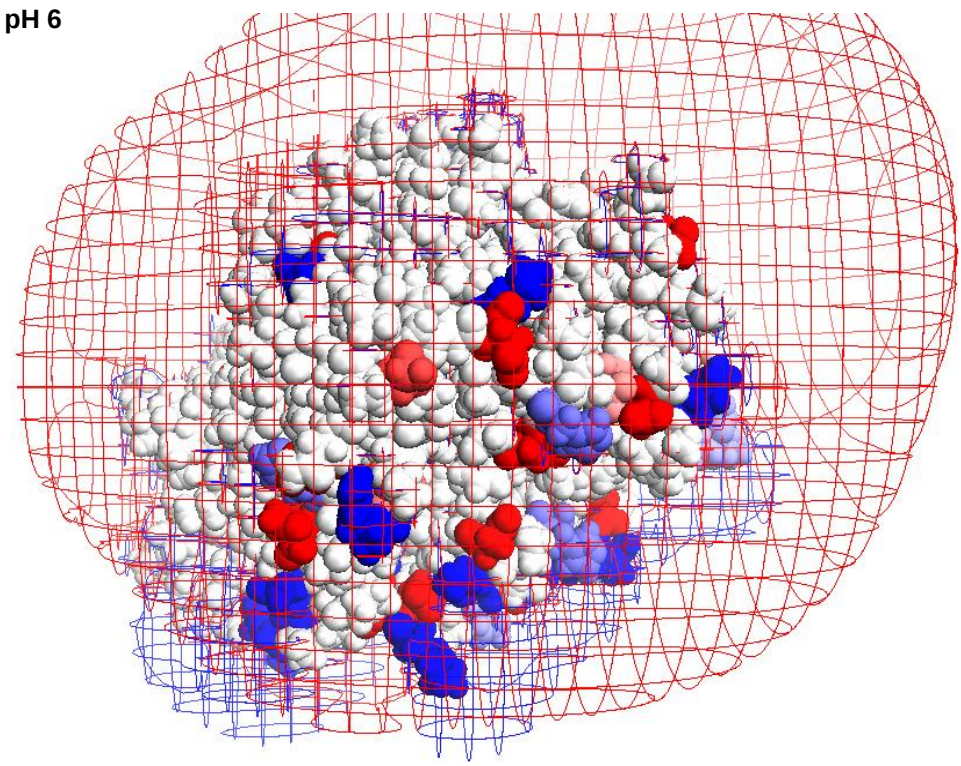

Figure 3.50. Back view of the electrostatic surface of *Tv* laccase at pH 6. Charge colour-code is as explained in Figure 3.44**.**

The back view of the protein at pH 6 (Figure 3.50), demonstrated once more a distribution of negative (red) and positive (blue) charges. There are a few positive residues in this area as well, to which AuNP-CALNN would preferentially bind.

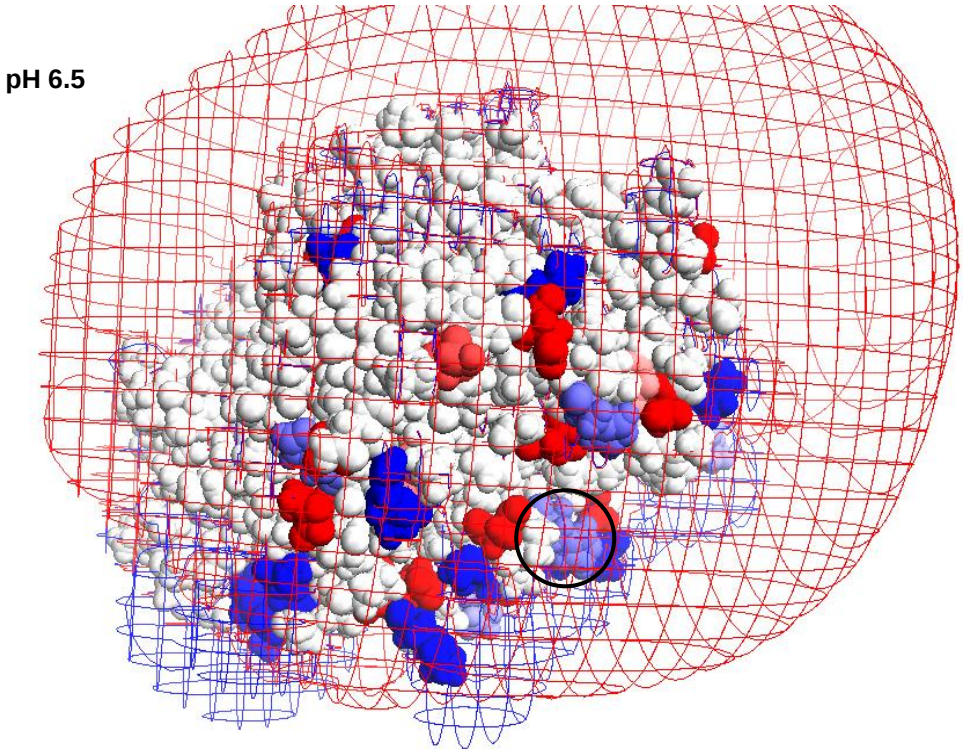

Figure 3.51. Back view of the electrostatic surface of *Tv* laccase at pH 6.5. Charge colour-code is as explained in Figure 3.44**.** The black circle marks a positive charge region at pH 6.5 that became neutral at pH 7.

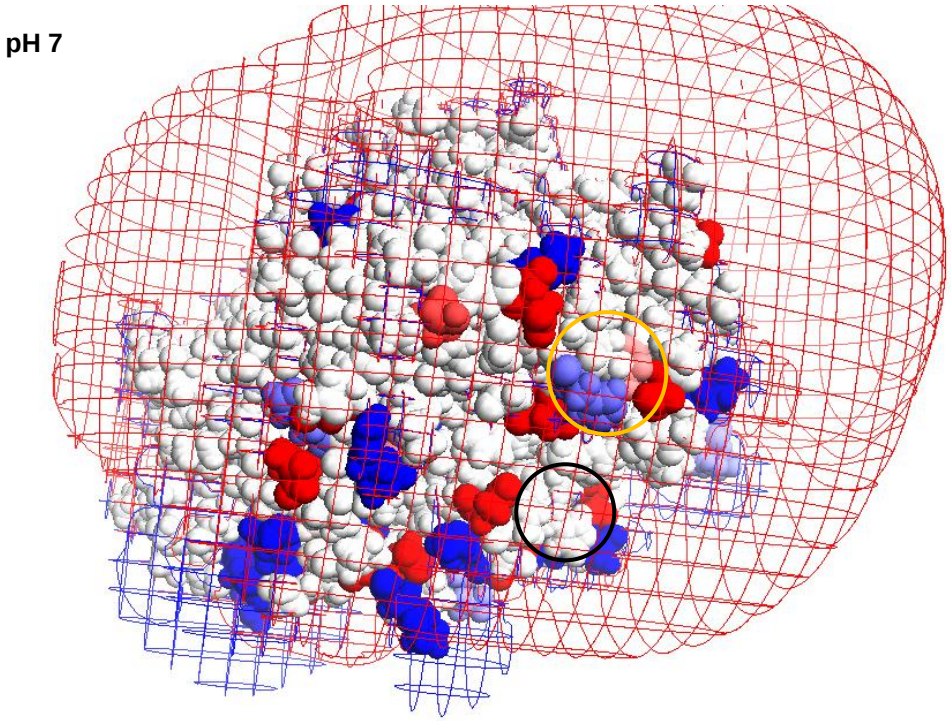

Figure 3.52. Back view of the electrostatic surface of *Tv* laccase at pH 7. Charge colour-code is as explained in Figure 3.44**.** The black circle marks a negative charge region at pH 6.5 that became neutral at pH 7. The yellow circle marks a positive charge region at pH 7 that became neutral at pH 7.5, and a negative region pH 6.5 that became more negative at pH 7.

When pH increased to 6.5, (Figure 3.51), no visual alteration was observed in the charge distribution at the surface of the protein in comparison with pH 6 (Figure 3.50).

However, when pH increased from 6.5 to 7 (Figure 3.52), it resulted in a charge change. In Figure 3.51, the black circle marks a positively charged area. This area became neutrally charged as pH increased to 7, as shown by the black circle in Figure 3.52. At pH 7 it was also possible to observe that the blue grid decreased in area, also seen in the front view at this pH.

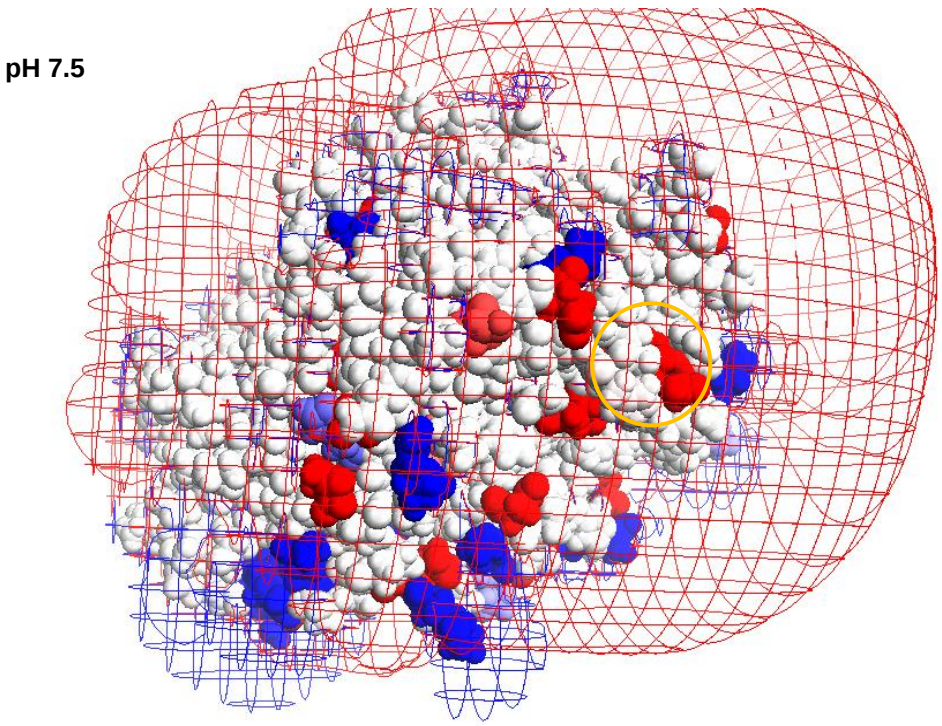

Figure 3.53. Back view of the electrostatic surface of *Tv* laccase at pH 7.5. Charge colour-code is as explained in Figure 3.44**.** The yellow circle marks a positive charge region at pH 7 that became neutral at pH 7.5, and a negative region pH 6.5 that became more negative at pH 7.

Another change occurred when pH changed from 7 (Figure 3.52) to 7.5 (Figure 3.53) and is demonstrated by the yellow circle in both images.

The yellow circle in Figure 3.52 shows a region with both a positive area (blue) and a negative area (light red). When pH increased to 7.5, the positive area became neutral (white), while the light red colour of the positive area became more intense, suggesting the charge in this area increased. At pH 8 and 8.5 (not shown here), the charge distribution in the structure remained identical to the one at pH 7.5.

3.8.2. Active site view

The image of the active site was taken without the side chains visible and at an angle that allowed to visualise the interior of the cavity containing the copper atoms.

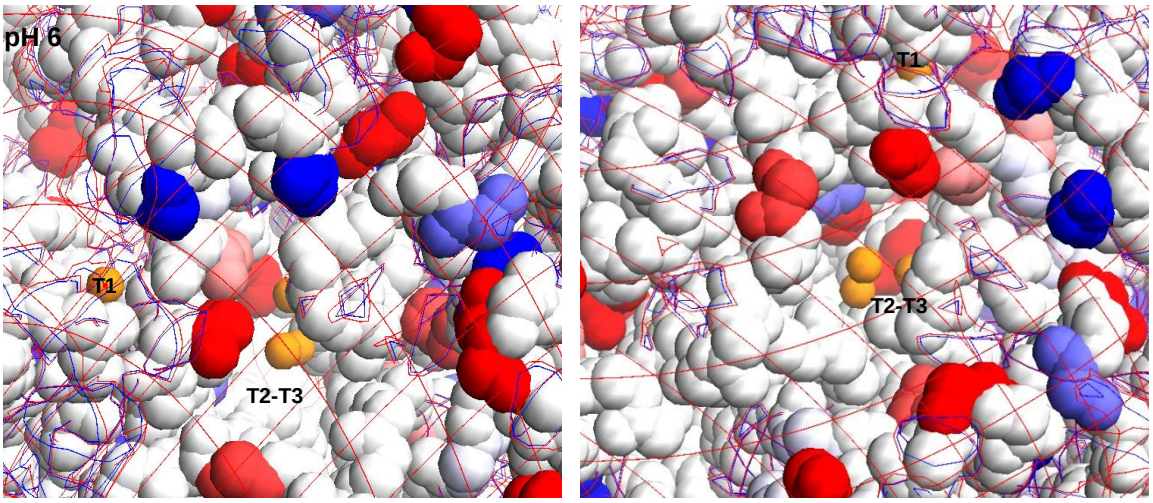

Figure 3.54. Two views from different angles of the active site of *Tv* laccase at pH 6. Charge colour-code is as explained in Figure 3.44. Copper atoms coloured in yellow.

The charge distribution in the active site at pH 6 can be seen in Figure 3.54.

The images revealed that the interior of the cavity, where coppers T1, T2 and T3 reside, is mostly surrounded by negative charges (red). The interior also revealed a small positive charged area (blue) inside the cavity. The predominance of negative charges in the active site has also been reported before[34]. It is thought to be related to the positive radical stabilization during the catalytic cycle[34].

Since it has been stated that the active site of laccases is highly conserved[32], *Rv* laccase active site might have the same charge distribution as *Tv* laccase.

Therefore, with the active site being mainly negative, AuNP-CALNN might not have the tendency to bind to the active site region and possibly cause enzymatic inactivation.

The charge distribution remained unchanged in this region as pH increased and consequently the images were not shown here.

3.8.3. General discussion

The electrostatic surface structures generated showed the charge distribution in the residues as well as the grids generated by Chemera under the conditions tested. The structures revealed a large negative grid (red) in one side of the protein. There was also a small positive grid area closer to the protein's surface on the opposite side of the structure. The smaller blue grid reflects weaker negative charges in the protein in comparison with positive areas. It was also apparent that there was an even distribution of residue charges throughout the protein.

As the pH increased to conditions further away from the *Tv* laccase isoelectric point (3.5[34]), the structure became gradually more negative as some positive residues became neutral and the blue grid reduced in area.

It is necessary to keep in mind that this study was just an approximation to real conditions, since in reality there are more parameters that influence the electrostatic surface. Nonetheless, it was still possible to have an idea of how charges are distributed and where conjugation with negative AuNPs might occur.

Electrostatic conjugation with negative AuNPs (as seen with the zeta potential experiments in section 3.6.1.) and this laccase would have the tendency to occur in the positive regions of the protein. The fact that the enzyme became less positive as pH increased might lead to a decrease in the ability and efficiency of conjugation between AuNPs and laccase.

In the case of *Rv* laccase, the similarity with *Tv* laccase suggest that there might be some level of similarity in charge distribution as well. Yet it is necessary to take into consideration that *Rv* laccase pI is reported to be 8.5[81]. It would be expected that in the pH range in question, there would be more positive charges than negative at the enzyme's surface.

Currently, the only way available to predict *Rv* laccase three-dimensional structure is by using the primary sequence known and perform homology replacement with structures of similar proteins. In the future, when the three-dimensional structure of *Rhus vernicifera* laccase is finally obtained, the same modelling method might be implemented to study its electrostatic surface.

Chapter IV: Conclusion

4.1. Conclusion

The unique proprieties of gold nanoparticles (AuNPs) have made them an ideal material for the immobilization of macromolecules. It was found that AuNPs were able to be used to successfully immobilize enzymes without activity loss and create stable bionanoconjugates (BNCs)[22]. In some cases, AuNPs provided an improvement in the catalytic activity of the enzymes[23]. These BNCs have been used in a wide variety of applications.

In this work, negatively-charged AuNPs were synthesised with the Turkevich method and functionalized independently with the ligands mercaptoundecanoic acid (MUA), and the peptide CALNN. These particles were then used to produce BNCs with the enzyme *Rhus vernicifera* (*Rv*) laccase, in order to study the influence of AuNP conjugation on the stability and activity of the enzyme.

The Turkevich method for the synthesis of AuNPs revealed to be highly reproducible and yielded particles with a maximum absorption around 520 nm as expected. From zeta potential experiments, these particles presented a superficial charge of -19.4 ± 1.05 mV. It was a value less negative than usual due to the time that occurred between the synthesis and this experiment, which might have allowed some level of aggregation to occur. After the synthesis, the particles were functionalized with MUA and CALNN and their UV-Visible spectra showed shifts of 3.9 and 1.9 nm, respectively, indicative of successful functionalization. Stability studies indicated that AuNP-CALNN were stable in the potassium phosphate buffer concentration from 10-100 mM, in the pH range from 6-8.5, and in methanol concentration from 0-0.5%.

Rhus vernicifera laccase solutions were evaluated for purity and composition. Both spectroscopic and SDS-PAGE experiments revealed that the solutions were not pure. SDS-PAGE revealed two bands, one with molecular weight above 96 kDa that was expected for *Rv* laccase, and another with molecular weight slightly above 26 kDa. After a process of separation by ultrafiltration, it could be concluded that the low molecular weight band did not seemed to be related to *Rv* laccase and could simply be a contaminant.

Native-PAGE experiments revealed that laccase had activity when in the presence of syringaldazine as substrate.

DLS studies revealed the hydrodynamic diameter of *Rv* laccase to be 5.65 ± 0.83 nm.

To evaluate the conjugation process between *Rv* laccase and AuNPs, zeta potential and agarose studies were performed. Zeta potential showed that AuNP-MUA aggregated in the presence of *Rv* laccase, therefore these were removed from the posterior experiments. On the other hand, BNCs with AuNP-CALNN were stable and showed an increase in superficial charge as the surface was increasingly covered with enzyme. The ratio [Lac] (μg/mL)/[AuNP-CALNN] (nM) used in the remaining experiments was 8.1 μg/mL of laccase (30 U/mL) to 1 nM AuNP-CALNN.

Agarose gels proved to not be a useful tool for BNC analysis. Additionally, after BNC centrifugation, only approximately 15% of laccase activity was found in the pellet.

Stability studies with syringaldazine (SYR) demonstrated that this substrate was heavily influenced by pH conditions of the medium. However, the quinone product from the reaction between laccase and SYR was stable under the pH range 6-8.5. With this in mind, a strategy to observe both the consumption of SYR and the formation of product was designed.

Rhus vernicifera laccase optimal activity for product formation was found at pH 7.5 and the BNCs produced were stable at pH 6-8.5. The kinetic experiments were performed with these BNCs in the same pH range and the results were compared with free laccase in the same conditions.

Kinetic studies were also performed with laccase conjugated with AuNP-CALNN through EDC/NHS cross-linking agent. The results showed high error in one of the enzymatic parameters (k_M). In the conditions tested, electrostatic conjugation occurred while conjugation with the cross-linking and its effects on laccase activity could not be proven. In certain situations, successful electrostatic conjugation might be preferential over chemical conjugation. Although it has advantages, the use of a cross-linking agent increments the conjugation procedure, can pose problems in protein orientation and adds additional costs to the process[93].

The kinetic results of laccase electrostatically adsorbed to AuNP-CALNN with less error, and therefore more reliable, were the ones obtained for product formation. In this case, at pH 6 laccase catalytic efficiency in the BNCs decreased 38% in comparison to free laccase. At pH 6.5 and 8.5 the catalytic efficiency was similar to the one of free laccase. The efficiency increased 67.27 % at pH 7, and approximately 100% at pH 7.5. At pH 8, the catalytic efficiency increased 29.98%.

These were very encouraging results with the exception of pH 6. In the other pH values there was either no significant negative influence or there was favourable influence from AuNPs conjugation on laccase activity. In cases where no improvements to laccase activity are necessary and laccase only needs to be immobilized to facilitate its removal from the media and be recycled, it is possible to do so in the pH range from 6.5 to 8.5.

Alternatively, if it is necessary to use laccase with higher efficiency to degrade phenol compounds, it is possible to immobilize the enzyme in stable AuNP-CALNN, in favourable pH conditions from 7 to 8.

Laccases have already shown to be cost-efficient in industrial applications[94,95]. Combining the already efficient capacities of laccase and the beneficial process of immobilization in AuNPs can benefit several industrial processes where free laccase is already implemented. In textile industry cotton bleaching is an important process[94,95]. Generally this process is carried out in alkaline conditions with hydrogen peroxide and high temperatures, but this leads to fabric damage and water waste to remove chemicals[94]. Laccases are able to replace chemicals and decrease damage to the fabric[94]. With low concentrations of this enzyme, the conditions of the process can be less aggressive. Enzyme immobilization also provides an additional step towards improving other industrial processes. When immobilized, the enzyme can be recycled and the production costs can decrease even further. This work showed that laccase can be successfully immobilized in AuNPs retaining or even improving catalytic efficiency at neutral and

alkaline pH. This laccase-AuNP-CALNN system might be a suitable option to render processes in delignification, waste water decontamination or wine clarification 'green' and even more cost-efficient.

The computational modelling of the electrostatic surface of a laccase with similarity with *Rv* laccase, showed that in the pH range in question, there was an homogeneous distribution of negative and positive charges in the surface. Positive charges are preferential for conjugation with AuNP-CALNN, but as pH increased some positive charged residues became neutral. It was possible to conclude that as the medium conditions become more alkaline, there might be a decrease in the efficiency of electrostatic conjugation between negative AuNPs and laccase. In the future, when *Rv* laccase's three-dimensional structure is available, it will be possible to understand in more detail how negative AuNPs interact with the enzyme surface, and possibly inferring how enzyme activity can be influenced.

References

1. Goodsell, D.S. *Bionanotechnology: Lessons from Nature*. 1-8 (Wiley-Liss Inc.: 2004).

2. Chan, W.C.W. Bionanotechnology progress and advances. *Biology of blood and marrow transplantation: journal of the American Society for Blood and Marrow Transplantation* **12**, 87-91 (2006).

3. Liz-marza, L.M. Tailoring Surface Plasmons through the Morphology and Assembly of Metal Nanoparticles. *Langmuir* 32-41 (2006).

4. Song, J.Y., Jang, H.-kyeong & Kim, B.S. Biological synthesis of gold nanoparticles using Magnolia kobus and Diopyros kaki leaf extracts. *Process Biochemistry* **44**, 1133-1138 (2009).

5. Kurniawan, F. New Analytical Applications of Gold Nanoparticles. (2008).

6. Turkevich, J., Stevenson, P., Hillier, J. A study of the nucleation and growth processed in the synthesis of colloidal gold. (1951).

7. Kimling, J. *et al.* Turkevich method for gold nanoparticle synthesis revisited. *The journal of physical chemistry. B* **110**, 15700-7 (2006).

8. Pedro V. Baptista, Maria Koziol-Montewka, J.P.-O., Doria, G. & Franco, R. Gold-nanoparticle-probe Based. *Clinical Chemistry* **52**, 1433-1434 (2006).

9. Doak, J., Gupta, R.K., Manivannan, K., Ghosh, K. & Kahol, P.K. Effect of particle size distributions on absorbance spectra of gold nanoparticles. *Physica E: Low-dimensional Systems and Nanostructures* **42**, 1605-1609 (2010).

10. Yang, Y., Matsubara, S., Nogami, M. & Shi, J. Controlling the aggregation behavior of gold nanoparticles. *Materials Science and Engineering: B* **140**, 172-176 (2007).

11. Lee, H., Lee, K., Kim, I.K. & Park, T.G. Synthesis, characterization, and in vivo diagnostic applications of hyaluronic acid immobilized gold nanoprobes. *Biomaterials* **29**, 4709-18 (2008).

12. Baptista, P.V. *et al. Nanoparticles in molecular diagnostics. Progress in molecular biology and translational science* **104**, 427-88 (2011).

13. Hussain, I., Nichols, R.J., Schiffrin, D.J., Brust, M. & Fernig, D.G. Rational and Combinatorial Design of Peptide Capping Ligands for Gold Nanoparticles. *J. Am. Chem. Soc.* 10076-10084 (2004).

14. Lee, Z. *et al.* Direct Imaging of Soft-Hard Interfaces Enabled by Graphene. *Nanoletters* **9**, 3365-3369 (2009).

15. Aubin-Tam, M.-E. & Hamad-Schifferli, K. Structure and function of nanoparticle-protein conjugates. *Biomedical materials (Bristol, England)* **3**, 034001 (2008).

16. Katz, E. & Willner, I. Integrated Nanoparticle – Biomolecule Hybrid Systems : Synthesis , Properties , and Applications Angewandte. *Angewandte Chemie* 6042-6108 (2004).doi:10.1002/anie.200400651

17. Petkova, G. a, Zaruba, K., Zvatora, P. & Kral, V. Gold and silver nanoparticles for biomolecule immobilization and enzymatic catalysis. *Nanoscale research letters* **7**, 287 (2012).

18. Xie, T. *et al.* Recent advance in the support and technology used in enzyme immobilization. *African Journal of Biotechnology* **8**, 4724-4733 (2009).

19. Luthuli, D.S. Analysis of the effects of Gold nanoparticles on the functional integrity of select serum proteins and heat shock proteins of By. (2012).

20. Ardao, I., Comenge, J., Benaiges, M.D., Álvaro, G. & Puntes, V.F. Rational nanoconjugation improves biocatalytic performance of enzymes: aldol addition catalyzed by immobilized rhamnulose-1-phosphate aldolase. *Langmuir : the ACS journal of surfaces and colloids* **28**, 6461-7 (2012).

21. Vidotti, M., Carvalhal, R.F., Mendes, R.K., Ferreira, D.C.M. & Kubota, L.T. Biosensors based on gold nanostructures. *Journal of the Brazilian Chemical Society* **22**, 3-20 (2011).

22. Tiwari, P.M., Vig, K., Dennis, V. a. & Singh, S.R. Functionalized Gold Nanoparticles and Their Biomedical Applications. *Nanomaterials* **1**, 31-63 (2011).

23. Lv, M. Preparative Biochemistry and Biotechnology Trypsin-Gold Nanoparticle Conjugates : Binding , Enzymatic Activity , and Stability. *Preparative Biochemistry and Biotechnology* **39**, 429-438 (2009).

24. Cortez, J. *et al.* Bionanoconjugates of tyrosinase and peptide-derivatised gold nanoparticles for biosensing of phenolic compounds. *Journal of Nanoparticle Research* **13**, 1101-1113 (2010).

25. Pingarron, J., Yanez-Sedeno, P., Gonzalez-Cortes, A. Gold nanoparticle-based electrochemical biosensors. *Electrochimica Acta* **53**, 5848-5866 (2008).

26. Ghosh, P., Han, G., De, M., Kim, C.K. & Rotello, V.M. Gold nanoparticles in delivery applications. **60**, 1307-1315 (2008).

27. Ambrosi, A., Airò, F. & Merkoçi, A. Enhanced gold nanoparticle based ELISA for a breast cancer biomarker. *Analytical chemistry* **82**, 1151-6 (2010).

28. Madhavi, V. & Lele, S.S. Laccase: properties and applications. *Bioresources* **4**, 1694-1717 (2009).

29. Riva, S. Laccases: blue enzymes for green chemistry. *Trends in biotechnology* **24**, 219-26 (2006).

30. Benfield, G., Bocks, S.M., Bromley, K. & Brown, B.R. Studies in fungal and plant laccases. *Phytochemistry* **3**, 79-88 (1964).

31. Yaropolov, A.I. & Ko, I.O.V.S. Laccase properties , catalytic mechanism , and applicability. *Applied Biochemistry and Biotechnology* **49**, (1994).

32. Alcalde, M. Laccases: Biological functions, molecular structure and industrial applications. *Industrial Enzymes* 461-476 (2007).

33. Huang, H., Zoppellaro, G. & Sakurai, T. Spectroscopic and kinetic studies on the oxygen-centered radical formed during the four-electron reduction process of dioxygen by Rhus vernicifera laccase. *The Journal of biological chemistry* **274**, 32718-24 (1999).

34. Piontek, K., Antorini, M. & Choinowski, T. Crystal structure of a laccase from the fungus Trametes versicolor at 1.90-A resolution containing a full complement of coppers. *The Journal of biological chemistry* **277**, 37663-9 (2002).

35. Chimera. *Accessed January 14, 2011* at <http://www.cgl.ucsf.edu/chimera/>

36. Nitta, K., Kataoka, K. & Sakurai, T. Primary structure of a Japanese lacquer tree laccase as a prototype enzyme of multicopper oxidases. *Journal of inorganic biochemistry* **91**, 125-31 (2002).

37. Torres-pacheco, I., Octavio, L.C. & Guanajuato, C. Laccases. **661**, 323-340 (2006).

38. Kunamneni, A., Plou, F.J., Ballesteros, A. & Alcalde, M. Laccases and their applications: a patent review. *Recent patents on biotechnology* **2**, 10-24 (2008).

39. Fernández-Fernández, M., Sanromán, M.Á. & Moldes, D. Recent developments and applications of immobilized laccase. *Biotechnology advances* (2012).doi:10.1016/j.biotechadv.2012.02.013

40. Ullah, M.A., Bedford, C.T. & Evans, C.S. Reactions of pentachlorophenol with laccase from Coriolus versicolor. *Appl. Microbiol Biotechnol.* **53**, 230-4 (2000).

41. Larsson, S., Cassland, P., Jönsson, L.J. & Jo, L.J. Development of a Saccharomyces cerevisiae Strain with Enhanced Resistance to Phenolic Fermentation Inhibitors in Lignocellulose Hydrolysates by Heterologous Expression of Laccase. *Appl. Environ. Microbiol.* **67**, 1163-1170 (2001).

42. Dagys, M. *et al.* Laccase–gold nanoparticle assisted bioelectrocatalytic reduction of oxygen. *Electrochemistry Communications* **12**, 933-935 (2010).

43. Faramarzi, M.A. & Forootanfar, H. Biosynthesis and characterization of gold nanoparticles produced by laccase from Paraconiothyrium variabile. *Colloids and surfaces. B, Biointerfaces* **87**, 23-7 (2011).

44. Babu, P.R., Pinnamaneni, R. & Koona, S. Occurrences , Physical and Biochemical Properties of Laccase. *Universal Journal of Environmental Research and Technology* **2**, 1-13 (2012).

45. Yun-Yang, W. *et al.* Purification and characterization of hydrosoluble components from the sap of Chinese lacquer tree Rhus vernicifera. *International Journal of Biological Macromolecules* **38**, 232-240 (2006).

46. Lu, R. & Miyakoshi, T. Studies on acetone powder and purified rhus laccase immobilized on zirconium chloride for oxidation of phenols. *Enzyme research* 375309 (2012).doi:10.1155/2012/375309

47. Shiba, T., Xiao, L., Miyakoshi, T. & Chen, C. Oxidation of isoeugenol and coniferyl alcohol catalyzed by laccases isolated from Rhus vernicifera Stokes and Pycnoporus coccineus. *Journal of Molecular Catalysis* 7-12 (2000).

48. Frasconi, M., Favero, G., Boer, H., Koivula, A. & Mazzei, F. Kinetic and biochemical properties of high and low redox potential laccases from fungal and plant origin. *Biochimica et biophysica acta* **1804**, 899-908 (2010).

49. Berg, J., Tymoczko, J. & Stryer, L. *Biochemistry*.

50. Michaelis, L., Menten, M.L., Johnson, K. a & Goody, R.S. The original Michaelis constant: translation of the 1913 Michaelis-Menten paper. *Biochemistry* **50**, 8264-9 (2011).

51. UCSF, Z.- http://zinc.docking.org/substance/2166843. *Accessed in June 15, 2012*

52. Harkin, J. & Obst, J. Syringaldazine, an Effective Reagent for Detecting Laccase and Peroxidase in Fungi. *Experimentia* **2**, 381-387 (1973).

53. Prasetyo, E.N., Willibald, W., Nyanhongo, G.S. & Guebitz, G.M. A unique two-way approach for the validation of total antioxidant capacity of serum samples. *European journal of clinical investigation* **42**, 432-8 (2012).

54. Bauer, R. & Rupe, C. Use of Syringaldazine in a Photometric Method for Estimating " Free " Chlorine in Water. *Analytical Chemistry* **43**, 421-425 (1971).

55. Nugroho Prasetyo, E. *et al.* Laccase-generated tetramethoxy azobismethylene quinone (TMAMQ) as a tool for antioxidant activity measurement. *Food Chemistry* **118**, 437-444 (2010).

56. Michota-Kaminska, A., Wrzosek, B. & Bukowska, J. Resonance Raman evidence of immobilization of laccase on self-assembled monolayers of thiols on Ag and Au surfaces. *Applied spectroscopy* **60**, 752-7 (2006).

57. Jans, H., Liu, X., Austin, L., Maes, G. & Huo, Q. Dynamic light scattering as a powerful tool for gold nanoparticle bioconjugation and biomolecular binding studies. *Analytical chemistry* **81**, 9425-32 (2009).

58. Light, Q.-elastic & Bloomfieldl, V.A. Quasi-Elastic Light Scattering applications in biochemistry and biology. *Ann. Rev. Biophys. Bioeng* **10**, 421-50 (1981).

59. Dynamic Light Scattering: An Introduction in 30 Minutes. *Malvern Instruments* 1-8

60. Zeta Potential theory. *Zetasizer nanoseries* 16.1-16-5

61. Zeta Potential: An Introduction in 30 Minutes. *Malvern Instruments* **2**, 1-6

62. Dror, R.O., Dirks, R.M., Grossman, J.P., Xu, H. & Shaw, D.E. Biomolecular Simulation: A Computational Microscope for Molecular Biology. *Annual Review of Biophysics* **41**, 429-452 (2012).

63. Luscombe, N.M., Greenbaum, D. & Gerstein, M. What is bioinformatics? An introdutions and review. *Yearbook of medical informatics* 83-100 (2001).

64. National Center for Biotechnilogy Information. *Accessed June - July 2012* at <http://www.ncbi.nlm.nih.gov/>

65. Protein Data Bank. *Accessed April 10, 2012* at <http://www.rcsb.org/pdb/home/home.do>

66. Kukić, P. & Nielsen, J.E. Electrostatics in proteins and protein-ligand complexes. *Future medicinal chemistry* **2**, 647-66 (2010).

67. Tech., V. H ++ Web-based computational prediction of protonation states of and pKa ionizable groups in macromolecules. *Accessed in June 10, 2012* at <http://biophysics.cs.vt.edu/>

68. Krippahl, L. Chemera. *Accessed in June, 2012* (2007).at <http://centria.fct.unl.pt/~ludi/chemera/index.html>

69. Haiss, W., Thanh, N.T.K., Aveyard, J. & Fernig, D.G. Determination of size and concentration of gold nanoparticles from UV-vis spectra. *Analytical chemistry* **79**, 4215-21 (2007).

70. Loureiro, C. Preparação de nanopartículas metálicas funcionalizadas com péptidos para aplicações em biossensores. (2011).

71. Sigma-Aldrich Enzymatic assay of laccase. *Accessed in November 2011 - June 2012* at <http://www.sigmaaldrich.com/technical-documents/protocols/biology/enzymatic-assay-of-laccase.html>

72. Thermo Scientific BCA Protein Assay. *Accessed June 20, 2012* at <http://www.piercenet.com/browse.cfm?fldID=02020101>

73. Rasband, W.S. ImageJ. at <http://imagej.nih.gov/ij/>

74. Image J Gels tutorial. at <http://rsbweb.nih.gov/ij/docs/menus/analyze.html#gels>

75. Krippahl, L. Chemera tutorial.

76. Gomes, I., Santos, N.C., Oliveira, M.A., Quintas, A. & Eaton, P. Probing Surface Properties of Cytochrome c at Au Bionanoconjugates. *J. Phys. Chem. C* 16340-16347 (2008).

77. Cavadas, M. Gold nanoparticle to antibody conjugates for diagnosis applications : molecular interactions and immunoassay development. (2011).

78. Eisenthal, R. & Danson, M. *Enzyme Assays*. (Oxford University Press: 2002).

79. Casella, L. *et al.* Enzymatic and spectroscopic studies on the activation or inhibition effects by substituted phenolic compounds in the oxidation of aryldiamines and catechols catalyzed by Rhus vernicifera laccase. *Journal of inorganic biochemistry* **100**, 2127-39 (2006).

80. Dwivedi, U.N., Singh, P., Pandey, V.P. & Kumar, A. Structure–function relationship among bacterial, fungal and plant laccases. *Journal of Molecular Catalysis B: Enzymatic* **68**, 117-128 (2011).

81. Martin, L. *Studies for the Prevention of Red Wine Browning – development of a molecular control for the Copper Enzyme laccase*. 1-27 (2001).

82. Biosciences, A. *Protein electrophoresis - Technical manual*.

83. Pereira, C.B. *et al.* Evaluation of laccases and melanization in clinical and environmental Cryptococcus neoformans samples by non-denaturing PAGE. *Journal of medical microbiology* **58**, 563-6 (2009).

84. Malvern Instruments Calculating distributions from DLS data (PDF). **di**, 1-4

85. Malvern Instruments *Zetasizer Nano series: Size theory*. 14.5 (Malvern Instruments:).

86. Klis, M. *et al.* Electroreduction of laccase covalently bound to organothiol monolayers on gold electrodes. *Electrochimica Acta* **52**, 5591-5598 (2007).

87. J.E.T. Andersen, M. Hallberg Jensen, P. Moller, J.U. No Title. *Electrochimica Acta* **41**, (1996).

88. Hanauer, M., Pierrat, S., Zins, I., Lotz, A. & Sönnichsen, C. Separation of nanoparticles by gel electrophoresis according to size and shape. *Nano letters* **7**, 2881-5 (2007).

89. George, E. & Marquis, J.K. *Enzymatic desulfurization of coal*. (1988).

90. Harp, D. Current Technology of Chlorine Analysis for Water and Wastewater. *Technical Information Series* (2002).

91. Hapiot, P., Jean, P., Neta, P. & Rolando, C. Electrochemical behavior of syringaldazine, a colorimetric redox agent. *Journal of Electroanalytical Chemistry* **353**, 255-235 (1993).

92. Dixon, M. & Webb, E.C. *Enzymes*. (Academic Press, Inc.: NY, 1975).

93. Ijeh, M. Covalent gold nanoparticle — antibody conjugates for sensitivity improvement in LFIA. (2011).

94. Couto, S.R. & Toca-herrera, J.L. Lacasses in the textile industry. **1**, 115-120 (2006).

95. Rodríguez Couto, S. & Toca Herrera, J.L. Industrial and biotechnological applications of laccases: a review. *Biotechnology advances* **24**, 500-13 (2006).

5. Appendix

I.

Enzymatic Assay of LACCASE
(EC 1.10.3.2)

PRINCIPLE:

Syringaldazine + O_2 + $\xrightarrow{\text{Laccase}}$ Oxidized Syringaldazine + $2H_2O$

CONDITIONS: T = 30°C, pH = 6.5, A_{530nm}, Light path = 1 cm

METHOD: Continuous Spectrophotometric Rate Determination

REAGENTS:

A. 100 mM Potassium Phosphate Buffer, pH 6.5 at 30°C
(Prepare 100 ml in deionized water using Potassium Phosphate, Monobasic, Anhydrous, Sigma Prod. No. P-5379. Adjust to pH 6.5 at 30°C with 1 M KOH.)

B. 0.216 mM Syringaldazine Solution
(Prepare 3 ml in absolute methanol using Syringaldazine, Sigma Prod. No. S-7896.)

C. Laccase Enzyme Solution
(Immediately before use, prepare a solution containing 25 - 50 units/ml of Laccase in cold deionized water.)

PROCEDURE:

Pipette (in milliliters) the following reagents into suitable cuvettes:

	Test	Blank
Deionized Water	------	0.50
Reagent A (Buffer)	2.20	2.20
Reagent C (Enzyme Solution)	0.50	------

Equilibrate to 30°C. Monitor the A_{530nm} until constant, using a suitably thermostatted spectrophotometer. Then add:

Reagent B (Syringaldazine)	0.30	0.30

PROCEDURE: (continued)

Immediately mix by inversion and record the increase in A_{530nm} for approximately 10 minutes. Obtain the $\triangle A_{530nm}$/minute using the maximum linear rate for both the Test and Blank.

CALCULATIONS:

$$\text{Units/ml enzyme} = \frac{(\triangle A_{530nm}/\text{min Test} - r\ A_{530nm}/\text{min Blank})(df)}{(0.001)(0.5)}$$

df = Dilution factor
0.001 = The change in A_{530nm}/minute per unit of Laccase at pH 6.5 at 30°C in a 3 ml reaction mix
0.5 = Volume (in milliliter) of enzyme used

$$\text{Units/mg solid} = \frac{\text{units/ml enzyme}}{\text{mg solid/ml enzyme}}$$

UNIT DEFINITION:

One unit will produce a $?A_{530nm}$ of 0.001 per minute at pH 6.5 at 30°C in a 3 ml reaction volume using syringaldazine as substrate.

FINAL ASSAY CONCENTRATION:

In a 3 ml reaction mix, the final concentrations are 73 mM potassium phosphate, 0.02 mM syringaldazine, 10% methanol, and 12.5 - 25.0 units laccase.

REFERENCES:

Ride, J.P. (1980) *Physiological Plant Pathology* **16**, 187-196

NOTES:

1. This assay is based on the cited reference.

II.

Compositions of some of the solutions used in the experimental procedures:

PBS: 100 mM potassium phosphate buffer and 50 mM NaCl

SDS-PAGE Running Buffer: 0.02 M trizma base, 0.19 M glycine and 10% SDS

Destaining solution: 40% methanol and 7% acetic acid

III.

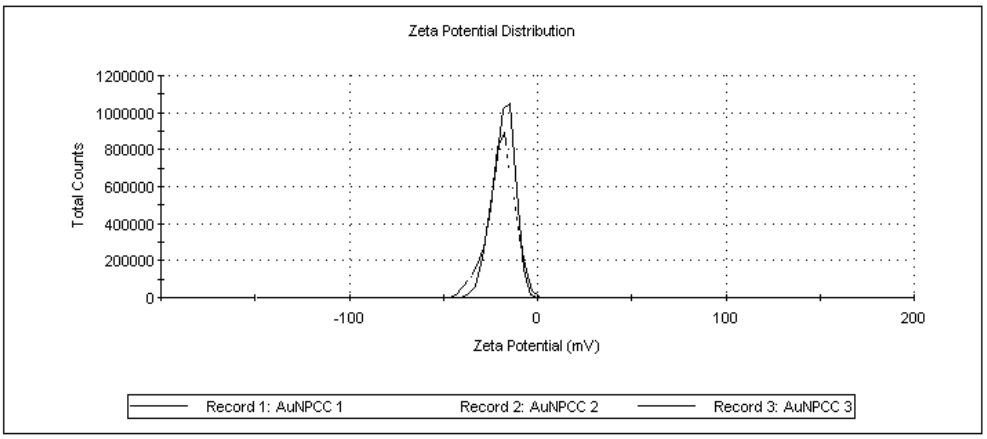

Figure 5.1. Graphical representation of the zeta potential distribution from three measurements of AuNP-Citrate acquired using the dynamic light scattering technique

IV.

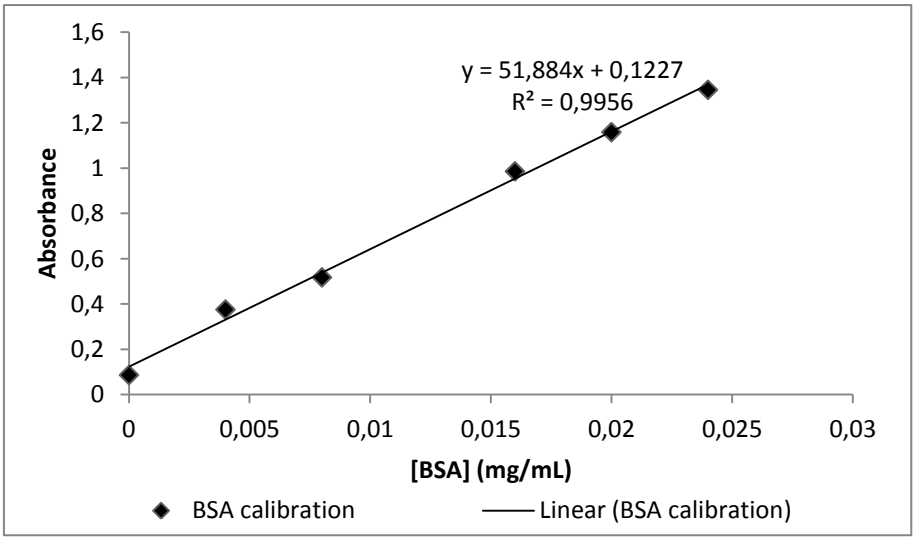

Figure 5.2. BSA calibration curve used to calculate the total protein concentration of two *Rv laccase* solution batches.

Table 5.1. Average absorbance values and respective dilution factors obtained for two *Rv laccase* solution batches and the concentration calculated from the equation in Figure 5.2.

Laccase sample	Average abs	Dilution factor (times)	Concentration (µg/mL)
1	0.320	20	76.054
2	0.311	20	72.457

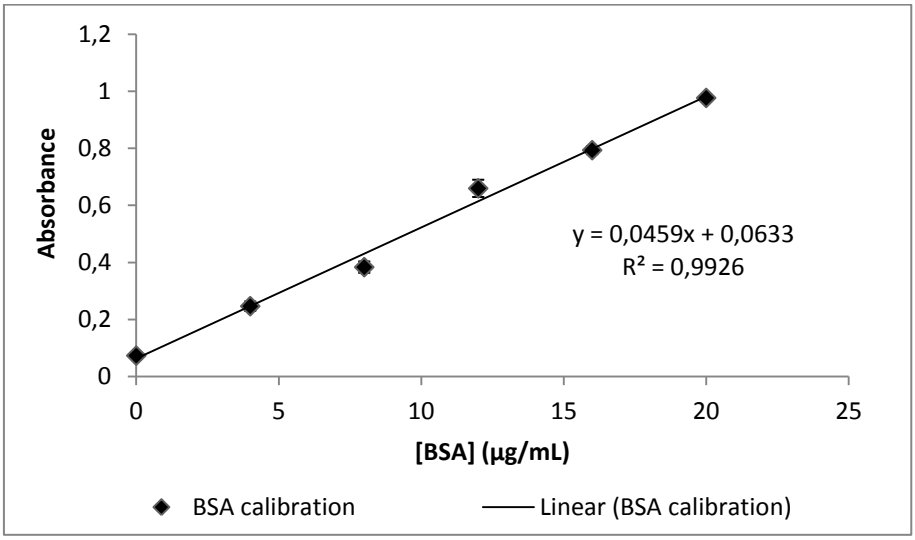

Figure 5.3. BSA calibration curve used to calculate the total protein concentration of the *Rv laccase* samples centrifuged in the 100 K and 10 K ultrafiltration devices.

Table 5.2. Average absorbance values and respective dilution factors obtained for the samples centrifuged in the 100 K and 10 K ultrafiltration devices and the concentration calculated from the equation in Figure 5.3.

Membrane pore (kDA)	Average Abs	Dilution factor (times)	Concentration (mg/mL)
10	0.432	200	1.608
100	0.274	100	0.459

V.

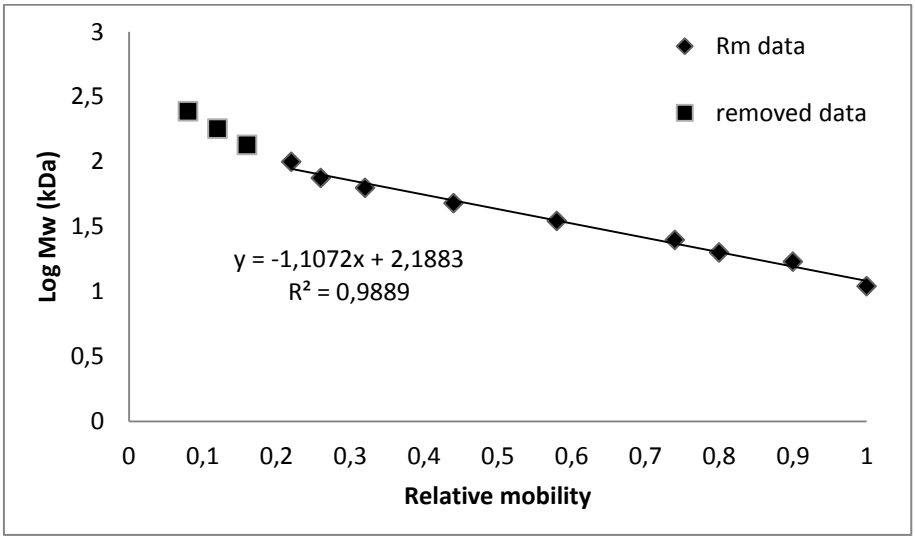

Figure 5.4. Calibration curve built with the relative mobility of the Protein II standard of low and high molecular weight proteins purchased from NZYTech.

VI.

a)

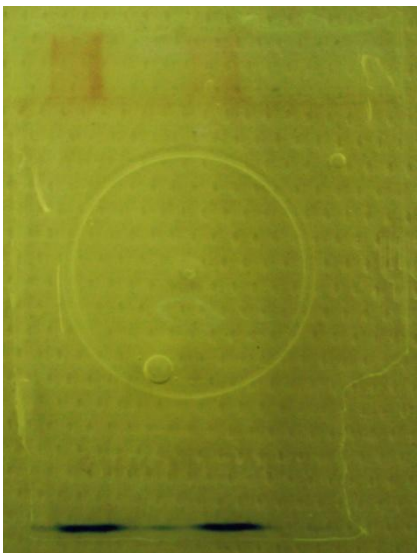

b)

Figure 5.5. a) Image of a native-PAGE gel performed at 180 V for one hour and stained for laccase activity with 1mM syringaldazine; **b)** Image of a native-PAGE gel performed at 75 V for three hour and stained for laccase activity with 1mM syringaldazine.

VII.

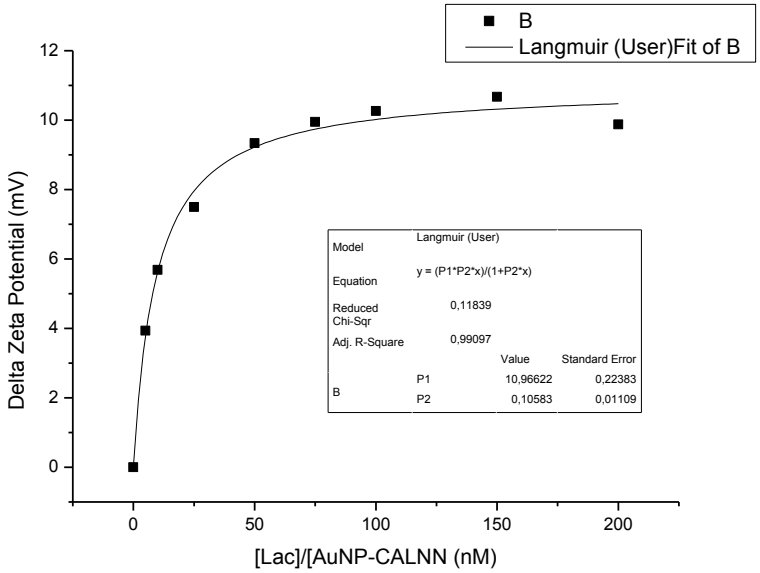

Figure 5.6. Graphical representation of the zeta potential variation values obtained for 1 nM AuNP-CALNN with increasing concentrations of laccase adsorbed to the surface. Table inset shows the data obtained with the fitting

VIII.

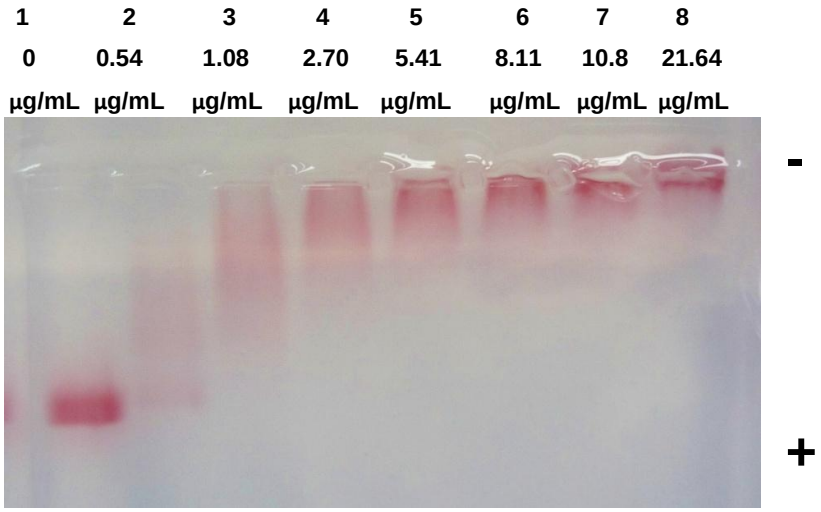

Figure 5.7. Image of a 0.5% agarose gel of BNC-CALNN with 1 nM AuNP-CALNN and increasing amounts of *Rv* laccase cross-linked to AuNPs. Above each lane is the concentration of laccase used. Gel performed at 75 V for 30 minutes.

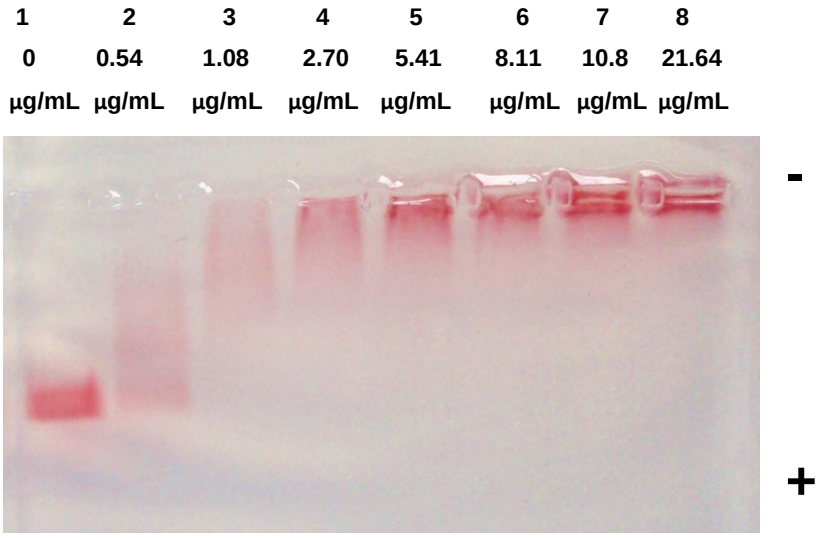

Figure 5.8. Image of a 0.5% agarose gel of BNC-CALNN with 1 nM AuNP-CALNN and increasing amounts of *Rv* laccase cross-linked to AuNPs. Above each lane is the concentration of laccase used. Gel performed at 100 V for 30 minutes.

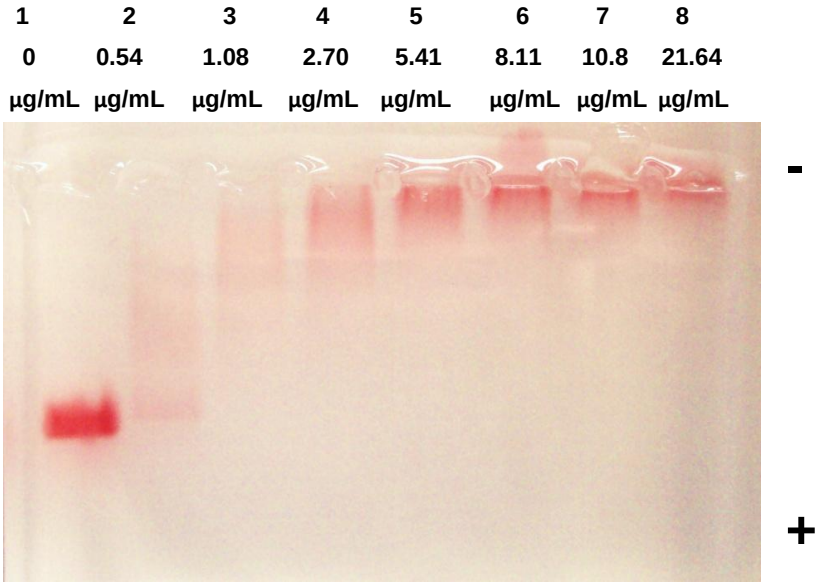

Figure 5.9. Image of a 0.5% agarose gel of BNC-CALNN with 1 nM AuNP-CALNN and increasing amounts of *Rv* laccase cross-linked to AuNPs. Above each lane is the concentration of laccase used. Gel performed at 150 V for 30 minutes.

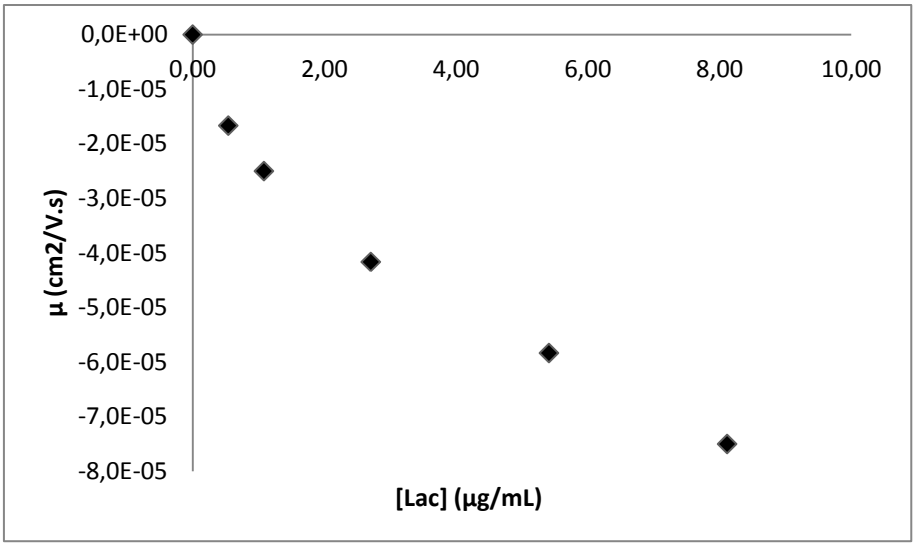

Figure 5.10. Graphical representation of the electrophoretic mobility from the bands in the gel in Figure 3.18.

IX.

Table 5.3. Michaelis-Menten parameters obtained for the reaction of SYR consumption of laccase conjugated with AuNP-CALNN with EDC/NHS. The errors were generated by the software Origin from the fitting of the Michaelis-Menten equation.

Substrate consumption						
pH	**V_M (min^{-1})**	**error**	**K_M (μM)**	**error**	**k_{cat} ($min^{-1}.U^{-1}.mL$)**	**k_{cat}/k_M ($min^{-1}.U^{-1}.mL.\mu M^{-1}$)**
6	0.169	0.049	50.03	33.6	5.63E-03	1.13E-04
6.5	0.156	0.025	29.28	16.14	5.20E-03	1.78E-04
7	0.113	0.042	26.5	20.6	3.77E-03	1.42E-04
7.5	0.133	0.028	21.73	15.34	4.43E-03	2.04E-04
8	0.404	0.24	179.41	66.2	1.35E-02	7.51E-05

Table 5.4. Michaelis-Menten parameters obtained for the reaction of product formation of laccase conjugated with AuNP-CALNN with EDC/NHS. The errors were generated by the software Origin from the fitting of the Michaelis-Menten equation.

Product formation						
pH	**V_M (min^{-1})**	**error**	**K_M (μM)**	**error**	**K_{cat} ($min^{-1}.U^{-1}.mL$)**	**k_{cat}/k_M ($min^{-1}.U^{-1}.mL.\mu M^{-1}$)**
6	0.159	0.012	14.05	9.83	5.30E-03	3.77E-04
6.5	0.138	0.015	6.75	2.89	4.90E-03	5.74E-04
7	0.202	0.05	14.19	10.03	6.73E-03	4.75E-04
7.5	0.245	0.027	9.22	3.33	8.17E-03	8.86E-04

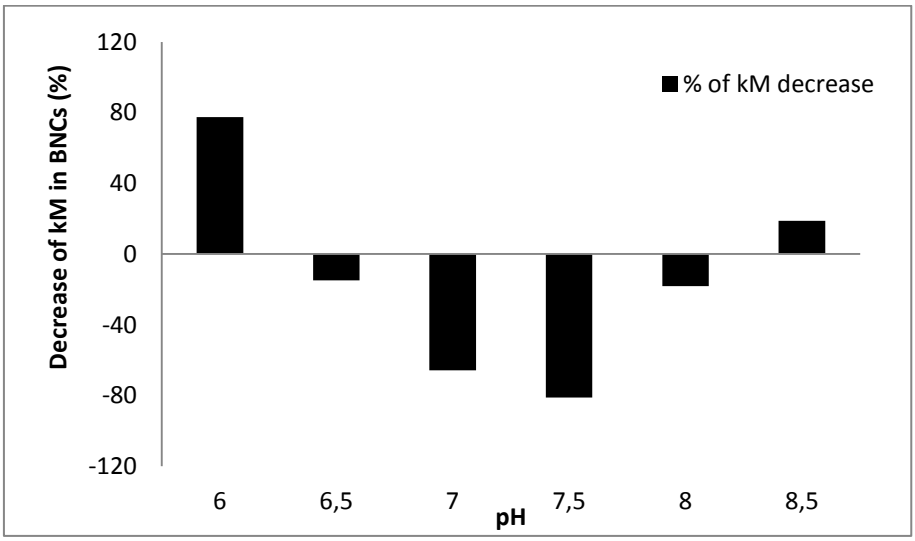

Figure 5.11. Graphical representation of the decrease of kM in BNCs in percentage in comparison with free laccase kM.